# POLYACRYLONITRILE / CARBON NANOTUBE COMPOSITE FIBERS: REINFORCEMENT EFFICIENCY AND CARBONIZATION STUDIES

A Dissertation
Presented to
The Academic Faculty

by

Han Gi Chae

In Partial Fulfillment
of the Requirements for the Degree
Doctor of Philosophy in the
School of Polymer, Textile, and Fiber Engineering

Georgia Institute of Technology
April 2008

# POLYACRYLONITRILE / CARBON NANOTUBE COMPOISTE FIBERS: REINFORCEMENT EFFICIENCY AND CARBONIZATION STUDIES

Approved by:


Dr. Satish Kumar, Advisor
School of Polymer, Textile, and Fiber Engineering
*Georgia Institute of Technology*

Dr. Samuel Graham
School of Mechanical Engineering
*Georgia Institute of Technology*

Dr. Anselm Griffin
School of Polymer, Textile, and Fiber Engineering
*Georgia Institute of Technology*

Dr. Donggang Yao
School of Polymer, Textile, and Fiber Engineering
*Georgia Institute of Technology*

Dr. Naresh N. Thadhani
School of Materials Science and Engineering
*Georgia Institute of Technology*



Date Approved: March 13, 2008

# ACKNOWLEDGEMENTS

First of all, the author would like to express his deepest appreciation to his advisor, Dr. Satish Kumar, for his invaluable guidance during the course of his study. His encouragement always made the author full of confidence.

The author would also like to thank Drs. Anselm Griffin, Naresh Thadhani, Samuel Graham, and Donggang Yao for their service on the thesis committee, and for invaluable suggestions and encouragement through the course of this study.

Many thanks go to Dr. Sreekumar T. Veedu for his help with the initial composite fiber spinning. The author would like to acknowledge to Dr. Tetsuya Uchida and Ms. Marilyn L. Minus for transmission electron microscopy study. The author also would like to thank Dr. Asif Rasheed and Mr. Young Ho Choi for assistance with FT-IR study and bi-component fiber spinning, respectively. The author would like to thank previous group members, Dr. Tao Liu, Dr. Young-Bin Park, Dr. Shanju Zhang, Dr. Hongming Ma, Dr. Xiefei Zhang, Dr. Chongfu Zhou, Dr. Jing Liu, Dr. Tong Wang, Dr. Huina Guo, and the current group members, Mr. Sudhakar Jaganathan, Mr. Beom-Jin Yoon, Mr. Rahul Jain, Mr. Yaodong Liu, Ms. Erika Johnson, and Mr. Ian Winters for their help and friendship.

The author is grateful to his parents, brother and sister for their support and understanding. The author is greatly indebted to his wife and son for their patience, love, and encouragement.

# TABLE OF CONTENTS

# LIST OF TABLES

# LIST OF FIGURES

Page

# SUMMARY

The objectives of this study are:

- To study the structure, processing, and properties of dry-jet wet spun polyacrylonitrile (PAN)/carbon nanotube (CNT) composite fibers.
- To study the structure, processing, and properties of gel spun PAN/CNT fibers.
- To study the stabilization and carbonized behavior of gel spun PAN and PAN/CNT fibers.
- To process small diameter PAN and PAN/CNT fibers using a combination of bi-component spinning and gel spinning, and to study the stabilization and carbonization behavior of these small diameter fibers.

Thesis introduction and brief review of literature is presented in Chapter 1. In Chapter 2, the reinforcement efficiency of single wall carbon nanotube (SWNT), double wall nanotubes (DWNT), multi wall nanotubes (MWNT), and vapor grown carbon nanofiber (VGCNF) in dry-jet wet spun PAN/CNT fibers is compared at 5 wt% CNT loading. Tensile properties of all the composite fibers were enhanced as compared to those of the control PAN fiber. Low strain properties, such as modulus and shrinkage, were most improved by the incorporation of SWNT. On the other hand, high strain properties, such as strength and work of rupture, were most enhanced by the incorporation of MWNT. It was concluded that the large interfacial area between CNT and the polymer matrix contributed to the improvement in low strain properties, and that long CNT length was important for high strain properties.

Gel spinning studies are presented in Chapter 3. Wide angle X-ray diffraction (WAXD) was used to study the structure of the gel spun fibers. Intermolecular spacing in gel spun PAN/CNT fiber was slightly lower than in gel spun PAN. PAN in the immediate vicinity of nanotube exhibited high orientation and good solvent resistance, and could be lattice imaged using high resolution transmission electron microscopy (HRTEM). Ultraviolet (UV) – visible (vis) spectra confirmed SWNT exfoliation in the highly drawn fiber. Mechanical and dynamic mechanical properties of the gel spun fibers are also reported.

Stabilization and carbonization studies on gel spun PAN and PAN/SWNT fibers are reported in Chapter 4. Differential scanning calorimetry (DSC) study shows that incorporation of 1 wt% SWNT affected the reactivity of about 30% PAN. PAN/SWNT shows the development of graphitic structure in the vicinity of carbon nanotubes when carbonized at 1100 °C, while PAN carbonized at this temperature was mostly disordered carbon. Development of graphitic structure at a relatively low carbonization temperature (1100 $^{o}$C) is commercially very important. Tensile strength and modulus of the carbonized PAN/SWNT fibers containing 1 wt% SWNTs are improved by 49% and 64% as compared to those of the carbonized PAN fiber, respectively.

In Chapter 5, PAN and PAN/CNT composite (99/1) fibers have been processed using core-shell and islands-in-a-sea bi-component cross-sectional geometry, and gel spinning. Shell and Sea component polymer are subsequently removed, and the core and islands component are stabilized and carbonized. Using this approach, PAN and PAN/CNT based carbon fibers, with an effective diameter as low as 1 μm have been processed. Islands PAN/CNT (99/1) based carbon fibers processed using this approach

exhibit a tensile strength of 4.5 GPa and tensile modulus of 463 GPa, while these values for the control PAN based carbon fiber processed under the similar conditions are 3.2 GPa and 337 GPa, respectively.

Conclusions and recommendations for future work are presented in Chapter 6.

# CHAPTER 1

# INTRODUCTION

## 1.1 Carbon Fibers

In the late 19th century, Edison produced carbon filament from cotton yarn, and used them for electric lamp light bulb[1]. Following this development, carbon filaments did not receive much attention due to the development of tungsten filament for light bulb application. Since 1950s, there has been significant demand for high performance (i.e. high strength, high modulus, and thermally stable) composite materials, which led to serious effort for investigating high strength carbon fiber. There have been mainly three different precursor fibers for producing carbon fibers; viscose rayon, polyacrylonitirle (PAN), and pitch[2]. However, viscose rayon-based carbon fibers are currently no longer available commercially.

### 1.1.1 PAN-Based Carbon Fiber

PAN was initially developed for producing textile fibers by DuPont in 1950s[3]. PAN turned out to be commercially important polymer due to its high carbon yield. PAN is generally synthesized by co-polymerization of acrylontrile (> 90%) and various co-monomers such as methyl acrylate, methyl metharcylate, vinylacetate, itaconic acid, and sodium methallyl sulphonate[3]. The molecular weight can have a wide range, from ~10,000 to several millions g/mol. For producing fibers, various spinning methods can be used such as wet spinning, dry-jet-wet spinning, gel spinning, and melt spinning. It is also known that dry-jet-wet and gel spinning can produce highly drawn fibers with the low

number of micro-voids throughout the fiber. For melt spinning, PAN polymer needs to be pretreated with plasticizer due to its high melting temperature, which is higher than its degradation temperature.

PAN-based carbon fibers are widely used in composites due to their high tensile and compressive strength. PAN-based carbon fibers are produced in the similar way as viscose rayon-based carbon fibers. These steps include oxidative stabilization (200 – 300 $^{o}$C), carbonization (up to 1700 $^{o}$C), and graphitization (2500 – 3000 $^{o}$C).

During stabilization controlled shrinkage is allowed to ensure that disorientation of molecules is minimized. Figure 1.1(a) shows the possible reaction schemes of PAN during the stabilization process, leading to the ladder structure polymer. The subsequent high temperature heat treatment (> 1000 $^{o}$C) under inert environment causes intermolecular reaction, leading to crosslinking between the ladder polymers as shown in Figure 1.1(b). The overall carbon yield from PAN fiber is about 50 - 60%. Further heat treatment (>1500 $^{o}$C) under inert environment leads to more ordered structure, resulting in higher modulus. As mentioned earlier, PAN-based carbon fibers have higher tensile strength (up to 7 GPa for 5 μm diameter carbon fiber) and relatively lower modulus as compared to those of the pitch-based carbon fibers.

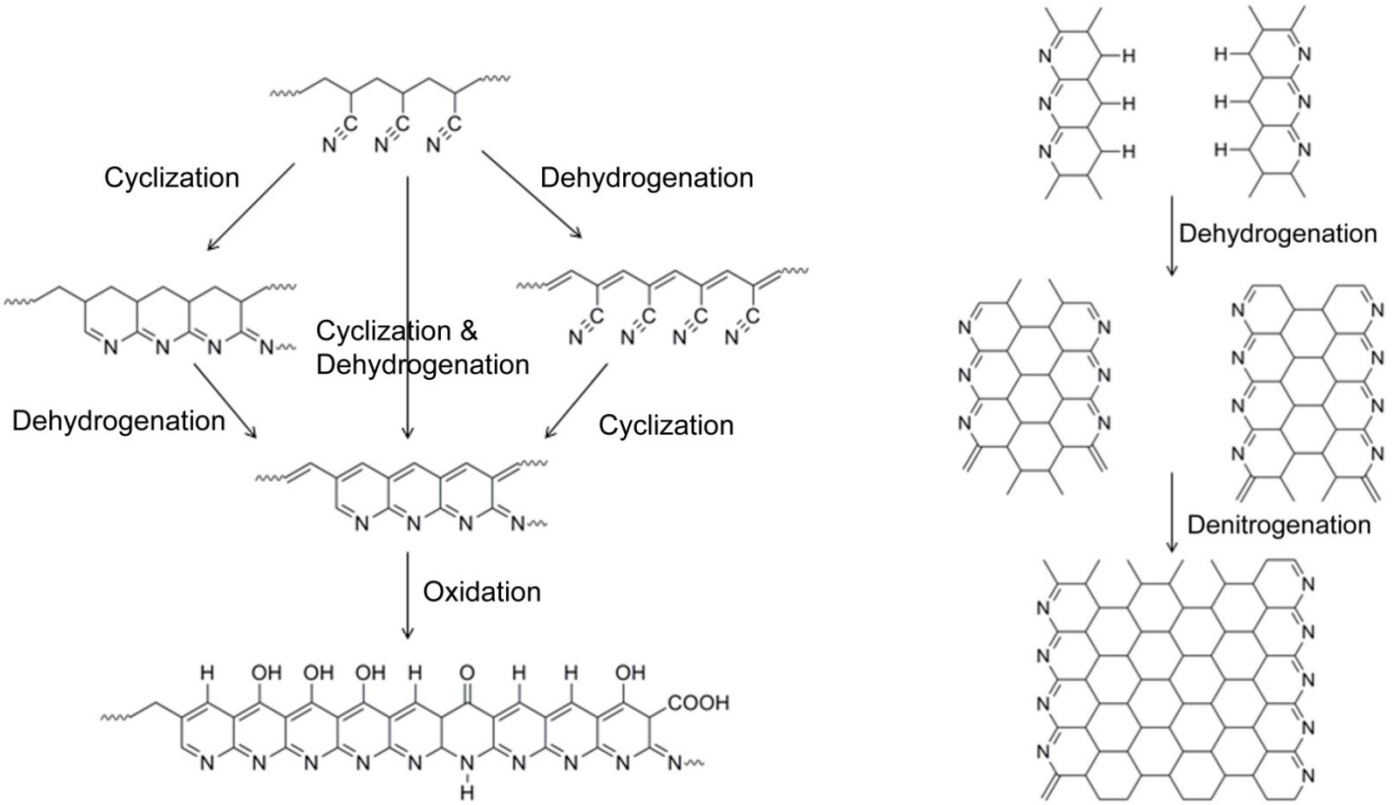


(a) (b)

Figure 1.1. Chemical reaction schemes during (a) stabilization and (b) carbonization of PAN fibers[4].

## 1.2 Carbon Nanotube (CNT)

Sumio Iijima (NEC, Japan) affected by fullerene research[5] decided to conduct transmission electron microscopy (TEM) study on this novel carbon material, and found highly perfect concentric tubular structure, multi wall carbon nanotube (MWNT, Figure 1.2)[6]. This tubular structure ranged in length from a few tens of nanometers to several micrometers, and in outer diameter from ~3 to 30 nm. End caps of these MWNT consist of the combination of pentagonal and heptagonal rings, as well as hexagons[7]. Subsequent studies resulted in the observation of SWNT[8, 9]. The synthesis of SWNT appeared to be extremely significant development, as they can have nearly ideal 1-dimensional structure.

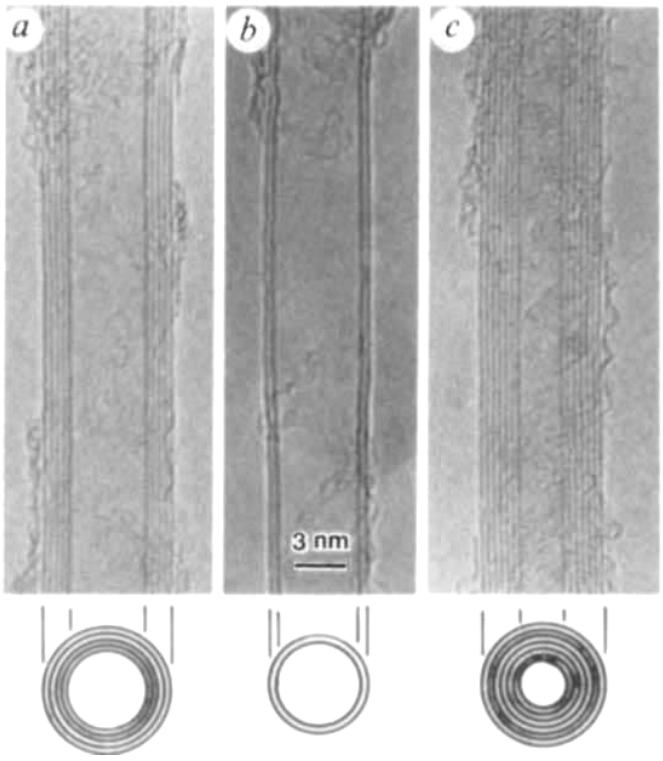


Figure 1.2 Transmission electron micrographs of microtubules of graphitic carbon. Parellel dark lines correspond to the (002) lattice images of graphite. (a) - (c) represent 5 wall, double wall, and 7 wall carbon nanotube, respectively[6].

### 1.2.1 Physical Properties of CNT[10-17]

1.2.1.1 Electronic Structure of CNT[15]

CNT can be described as a graphene sheet rolled into a cylindrical shape (Figure 1.3) so that the structure is one-dimensional with axial symmetry, and in general exhibiting a spiral conformation, so called chirality. CNT can be classified into achiral (armchair and zigzag) and chiral tube. CNTs, whose mirror image have an identical structure to the original, are achiral tubes, and those whose mirror image cannot be superimposed onto the original structure are chiral tubes.

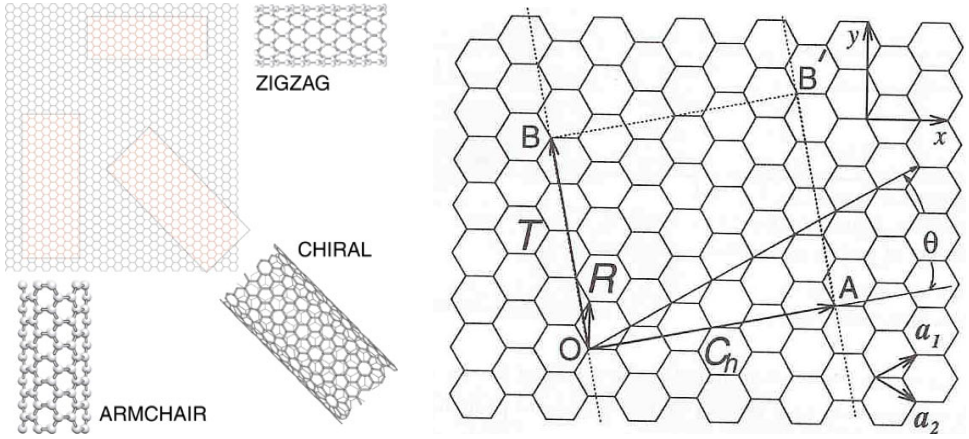


Figure 1.3 Drawings of different types of SWNTs based on the different chiral vector[18], and details of vectors defining the structure of CNTs where $C_h$, $T$, $R$, and θ are chiral vector, translational vector, symmetry vector, and chiral angle[15].

In order to specify the structure of CNTs, the chiral vector ($C_h$) is the most important parameter.

$$C_h = na_1 + ma_2 \equiv (n, m)$$

where, n and m are integers, and a is the lattice constant of graphite structure (2.49 Å).

The relations to obtain metallic or semiconducting CNT are as follows. For metallic CNT, the difference between n and m values should be multiple of 3. Therefore, armchair tubes are always metallic and zigzag tubes when n is multiple of 3 are also metallic. The zigzag tubes whose n value is not the multiple of 3 and chiral tubes with n-m ≠ 3 are semiconducting CNTs.

Since the CNTs have quantized 1D electronic structure, the most distinctive feature of CNT is showing discrete energy state in density of states, which is called van Hove singularities (vHs). Figure 1.4 show the density of states diagram for (10,0) and (9,0) tubes, and the density of state of graphite sheet for comparison. There is no discrete energy level for graphite while the density of state of CNTs show vHs. It should also be noted that (10,0) tube has density of state value of zero at Fermi level ($E$=0) while (9,0) tube has non-zero density of state. As discussed earlier, (10,0) tube is semiconducting zigzag tube and (9,0) is a metallic zigzag tube due to the continuity of density of state at Fermi level. In addition, the band gap energy is inversely proportional to the CNT diameter as expressed by the following equation.

$$E_g = \frac{|t|a_{cc}}{d_t}$$

where |t| is overlap integral, $a_{cc}$ is the distance between adjacent carbon atoms, and $d_t$ is CNT diameter.

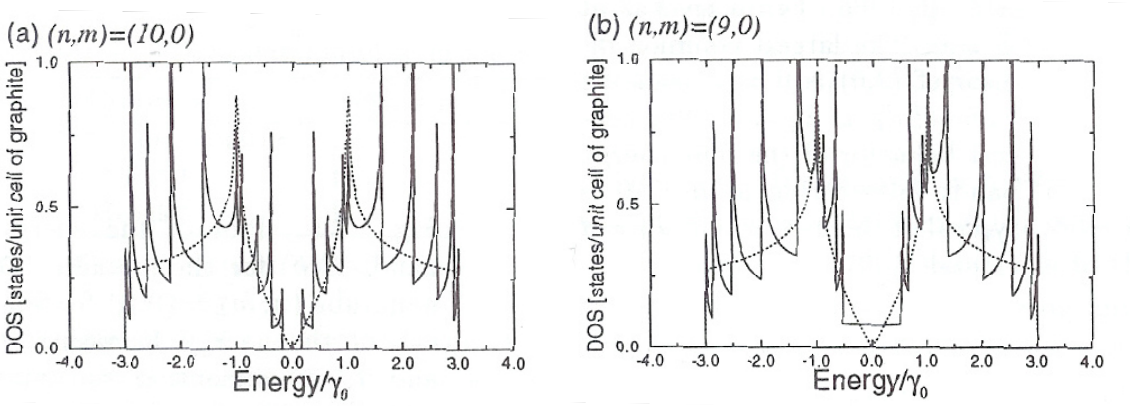


Figure 1.4 1D electronic structure of (a) (10,0) tube and (b) (9,0) tube[15]. For comparison, the density of state of 2D graphite sheet is also presented as dotted line.

The understanding of CNT electronic structure is very important to spectroscopic characterization of CNT such as Raman spectroscopy, UV-vis-NIR spectroscopy, and Fluorescence spectroscopy. For example, Raman spectra of CNT can be used to calculate the orientation of CNT under external force field and assess the interaction of CNT with its environment. Further, CNT diameter can be calculated from radial breathing mode (RBM) band. The ratio of tangential band (G band) to disorder band (D band) can be used for qualitative assessment of CNT perfectness. From UV-vis-NIR spectroscopy, one can assess the exfoliation state of CNT as well as its interaction with the environment.

### 1.2.1.2 Mechanical Properties of CNT

Theoretical and experimental results also showed that SWNT and MWNT can have very high elastic modulus (close to that of graphite, 1060 GPa), and their tensile strength reaches to 90 GPa[17, 19-24]. The properties of CNTs are listed in Table 1.1 and compared with the high performance fibers.

Table 1.1 Typical properties of CNTs, vapor grown carbon nano fiber (VGCNF) and commercial high performance fiber.

| | SWNT[10, 25-29] | DWNT[30] | MWNT[23, 31-33] | VGCNF[34-37] | Carbon fiber[38] | Zylon®[39, 40] | Spectra®[39, 41] | Kevlar 49®[39, 42] |
|---|---|---|---|---|---|---|---|---|
| Tensile strength (GPa) | 23 - 63 | | | 3 - 20 | 4 - 7 | 5.8 | 3.1 | 3.6 - 4.1 |
| Tensile modulus (GPa) | 640 | - | 1060 | 50 - 775 | 150 - 950 | 270 | 105 | 130 |
| Elongation at break (%) | 5.8 | 28 | - | - | 0.5 - 2.5 | 2.5 | 2.5 | 2.8 |
| Density ($g/cm^3$) | 1.3 - 1.5 | 1.5 | 1.8 - 2.0 | 1.9 - 2.1 | 1.7 - 2.2 | 1.56 | 0.97 | 1.44 |
| Electrical conductivity (S/m) | $\sim 10^6$ | | | | $5.5\times10^4$ - $9\times10^5$ | $< 10^{-13}$ | | |
| Typical diameter | 1 nm | ~5 nm | ~20 nm | 60-100 nm | 5 - 15 μm | | | |

1.2.1.3 Thermal Properties of CNTs

Theoretical thermal conductivity of an individual SWNT has been predicted to be as high as 6600 W/mK at room temperature[11], and an experimental value of 3000 W/mK has been reported for a single MWNT[43]. Theoretical calculations also suggest that the thermal conductivity of SWNT is not only related to their diameter and the temperature, but also related to their chirality[44]. High thermal conductivity materials are quite attractive for thermal management applications[45].

1.2.1.4 Electrical Properties of CNTs

The electrical conductivity of SWNT films and fibers has been reported[46, 47] to be in the range of $10^4$-$10^5$ S/m, while the conductivity of the individual nanotubes and nanotube ropes has been measured to be on the order of $10^6$ S/m[10]. According to the percolation theory, Figure 1.5 exhibits the effect of SWNT bundle diameter and length on the electrical percolation concentration of SWNT in polymer matrix[48, 49].

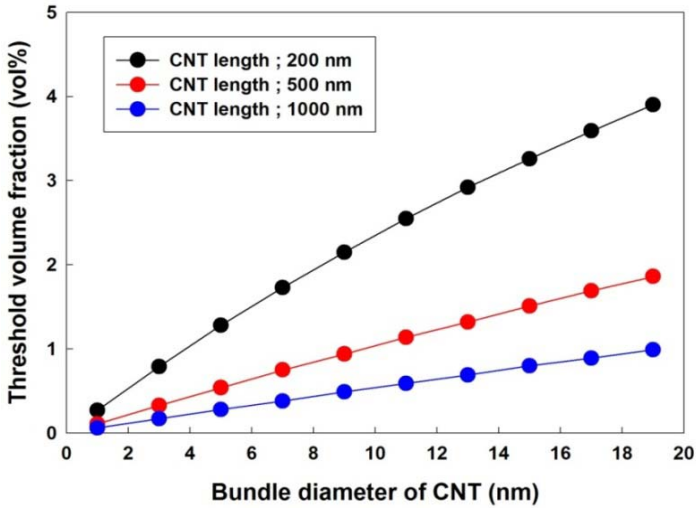


Figure 1.5 The calculated percolation threshold volume fraction of CNT as a function of bundle diameter and length of CNTs.

1.2.1.5 Optical Properties of CNTs

Due to the unique 1D electronic structure of CNT, especially SWNT, as discussed earlier, the optical properties measured by UV-vis-NIR spectroscopy, fluorescence, and Raman spectroscopy are critical methods to characterize the interaction and orientation of composite materials as discussed earlier. In addition, carbon nanotubes exhibit intrinsic anisotropic optical properties. Orientation of single and double wall carbon nanotubes can be determined using the resonance enhanced Raman spectra as a function of polarization direction[47, 50-52]. The absorbance due to SWNT van Hove transitions has also been shown to be dependent on the polarization direction[53].

## 1.3 Dispersion and Orientation of CNT in Polymer Matrix

SWNT agglomerate into 5 to 100 nm diameter ropes[54], and form hexagonal lattice within the rope with binding energy between the tubes being of the order of 900 meV/nm[55]. Therefore, counterbalancing the van der Waals interaction is one of the key challenges for dispersing and exfoliating SWNT. In addition, SWNT ropes have highly entangled structure. DWNT, MWNT, and VGCNF generally exist as individuals and do not aggregate into bundles as SWNTs do. However, they can also be entangled, requiring significant effort for their dispersion. Physical and chemical approaches have been pursued to unentangle, disperse, and exfoliate nanotubes[55-104].

CNTs show highly anisotropic electrical, optical, mechanical, and thermal properties as discussed. Physical properties of CNT fibers and films, and their composites strongly depend upon the CNT orientation in the bulk sample. Therefore, for good

understanding of the properties of CNT based materials, accurate orientation determination is necessary. Orientation of SWNT and DWNT can be determined from Raman spectroscopy and the orientation of MWNT and VGCNF can be determined from wide angle X-ray diffraction. Intensity of the Raman G band in the oriented systems depends on the polarization direction. The Raman spectra can be measured in the VV (polarizer and analyzer are parallel to each other). The detailed methods to calculate the degree of orientation are described elsewhere[50, 52, 105-107]. The orientation of MWNTs and that of the vapor grown carbon nano fibers (VGCNF) can be determined using WAXD. MWNTs and VGCNFs have layered graphitic structure. From the graphite (002) azimuthal scan, orientation of the axis perpendicular to the (002) plane (i.e. the c-axis) can be calculated. Based on the orthogonality condition, orientation of the MWNT can be obtained as described elsewhere[108, 109]. Due to the stacked cup geometry, the orientation of VGCNF needs to be calculated by different way, which is reported elsewhere[37].

### 1.4 Polymer/CNT Composite Films and Fibers

Significant breakthroughs have been reported in processing CNT films and fibers[46, 51, 81, 110-120]. CNTs are also incorporated in numerous polymer matrix by various methods[60, 61, 65, 66, 81, 89, 98, 121-127] with enhanced physical and mechanical properties[47, 58, 81, 113, 117, 120, 128-161]. Among them, PAN/CNT composites are of great current interest. These composites are processed using solvents such as *N*,*N*-dimethylacetamide (DMAc), *N*,*N*-dimethylformamide (DMF), or dimethylsulfoxide (DMSO) using conventional solution spinning, gel spinning, electrospinning, or by film casting. The results reveal that PAN

has strong interaction with CNTs, resulting in enhanced physical and mechanical properties of composite films and fibers.

Sreekumar et al.[47] prepared PAN/SWNT composite fibers containing up to 10 wt% SWNT by conventional dry-jet-wet spinning. Dynamic mechanical analysis exhibited that the dynamic modulus of PAN/SWNT (10 wt% SWNT) fibers at 150 $^{o}$C is an order of magnitude higher than that of the control PAN fibers, and the glass transition temperature of PAN/SWNT (10 wt% SWNT) was about 40 $^{o}$C higher than the control PAN fiber. The remarkable thermal shrinkage reduction of PAN/SWNT fiber at 200 $^{o}$C was also observed. Further, the composite fibers soaked in DMF were just disintegrated, while the control fibers dissolved readily. The subsequent TEM study showed the partial exfoliation of SWNT (~11 nm bundle size as compared to the neat SWNT bundle diameter of ~ 37 nm)[162].

The limited oxidative stabilization study[163] was also carried out and showed that the composite fibers required less stress than the control PAN fibers to keep the constant fiber length during stabilization. This indicates that in PAN/CNT one can maintain the molecular orientation readily in order to obtain high strength and high modulus carbon fiber. The improved tensile properties of the stabilized PAN/SWNT fibers were observed, which suggests the carbonized composite fiber would also have superior properties.

Guo et al.[141] reported that PAN/SWNT composite films have been processed with unique combination of tensile properties, electrical conductivity, dimensional stability, low density, solvent resistance, and thermal stability. PAN molecular motion above the glass transition temperature ($T_g$) in the composite film is significantly suppressed. SEM studies showed that rope diameter in the SWNT powder was 26 nm, while in 60/40

PAN/SWNT film, the rope diameter was 40 nm, suggesting that the PAN molecules either cover the nanotube bundles, or intercalate them, or both.

Ge et al.[164] prepared PAN/surface oxidized MWNT nanofiber sheets by electrospinning. Wide angle X-ray diffraction study showed the higher orientation of MWNT as compared to that of the PAN crystals. The electrical conductivity of the PAN/MWNT composite nanofibers containing 20 wt% nanotubes was 100 S/m.

Ye et al.[165] studied the rupture behavior of PAN/SWNT and PAN/MWNT composite sheets produced by elecctrospinning. A two-stage rupture behavior of the composite fibers under tension, including crazing of polymer matrix and pull-out of carbon nanotubes, has been observed. CNTs reinforce the polymer fibers by hindering craze propagation, reducing stress concentration, and dissipating energy by pullout. It was shown that distribution of nanotubes in the polymer matrix and interfacial adhesion between nanotubes and the polymer are two major factors determining the reinforcement effect of carbon nanotubes in polymer fibers. They also carbonized PAN/SWNT composite to form SWNT/carbon yarns[166]. Atomic force microscopy (AFM) experiment showed significantly improved moduli of carbonized PAN/SWNT yarns as compared to that of the control sample (more than the rule of mixtures prediction).

Koganemaru et al.[167] prepared composite films of PAN and MWNT by gelation and crystallization. They also stabilized and carbonized the drawn gel films. The MWNTs within the PAN matrix promote the formation of a condensed aromatic ladder structure during the stabilization process and play an important role in preparing PAN-based carbon material with high carbon quality and high mechanical properties. When the

stabilized composites with 10 wt% MWNTs are carbonized at 1000 $^{o}$C, the modulus reaches 37.5 GPa, and the electrical conductivity reached $10^4$ S/m.

## 1.5 Objectives of Thesis

Polyacrylonitrile (PAN) fiber is the most common precursor for producing high strength carbon fiber with high compressive strength. Carbon nanotubes (CNTs), one of the novel carbon allotropes, are often heralded as the ultimate reinforcement due to their exceptional mechanical properties. The objectives of this study are:

- To study the structure, processing, and properties of dry-jet wet spun polyacrylonitrile (PAN)/carbon nanotube (CNT) composite fibers.
- To study the structure, processing, and properties of gel spun PAN/CNT fibers.
- To study the stabilization and carbonized behavior of gel spun PAN and PAN/CNT fibers.
- To process small diameter PAN and PAN/CNT fibers using a combination of bi-component spinning and gel spinning, and to study the stabilization and carbonization behavior of these small diameter fibers.

# CHAPTER 2

# REINFORCEMENT EFFICIENCY OF VARIOUS TYPES OF CNTS IN PAN FIBERS SPUN BY CONVENTIONAL SOLUTION SPINNING

## 2.1 Introduction

Which type of carbon nanotube will have the best reinforcement efficiency? This question has received little attention to date[168]. Also there are few reported fiber studies[169], comparing the reinforcement efficiencies of different types of nanotubes. Here, the reinforcement efficiency of SWNTs, DWNTs, MWNTs, and VGCNFs has been compared in polyacrylonitrile fiber at 5 wt% nanotube content.

## 2.2 Experimental

### 2.2.1 Materials

PAN (molecular weight 100,000 g/mol) obtained from Japan Exlan Co. Ltd. was dried *in vacuo* at 90 $^{o}$C. SWNTs were obtained from Carbon Nanotechnologies, Inc. (Houston, TX), DWNTs from Nanocyl, Co. (Belgium), MWNTs from Iljin Nanotech, Co. (Korea), and VGCNFs (PR-24-HT, heat treated at 2850 $^{o}$C) from Applied Sciences, Inc. (Cedarville, OH). The amount of catalytic impurity in each type of nanotube was estimated from the thermogravimetric analysis (TGA) under air based on the residual weight[170]. Based on this analysis, the impurity was 2.4, 5.4, 2.5, and 0.3 wt% in SWNT, DWNT, MWNT, and VGCNF, respectively. *N,N*-dimethylacetamide (DMAc) was obtained from Sigma-Aldrich, Co. and was used as received.

### 2.2.2 Solution Preparation

CNTs (1.5 g) were dispersed in 300 mL DMAc using simultaneous sonication (Cole-Parmer 8891R-DTH, 80 W, 43 kHz) and stirring, until dispersion reached optical homogeneity. SWNTs, MWNTs, and VGCNFs formed optically homogeneous dispersion in less than 10 hours of sonication, while highly entangled DWNTs required continuous sonication for 2 weeks before optically homogenous dispersion could be obtained. 28.5 g PAN was separately dissolved in 150 mL DMAc at 70 $^{o}$C, and PAN/DMAc solution was added to the CNT/DMAc dispersion and homogenized while stirring. Excess solvent was evaporated to obtain the desired solution concentration of 30 g solids (PAN+CNT) in 150 mL DMAc. Accounting for impurity, CNT content, in each case was 5$\pm$0.03 wt% with respect to the weight of the polymer.

### 2.2.3 Electrical Conductivity Measurement of PAN/SWNT/DMAc Solution

The PAN/SWNT/DMAc solution prepared by above method was stirred by high shear mixing impeller for 2 weeks. Leica DMRX Optical Microscope manufactured by Leica Microsystems equipped with a Sony digital photo camera DKC-5000 was used to assess the optical homogeneity of the composite solution. For solution electrical conductivity measurement, a cell shown in Figure 2.1 was used. The applied DC (direct current) and current step through the electrode were in the range of 0.01 to 0.45 μA with the step of 110 nA, respectively. Delay time between each measurement was set to be 180 s. Based on the collected voltage and geometrical consideration of the cell, one can calculate electrical conductivity of the solution. UV-vis-NIR spectra were recorded on a

Cary 5G (Varian) spectrometer using a 10 mm quartz cell. For sample preparation, 1 g of composite solution was collected and 20 mL of DMAc was added to the solution followed by stirring with magnetic bar for 10 min. The same concentration of PAN/DMAc solution was prepared and used for baseline subtraction.

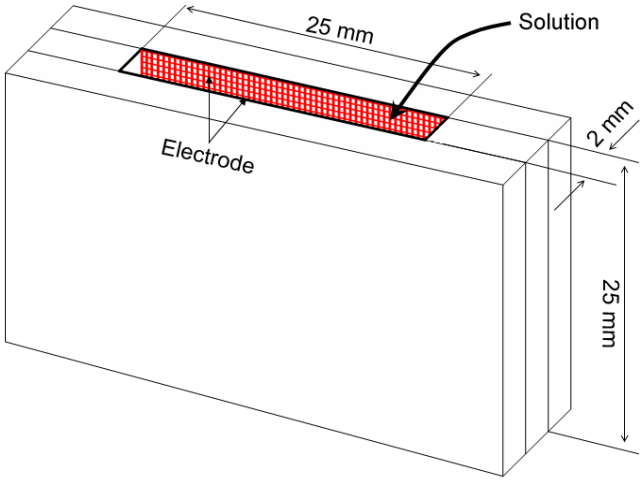


Figure 2.1 The schematic diagram for electrical conductivity measurement. The spacer and substrate for electrodes were made by glass slides. The nickel plate was cut to be used as electrodes. The glass parts were assembled by silicon adhesives.

### 2.2.4 Fiber Spinning

The PAN/CNT/DMAc solutions were spun at room temperature by dry-jet-wet spinning using the small scale spinning system manufactured by Bradford University Research Ltd. The air gap between spinneret (single hole, 500 μm diameter) and the coagulation media was about 2 cm. The schematic of the spinning set up is shown in Figure 2.2. A 635 mesh (20 μm) stainless steel filter pack (TWP, Inc.) was used in the spinning line. DMAc/water volumetric ratios in the coagulation baths (baths 1 and 2) and drawing bath (bath 3) were 60/40, 10/90, and 0/100, respectively, while the two coagulation baths were maintained at 30 $^{o}$C and the drawing bath at 100 $^{o}$C. An in-line heater was used for fiber drying and was maintained at 130 $^{o}$C. There was no fiber

drawing in the two coagulation baths. Fiber was drawn between 1st and 2nd rollers, and fibers were allowed to relax and dried in the heating block. Take-up roller speed was set to be a little lower (19.4 m/min) than the 2nd roller speed (20 m/min). The final draw ratio of the control PAN and for each composite fiber was 10. The fibers were further dried in a convection oven at 50 $^{o}$C for 1 week at constant length.

### 2.2.5 Mechanical Properties

Fiber mechanical properties were determined using RSA III solids analyzer (Rheometric Scientific, Co.). The gauge length and crosshead speed for the tensile tests were 25 mm and 0.1 mm/s, respectively. For tensile tests, at least 10 filaments were tested in each case.

### 2.2.6 Dynamic Mechanical and Thermo-Mechanical Properties

Dynamic mechanical tests were conducted at 10 Hz at a heating rate of 2$^{o}$ C/min, and on bundles of 10 filaments at 25 mm gauge length. Thermal shrinkage was determined using thermo-mechanical analyzer (TMA 2940, TA Instruments) at 15 MPa pre-stress and at a heating rate of 10 $^{o}$C /min.

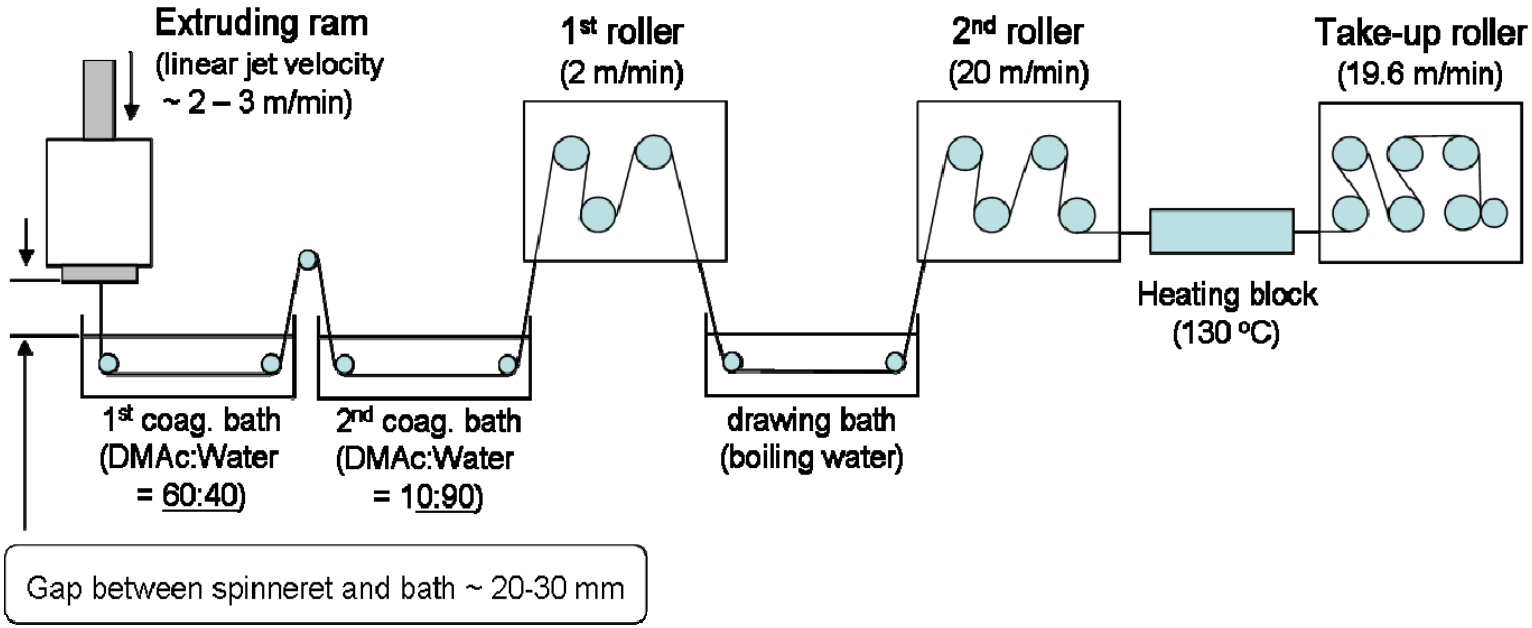


Figure 2.2. The schematic diagram of the dry-jet-wet fiber spinning set up.

### 2.2.7 Raman Spectroscopy

Raman spectra were collected in the back scattering geometry using a Holoprobe Research 785 Raman Microscope made by Kaiser Optical System using 785 nm excitation laser with polarizer and the analyzer parallel to each other. Spectra were collected when the fiber axis was at 0, 5, 10, 20, 30, 40, 50, 60, 70, 80, 85, and 90° from the polarization direction[52]. The SWNTs and DWNTs orientation in the composite fiber was determined from the peak intensity of tangential band (ca. 1590 $cm^{-1}$) assuming Gaussian intensity distribution with respect to the polarization direction.

### 2.2.8 WAXD Analysis of PAN/CNT Composite Fibers

Wide angle X-ray diffraction (WAXD) patterns were obtained on multifilament bundles by Rigaku Micromax-007 (operated at 45 kV, 0.66 mA, $\lambda$=1.5418 Å) using Rigaku R-axis IV++ detection system. The diffraction patterns were analyzed using AreaMax V. 1.00 and MDI Jade 6.1. PAN orientation was determined from the (200,110) azimuthal scans ($2\theta$=16.7°) using the previously described procedure[47]. PAN crystallinity was determined by area-calculation of deconvoluted integrated diffraction patterns. In PAN/MWNTs and PAN/VGCNFs composite fibers, the graphite peak was also present and was excluded from the PAN crystallinity calculation. The PAN crystal size was determined from the peak at $2\theta$=16.7° using the Scherrer equation with K=0.9.The orientation of MWNTs in the composite fiber was determined from the graphite (002) azimuthal scan obtained from X-ray diffraction. From the orientation factor of the graphite plane normal, -0.455, orientation factor of the graphite plane was determined to be 0.91 on the assumption of the symmetry of orientation along the *a* and *b* axes. The orientation of the VGCNF was also determined from the graphite (002) azimuthal scan. The graphene layers in VGCNFs make an angle of 15° to the fiber axis. Therefore, to determine the orientation of VGCNFs, the azimuthal scan profile was fitted by two

Gaussian peaks, with peak positions located at ±15° around the equator as described elsewhere[37].

### 2.2.9 Morphology of Composite Fibers

Fiber tensile fractured surfaces were observed on the gold coated samples by scanning electron microscopy (LEO 1530 SEM operated at 15 kV). Transmission electron microscopy (TEM) specimens for the composite fibers were prepared by detachment method using parlodian[171]. Bright field TEM images were recorded on Mitsubishi Microscope Film using JEM 2000EX (operated at 200 kV).

## 2.3 Results and Discussion

### 2.3.1 Properties of Pristine CNTs

Figure 2.3 shows the bright field TEM and SEM images of various nanotubes used in this study. As expected, SWNTs show 5 - 50 nm diameter bundles or ropes, with an average diameter of about 30 nm. Diameters of DWNTs were about 5 nm, and they mostly existed as individual tubes, however these were highly entangled. The average diameter of MWNTs was about 20 nm, and these also existed as mostly individuals, however these were highly entangled. Diameter of VGCNF was about 60 nm and they appeared to be relatively free of entanglements. As mentioned in the experimental section, DWNTs, due to high degree of entanglement, were the most difficult to disperse. By comparison SWNTs and MWNTs were readily dispersed by sonication, suggesting a relatively less entangled structure in these two types of nanotubes.

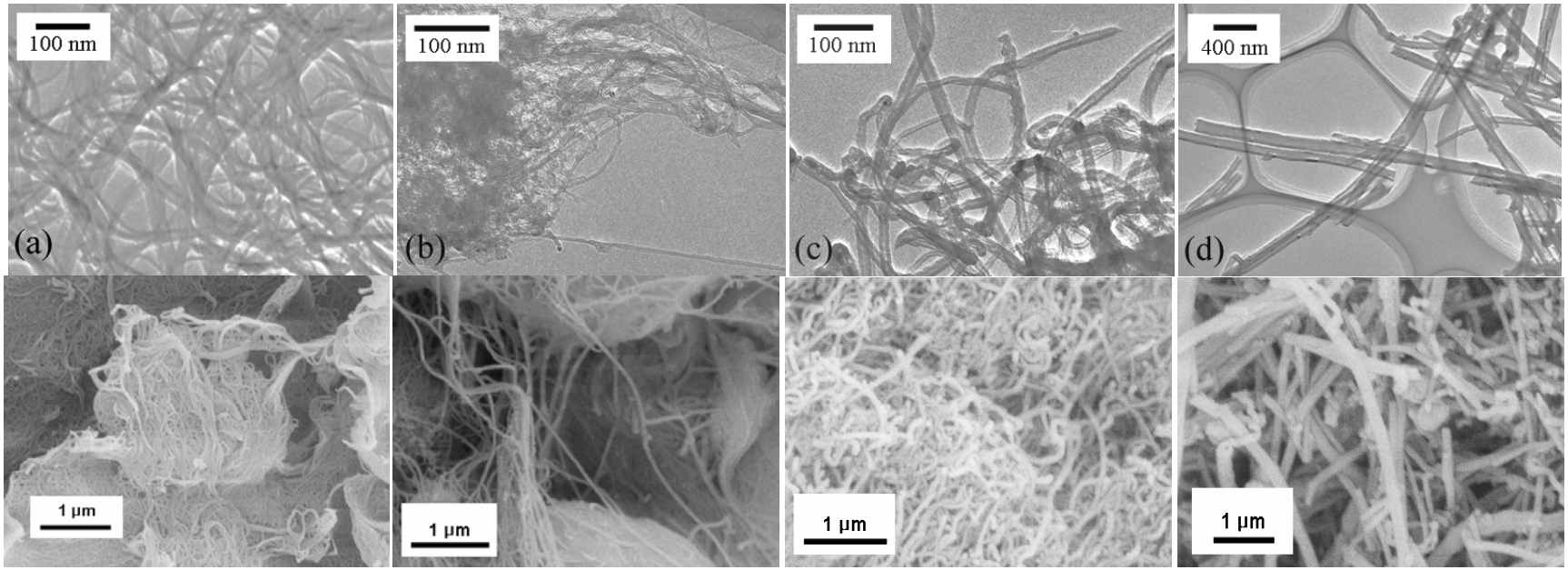


Figure 2.3. Bright field TEM and SEM images of carbon nanotubes used in this study: (a) SWNT, (b) DWNT, (c) MWNT, and (d) VGCNF.

TGA plots indicate that SWNT, DWNT, MWNT, and VGCNF degradation peaks in air at about 440, 500, 600, and 700 $^{o}$C, respectively (Figure 2.4(A)). Degradation in MWNT and VGCNF is delayed due to the existence of the layered graphitic structure in these. For comparison, TGA analysis results in nitrogen (Figure 2.4(B)) show that all nanotubes do exhibit degradation in the 800-1000 $^{o}$C range. SWNT exhibit the most degradation followed by SWNT, MWNT, and VGCNF.

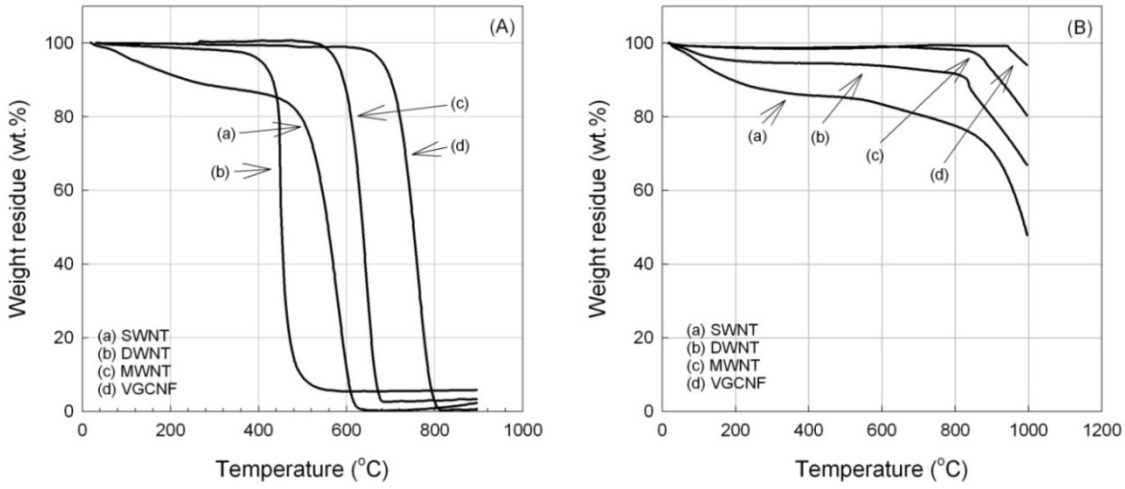


Figure 2.4. Thermogravimetric plots for pristine (a) SWNT, (b) DWNT, (c) MWNT, and (d) VGCNF powder at a heating rate of 10 ºC/min in (A) air and (B) nitrogen.

Raman spectra (Figure 2.5) show that the intensity of the disorder band (ca. 1300 cm$^{-1}$) in MWNTs and in VGCNF is quite high, suggesting highly defective graphitic structure in these two cases. Among the four types of tubes, SWNTs appear to have the highest perfection followed by DWNTs.

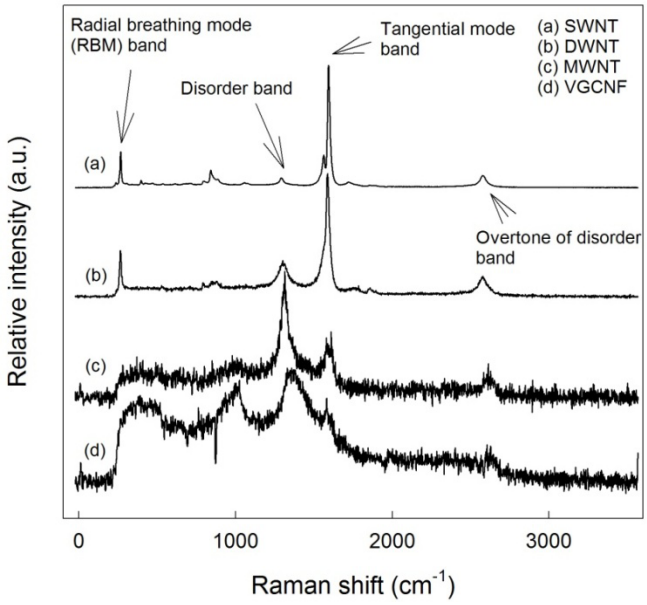


Figure 2.5. Raman spectra for pristine (a) SWNT, (b) DWNT, (c) MWNT, and (d) VGCNF powder.

### 2.3.2 Optical Homogeneity of PAN/CNT/DMAc Composite Solution

During spinning solution preparation, the optical homogeneity has been checked by optical microscopy. As mentioned in the experimental section, all the nanotube/PAN solution showed optical homogeneity by simultaneous sonication and high shear stirring for 10 hr except DWNT. Figure 2.6 shows optical micrographs of SWNT and DWNT solutions as a function of stirring and sonication time. While the SWNT solution exhibited homogeneous dispersion, DWNT solution even after 7 days of sonication and stirring contained small DWNT aggregates visible under the optical microscopy. By extensive sonication and stirring for about 2 weeks, nearly homogeneous solution could be obtained and the spinning solution was prepared. Therefore, one can expect the highly entangled DWNT structure and significant reduction in DWNT length due to the long exposure time of DWNT to sonication.

### 2.3.3 Effect of High Shear Mixing on the Electrical Conductivity and UV-vis-NIR Spectra of PAN/SWNT/DMAc Solution

The resolution of optical microscope (OM) is limited to about 350 nm. Even though optical homogenenity of the solution is necessary to obtain well dispersed CNTs composite solution, there is no way to assess the degree of dispersion or exfoliation with OM once we have particle size less than the optical resolution. As shown in Figure 2.6, the SWNT/DMAc solution after 1 hr sonication exhibited very poor dispersion, while the addition of PAN into the SWNT/DMAc solution after 10hr sonication facilitated the SWNT dispersion. It is also observed that, after 5 day high shear mixing, there is little change in optical homogeneity of the solution. PAN is also known to be one of the polymers that have good interaction with CNTs. Several studies have shown that PAN molecules can wrap around the CNTs. Therefore, one can expect the SWNT exfoliation via intercalation of PAN molecules into the inter-tube spacing of SWNT bundle by applying high shear mixing, whereas the optical homogeneity does not change significantly. As mentioned in Chapter 1, electrical conductivity of SWNT composite materials is strongly dependent on the exfoliation as well as aspect ratio. To date, most of the electrical conductivity measurement has been carried out for the solid state composite films and fibers. The only way to verify the exfoliation effect was changing CNT concentration during processing. Measurement of electrical conductivity of solution during high shear mixing can be used to assess the degree of exfoliation in solution. The electrical conductivity increased monotonically as a function of shearing time, suggesting enhanced SWNT dispersion and exfoliation (Figure 2.7). It is noteworthy that for low current level (0.01 and 0.1 μA), the electrical conductivity increases abruptly after 7 days

of high shear mixing. Figure 2.8 shows UV-vis-NIR spectra of the composite solution. In the beginning of high shear mixing, one could observe van Hove transitions, which are finger-prints for SWNT exfoliation. However, as mixing time goes by, the absolute optical absorbance increases. This indicates increase of individual SWNT population in the solution. Especially, there is abrupt increase in absorbance between $9^{th}$ and $13^{th}$ day stirring, which is almost consistent with the electrical conductivity result. It is clearly shown that the combination of electrical conductivity and UV-vis-NIR spectra can be used to monitor SWNT dispersion and exfoliation.

Besides assessing the exfoliation, one can also notice that the electrical conductivity at high current level (0.34 and 0.45 μA) exhibits relatively high value at shorter mixing time and less sensitivity to mixing time. This indicates that at low current, the mobility of suspended SWNT in solution is prohibited by the high viscosity of solution, which results in the preservation of percolation network. Therefore, the conductivity at low current is relatively higher or comparable to that of high current measurement, once SWNT exfoliation occurs. However, the breakage of percolation in solution could be expedited by applying high current, i.e. stronger electric field strength. The schematics in Figure 2.7 represent the SWNTs in solution at different current and degree of exfoliation, showing the effect of SWNT alignment with the electric field strength and exfoliation.

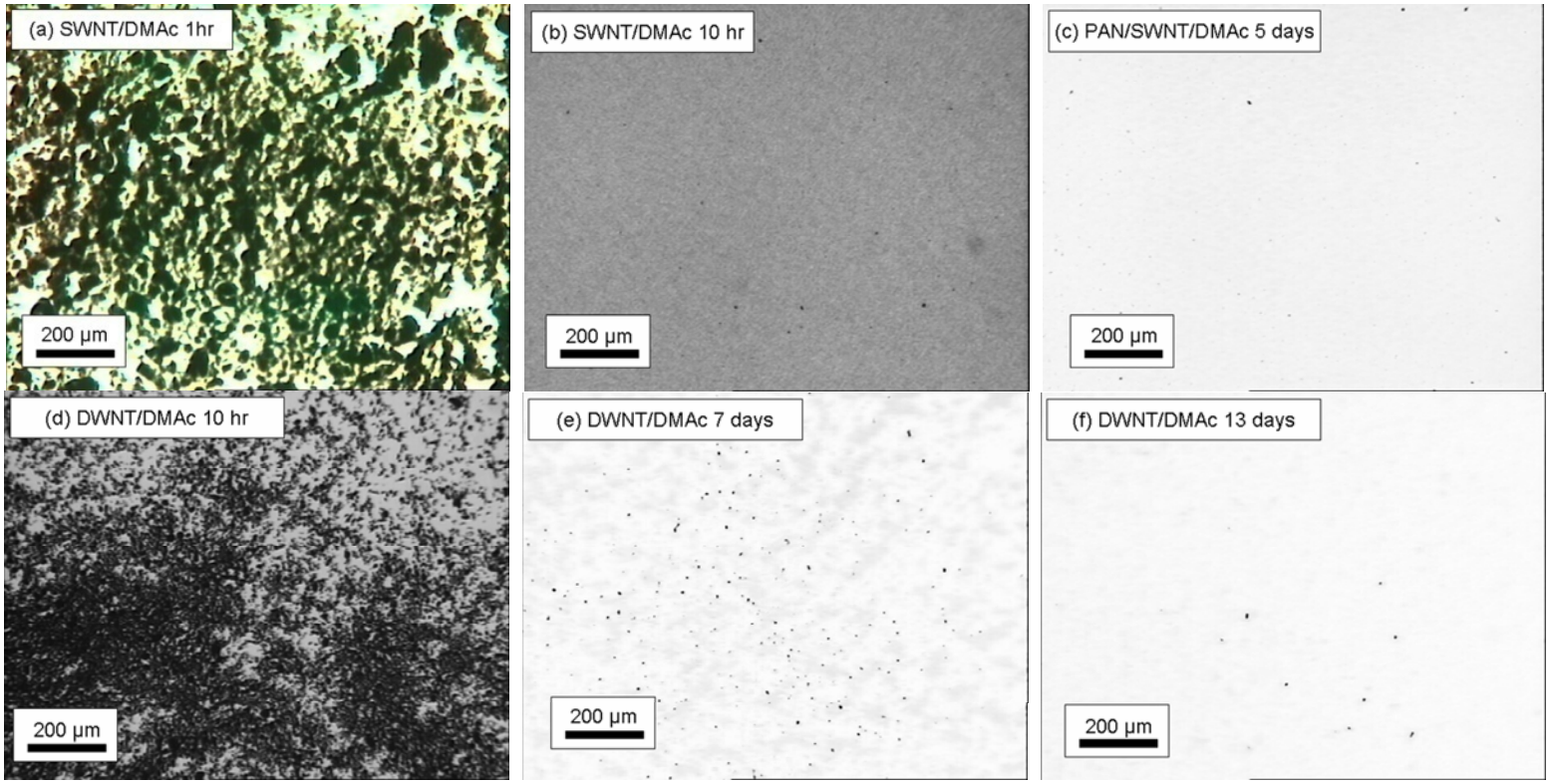


Figure 2.6 Optical micrographs of (a)-(c) SWNT/DMAc and PAN/SWNT/DMAc solution, and (d)-(f) DWNT/DMAc and PAN/DWNT/DMAc solution as a function of sonication and stirring time.

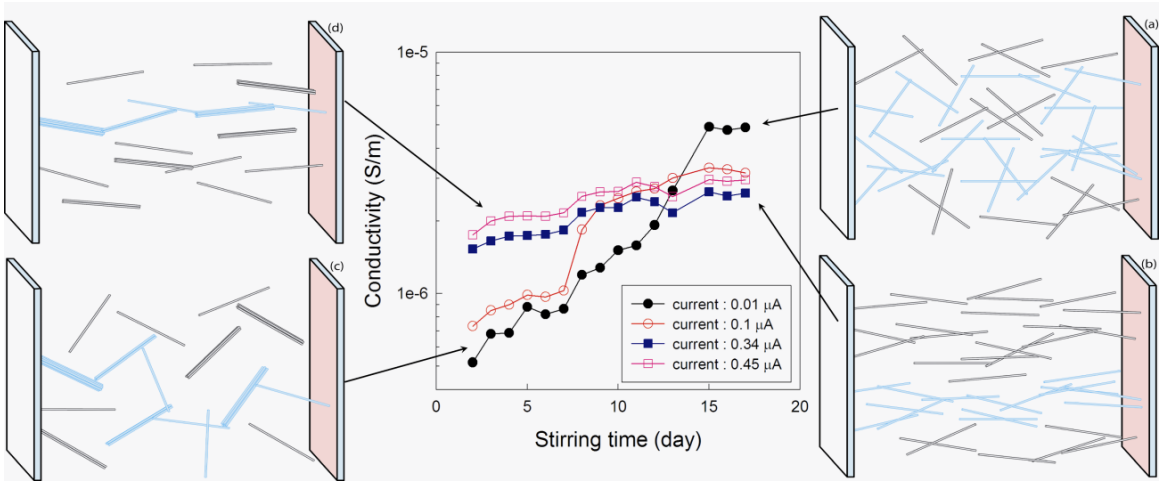


Figure 2.7 Electrical conductivity of PAN/SWNT/DMAc solution as a function of high shear mixing time and schematics describing the status of SWNT in solution.

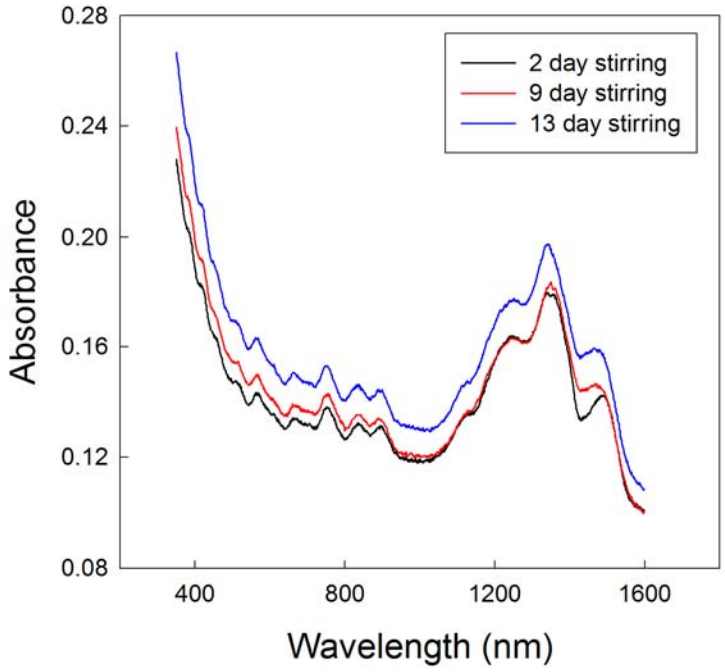


Figure 2.8 UV-vis-NIR spectra for PAN/SWNT/DMAc solution as a function of high shear mixing time.

### 2.3.4 Mechanical Properties and Dimensional Stability of PAN/CNT Composite Fibers

Mechanical properties and various structural parameters for the control PAN and the composite fibers are listed in Table 2.1. All composite fibers exhibit improved mechanical properties over the control PAN. Increase in modulus and decrease in shrinkage is the highest in SWNT containing fibers, while increase in tensile strength, strain to failure, and toughness was the highest in MWNTs containing fibers. Improvement in all the properties in PAN/DWNTs and PAN/VGCNFs composite fibers was intermediate to that of PAN/SWNTs and PAN/MWNTs. While conventional fillers and reinforcements improve modulus and strength at the expense of strain to failure and toughness, all nano carbon reinforcements used in this study improved all mechanical properties, including up to 230% improvement in fiber toughness (with just 5 wt.% MWNTs) as measured from the area under the stress-strain curve.

Storage modulus at 140 $^{o}$C is enhanced by almost a factor of 6 (for SWNT containing fibers), while the tan δ peak temperature increased from 100 $^{o}$C for the control PAN to 109 $^{o}$C for the PAN/SWNTs composite, and the magnitude of the tan δ peak decreased from >0.3 for the control PAN to below 0.2 for the composite fibers (Figure 2.9). Storage moduli in the entire temperature range for the MWNT and VGCNF containing composite fibers were quite comparable to each other. On the other hand, the storage modulus of the composite containing DWNT was substantially higher than that of the control fiber, above the glass transition temperature, while it only exhibited a moderate increase at room temperature. Width of the tan δ vs. temperature plot for the composite fibers (except SWNT containing fibers) is significantly reduced as compared

to that of the control PAN. This suggests a narrower spectrum of relaxation times in the composites than in PAN, a result of polymer interaction with the nanotubes. In the case of SWNT containing fibers, tan δ peak is broadened towards high temperature. We conjecture that PAN interactions with SWNT are stronger than with other larger diameter nanotubes, and that PAN segments closer to the SWNT exhibit tan δ loss at higher temperature than the segments farther from it, leading to the broadening in the high temperature region. Intercalation of PAN in the SWNT bundle may also be partially responsible for the tan δ broadening behavior.

SWNT containing fibers exhibited most improvement in the thermal shrinkage behavior, followed by MWNTs, VGCNF, and DWNT, respectively (Figure 2.10). In the control PAN fiber, as there are no nanotubes, amorphous chains are free to relax, unless constrained by the crystalline regions. In the PAN-CNT composite, due to polymer nanotube interaction, an additional constraint is imposed on the PAN molecules, resulting in improved thermal shrinkage performance. DWNT containing samples exhibit poor performance due to high degree of entanglement and agglomeration. Under comparable spinning conditions, PAN orientation factors in the composite fibers were 0.62, 0.60, 0.57, and 0.53 for SWNT, MWNT, VGCNF, and DWNT containing fibers, while the orientation of the control PAN fiber was 0.52. All types of CNTs, including VGCNF, resulted in enhanced polymer orientation, with SWNT resulting in most enhancements. Normally fibers with high degree of orientation results in large thermal shrinkage, and unoriented fiber would exhibit no entropic shrinkage. Considering that the nanotube containing fibers exhibit higher orientation than the control PAN, the reduction in their

thermal shrinkage conveys stronger PAN-CNT interaction than if the PAN orientation in the composite was the same as in the control PAN.

### 2.3.5 Structural Analysis of PAN/CNT Composite Fibers

Integrated radial WAXD scans, including the deconvoluted scans and the flat plate photographs for various fibers are given in Figure 2.11. The crystallinity of the control PAN fiber was only marginally higher than that of the composite fibers. However, PAN crystal size obtained from (200,110) peak, was larger in all composite fibers, and 35% larger in SWNT and MWNT containing fibers than the control PAN. As was the case with orientation, composite fiber containing DWNTs exhibited the smallest increase in crystal size. PAN is currently the predominant precursor for carbon fibers. Stabilization and carbonization studies on PAN/carbon nanotubes composites point to the potential of this composite system as a precursor for next generation carbon fiber[163, 167]. Fibers with larger PAN crystals and higher polymer molecular orientation are expected to lead to a more perfect and higher orientation carbon fiber with improved mechanical properties.

Table 2.1 Structural parameters and properties of control PAN and PAN/CNT composite fibers.

| | Control PAN | PAN/SWNT | PAN/DWNT | PAN/MWNT | PAN/VGCNF |
|---|---|---|---|---|---|
| Tensile modulus (GPa) | 7.8 ± 0.3 | 13.6 ± 0.5 | 9.7 ± 0.5 | 10.8 ± 0.4 | 10.6 ± 0.2 |
| Tensile strength (MPa) | 244 ± 12 | 335 ± 9 | 316 ± 15 | 412 ± 23 | 335 ± 13 |
| Strain to failure (%) | 5.5 ± 0.5 | 9.4 ± 0.3 | 9.1 ± 0.7 | 11.4 ± 1.2 | 6.7 ± 0.3 |
| Work of rupture (MPa) | 8.5 ± 1.3 | 20.4 ± 0.8 | 17.8 ± 1.7 | 28.3 ± 3.3 | 14.0 ± 1.0 |
| Shrinkage at 160 $^{o}$C (%) | 13.5 | 6.5 | 11.5 | 8.0 | 11.0 |
| $T_g$ [a] ($^{o}$C) | 100 | 109 | 105 | 103 | 103 |
| $f_{PAN}$ | 0.52 | 0.62 | 0.53 | 0.60 | 0.57 |
| $f_{CNT}$ | - | 0.98 | 0.88 | 0.91 | 0.91 |
| Crystal size (nm) | 3.7 | 5.0 | 4.1 | 5.0 | 4.4 |
| Crystallinity (%) | 58 | 54 | 57 | 55 | 55 |

a. Tan δ peak temperature

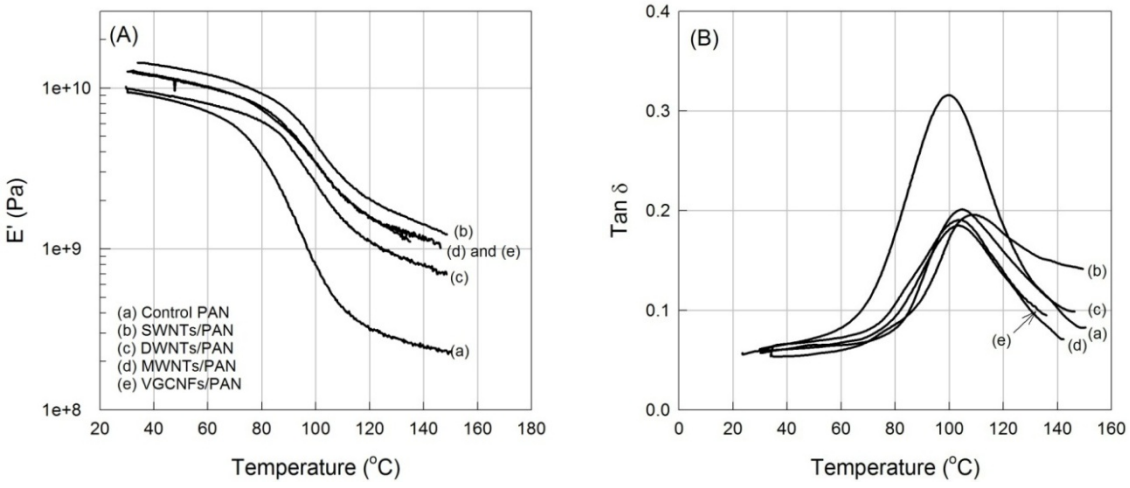


Figure 2.9 (A) Storage modulus and (B) Tan δ versus temperature plots of various composite fibers.

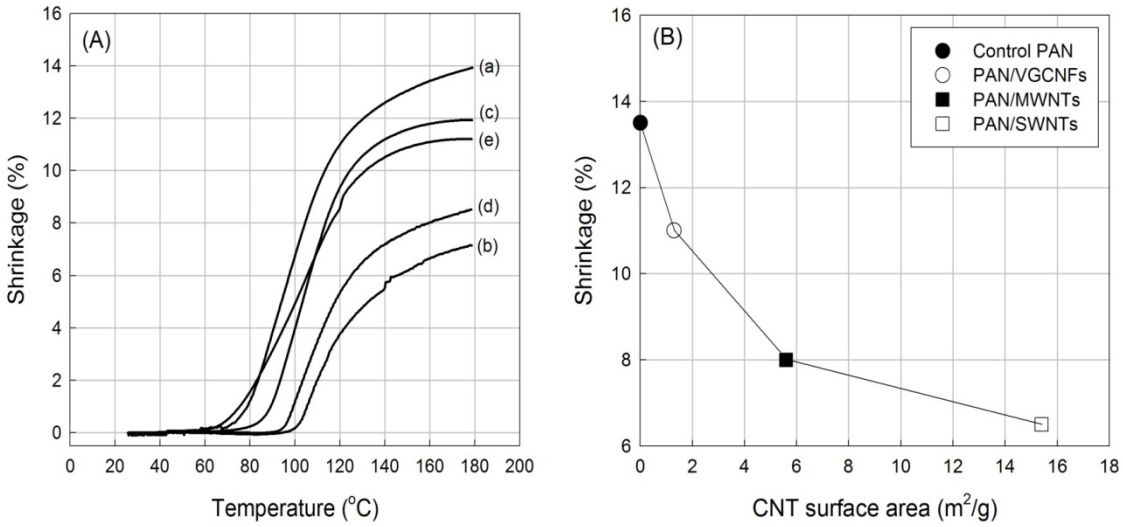


Figure 2.10 (A) Thermal shrinkage in various fibers as a function of temperature. Figure legend same as in Figure 2.10(A). (B) Thermal shrinkage in various fibers at 160 °C as a function of CNT surface area.

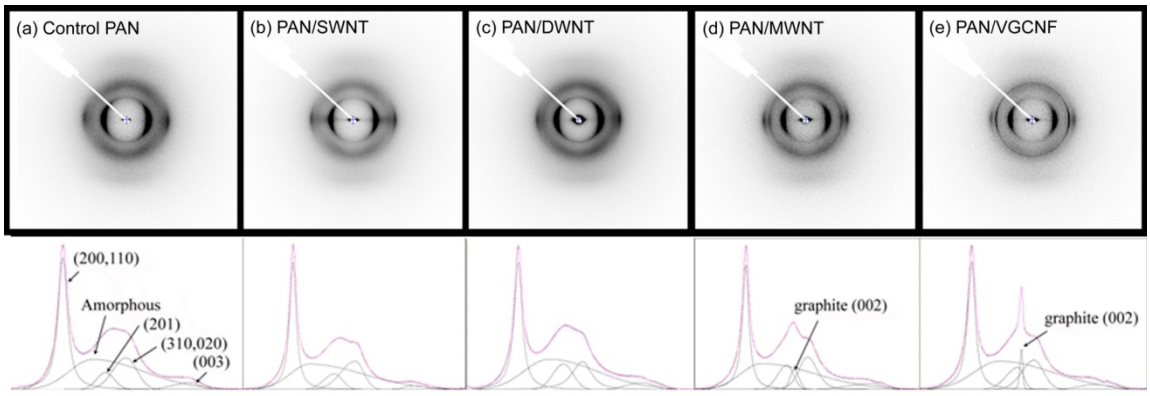


Figure 2.11 2D WAXD patterns of various PAN and PAN/CNT fibers. The bottoms figures show the integrated radial scans of each WAXD pattern and peak deconvolution for crystallinity calculation.

### 2.3.6 Morphological Studies of PAN/CNT Composite Fibers

Tensile fractured surfaces reveal fibrillar structure in both the control PAN and the PAN/CNTs composite fibers (Figure 2.12). Many more fibril ends are observed in PAN/SWNT fiber than in PAN/MWNT fiber. SWNT bundles are known to be surrounded by PAN molecules[141, 144], and we suggest that the fibril ends observed in PAN/SWNT composite are PAN wrapped SWNTs bundles (Figure 2.12b). The fact that numerous fibril ends are visible in PAN/SWNT than in PAN/MWNT, suggests that SWNT or SWNT bundles are much shorter than MWNTs.

Higher tensile strength and higher toughness of the PAN/MWNT fiber, over that of the PAN/SWNT fiber is attributed to longer MWNTs than SWNTs. This behavior is analogous to the increased tensile strength with increasing molecular weight in polymers[172-175].

Bright field TEM images of thin peeled composite fibers as well as the schematics showing the presence of carbon nanotubes are shown in Figure 2.13. SWNTs, MWNTs, as well as VGCNFs are mostly oriented along the fiber axis. However these are not quite

straight, as kinked, bent, and curved nanotubes were generally observed. SWNT bundle diameter in the composite fiber is about 10 nm[162]. This represents partial exfoliation of the SWNT bundles, as the diameter of the SWNT ropes in the powder used in this study was about 30 nm. SWNT, MWNT, and VGCNF agglomeration was not observed in these composite fibers. Occasionally MWNTs with orientation perpendicular to the fiber axis were also observed. SWNT bundles were typically 100 to 300 nm long (Figure 2.13a), while MWNTs longer than 1 μm were often observed (Figure 2.13c). VGCNFs also survived the sonication and fiber processing conditions, and were also typically longer than 1 μm. However due to the stacked cup geometry[168, 176], the strength of the VGCNF is lower than that for the MWNTs, resulting in lower tensile strength improvement in PAN/VGCNF than in PAN/MWNT. In PAN/DWNT composite fiber, the dispersed nanotubes were mostly individuals and well oriented. However, TEM images also reveal the presence of entangled and unoriented DWNTs globules (Figure 2.13b). The limited property improvements in PAN/DWNT composite fibers are a result of the presence of these unoriented and entangled DWNT globules. The size of these DWNT globules is in the range of 50 to 200 nm, which is below the resolution limit of the optical microscope and explains why solutions containing such globules appeared to be mostly optically homogeneous.

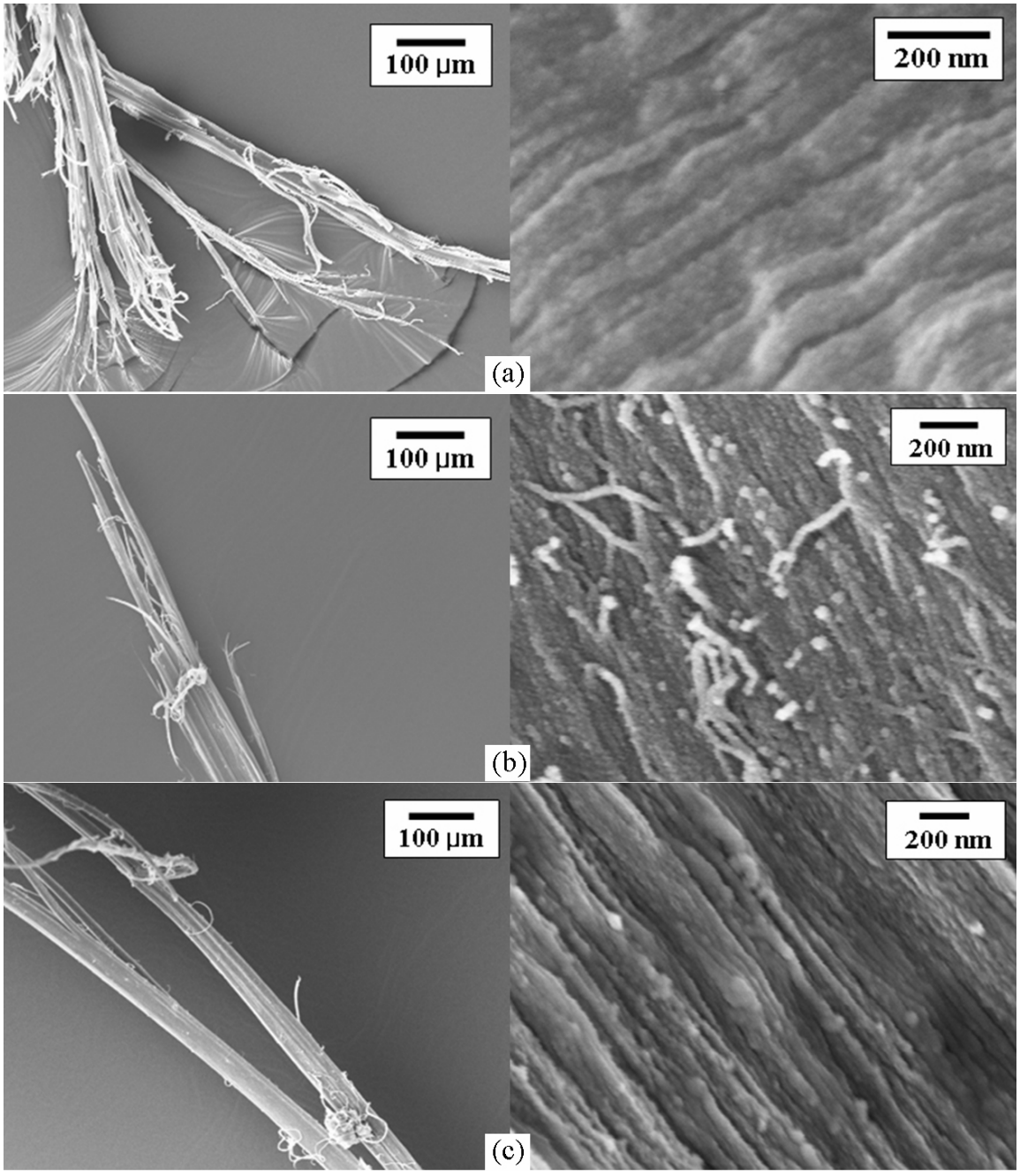


Figure 2.12 SEM images of the tensile fractured surfaces; (a) control PAN, (b) PAN/SWNTs, and (c) PAN/MWNTs fibers.

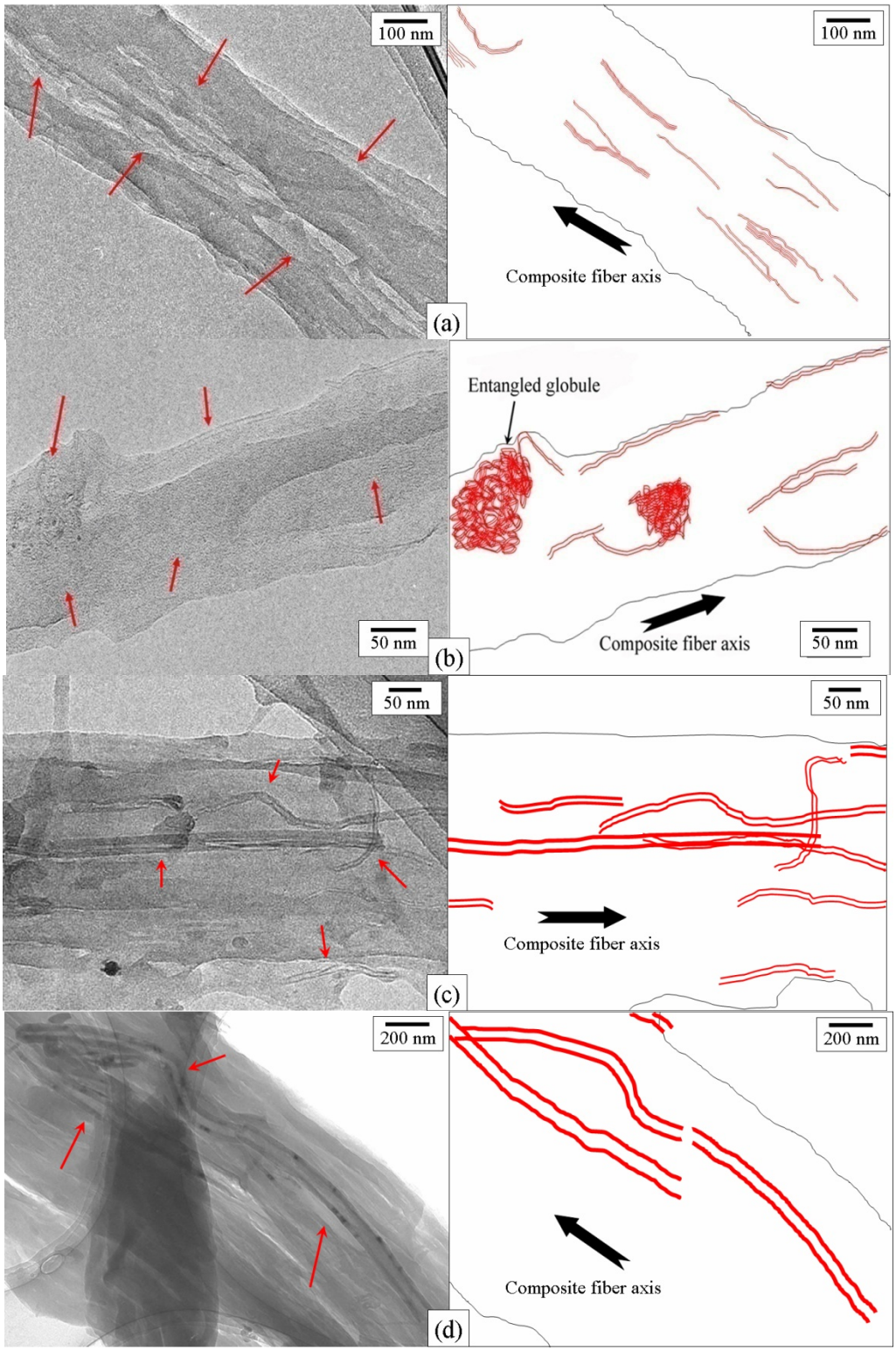


Figure 2.13 Bright field TEM images and the schematics showing the presence of carbon nanotubes in various composite fibers; (a) PAN/SWNTs, (b) PAN/DWNTs, (c) PAN/MWNTs, and (d) PAN/VGCNFs.

### 2.3.7 Effect of Interfacial Area between PAN and CNT on the Physical Properties of Composite Fibers

The enhancements in tensile and dynamic mechanical properties as well as reduced thermal shrinkage, all point to interaction between carbon nanotubes and the PAN matrix. The question is what factors are responsible for different levels of property improvements with different nanotubes. Low strain properties (modulus and thermal shrinkage) were most improved in PAN/SWNT, while high strain properties (tensile strength, strain to failure, and toughness) were most improved in PAN/MWNT. As addressed above, the improvements in high strain properties are a result of longer MWNT than SWNTs. The improvements in low strain properties are dominated by the polymer/CNT interaction which will depend on the interfacial area. Strength of the interaction may also depend on the nanotube curvature, as due to higher non planar strains arising from pyramidalization of the conjugated carbon atoms and π-orbital misalignment between adjacent pairs of conjugated carbon atoms[177, 178], smaller diameter tubes would provide stronger interaction than the larger diameter tubes. This would favor SWNTs over DWNTs and MWNTs. At 5 wt% nanotube loading, the calculated polymer/CNT interfacial area for various types of nanotubes along with their diameters and densities are listed in Table 2.2. The trend of the interfacial area for SWNTs (10 nm diameter bundle) > MWNTs > VGCNFs is in qualitative agreement with the reduction in thermal shrinkage (Figure 2.10B). The interfacial area for the DWNTs is higher than that of the SWNT bundles (10 and 20 nm diameter) however, as mentioned earlier, the PAN/DWNT composite fiber contained DWNT globules, which limited the property improvements in this system. Based on the TEM observations, the length of the dispersed

DWNTs in the composite fiber was comparable to the length of the SWNT bundles. Considering the fact that DWNTs were sonicated for nearly two weeks as opposed to 10 hours of sonication for SWNTs, suggests that DWNTs were originally much longer than SWNTs, leading to greater degree of entanglement for the former. The interfacial area calculations further suggest that well dispersed DWNTs (surface area 26.6 $m^2/g$ at 5 wt% DWNTs) and well dispersed and fully exfoliated SWNTs (surface area 154 $m^2/g$ at 5 wt% SWNTs) would lead to further enhancement in modulus and other low strain properties such as thermal shrinkage, glass transition temperature, as well as modulus improvement above the glass transition temperature. Retention of the SWNT and DWNT length would also lead to further improvements in the high strain properties (strength, strain to failure, and toughness).

Modulus of the composite films and fibers depends significantly on the nanotube orientation and exfoliation[179]. Modulus of the composite fiber was estimated using the following equation:

$$E_{composite} = (E_{PAN})_{comp} V_{PAN} + (E_{CNT})_{II} V_{CNT}$$

where, $(E_{PAN})_{comp}$, $(E_{CNT})_{II}$ are the moduli of the two components along the fiber axis and $V_{PAN}$, and $V_{CNT}$ are their volume fractions. $(E_{PAN})_{comp}$ for each composite fiber was estimated based on the modulus of the control PAN as well as the PAN orientation in the control PAN and in the respective composite fiber. Effective $(E_{CNT})_{II}$ for SWNT, and MWNT along the composite fiber axis was calculated using the following continuum mechanics equation[180], as described elsewhere[47, 179]:

Table 2.2. Physical carbon nanotube parameters, as well as theoretical and experimental moduli of the various composite fibers.

| | Diameter (nm) | CNT Density ($g/cm^3$) | CNT wt.% | CNT vol.% | PAN/CNT interface area in the composite fiber at 5 wt.% loading ($m^2/g$) | PAN/CNT Composite Fiber Tensile modulus (GPa) | |
|---|---|---|---|---|---|---|---|
| | | | | | | Theoretical | Experimental |
| VGCNF | 60 | 1.95[181] | | 3.1 | 1.3 | 9.7 | 10.6 |
| MWNT | 20 | 1.8[181] | | 3.3 | 5.6 | 10.7 | 10.8 |
| SWNT Bundle | 20 | 1.3[26] | 5.0 | 4.6 | 7.7 | 11.9 | - |
| | 10 | | | | 15.4 | - | 13.6 |
| | 4.5 | | | | 34.2 | 21.4 | - |
| DWNT | 5 | 1.5[182] | | 4.0 | 26.6 | - | 10.8 |
| Exfoliated SWNT | 1 | 1.3[26] | | 4.6 | 154 | 29.7 | - |

$$\frac{1}{(E_{CNT})_{II}} = \frac{1}{E_1}\langle \cos^4\theta \rangle + \frac{1}{E_2}\langle \sin^4\theta \rangle + \left(\frac{1}{G_{12}} - \frac{2\nu_{12}}{E_1}\right)\langle \sin^2\theta \cos^2\theta \rangle$$

$$= \frac{1}{E_2} + \left(\frac{1}{G_{12}} - \frac{2\nu_{12}}{E_1} - \frac{2}{E_2}\right)\langle \cos^2\theta \rangle + \left(\frac{1}{E_1} + \frac{1}{E_2} - \frac{1}{G_{12}} + \frac{2\nu_{12}}{E_1}\right)\langle \cos^4\theta \rangle$$

where $E_1$, $E_2$, and $G_{12}$ are the longitudinal, transverse, and in-plane shear moduli, respectively, and $\nu_{12}$ is the Poisson's ratio. Elastic constants and Poisson's ratios for various nanotubes used in this study were obtained from the literatures[25-27, 29, 181, 183] and are listed in Table 2.3. Due to variation in diameter and chirality, the shear modulus of SWNT bundle dependence on its diameter[28]. Shear modulus of the 20 nm diameter bundle was reported to be 1 GPa, while that for the 4.5 nm diameter bundle it was about 6 GPa. Based on the shear modulus of graphite (4.5 GPa) and the geometric packing factor, it was estimated that the shear modulus of nanotubes with homogeneous diameters should approach 19.5 GPa. Values of axial modulus and shear modulus between the planes for MWNTs are based on the reported values for graphite[31]. Calculations[184] of axial and shear moduli for various diameter tubes suggest that for 20 nm diameter MWNT tubes, values of $E_1$ and $G_{12}$ listed in Table 2.3 based on graphite elastic constants are quite reasonable. Poisson's ratio of 0.14 was also extrapolated based on the calculations reported in reference[184]. Graphite planes in VGCNFs make an angle of 15° to the nano fiber axis[37]. Modulus of VGCNF calculated using equation 2 and the misorientation angle of 15°, represents the modulus along the VGCNF axis, which we term as $E_{CNT}$. Thus axial modulus of VGCNF ($E_{CNT}$) was determined to be 50 GPa[37]. The effective VGCNF

modulus along the composite fiber axis, $(E_{CNT,})_{II}$ was estimated to be 44.3 GPa based on the axial VGCNF modulus of 50 GPa and the VGCNF orientation in the composite fiber.

Table 2.3 The elastic constants of SWNTs and MWNTs.

| | SWNTs | | | MWNTs |
|---|---|---|---|---|
| | 1 nm | 4.5 nm | 20 nm | |
| $E_1$ (GPa) | | 640[25-27, 29] | | 1060[31] |
| $E_2$ (GPa) | | 15[27] | | 50[183] |
| $G_{12}$ (GPa) | 19.5[28] | 6[28] | 1[28] | 4[31] |
| $\nu_{12}$ | | 0.17[27] | | 0.14[184] |

Calculated composite fiber moduli as a function of Herman's orientation factor for various nanotubes are plotted in Figure 2.15. Due to the graphite plane misorientation in the VGCNFs, the modulus of the composite fiber is relatively insensitive to the VGCNF orientation, and even at the ideal VGCNF orientation, the modulus of the composite fiber is relatively low. MWNT and SWNT containing fibers exhibit significant modulus dependence on orientation and on SWNT exfoliation. For example, the modulus of the fiber containing 5 wt% MWNT is predicted to be 15 GPa at MWNT orientation of 0.98, while for the ideal MWNT orientation (orientation factor 1), it is predicted to be 34 GPa. This is assuming that the PAN orientation is the same as observed in PAN/MWNT fiber reported in Table 2.1. However, PAN orientation is also likely to increase with increase in CNT orientation. Therefore, the calculated modulus values in Figure 10 represent a lower limit. By comparison, calculated modulus of SWNT containing fibers is predicted to be higher, even at lower orientation, provided SWNT bundles are at least partially exfoliated. For example, at SWNT orientation of 0.98, the modulus of the

PAN/SWNT composite fiber is predicted to be 21, and 29 GPa for the SWNT bundle diameter values of 4.5, and 1 nm diameters.

The experimentally observed moduli for SWNT and MWNT containing composite fibers are in excellent agreement with the theoretical values (Table 2.2). The experimental value of 13.6 GPa for the PAN/SWNT composite is in between the predicted value of 11.9 GPa for 20 nm diameter rope and 21.4 GPa for the 4.5 nm diameter rope. From TEM studies, the rope diameter in the PAN/SWNT composite fiber was estimated to be about 10 nm. The experimental modulus for VGCNF containing composite fiber is somewhat higher than the theoretical values. VGCNF exhibit two types of morphologies, where a second outer layer is composed of highly oriented graphite. The presence of such VGCNF will result in higher observed modulus than the value calculated based on the morphology where all graphite layers are oriented at 15° to the nano fiber axis[37].

## 2.4 Conclusions

This study shows that polymer/CNT composite fibers can be solution processed using SWNT, DWNT, MWNT, as well as VGCNF. All nanotubes exhibit improvements in tensile, dynamic mechanical, and thermal shrinkage properties and result in higher polymer orientation and crystallite size. The increased polymer orientation and crystal size point to the potential of PAN/CNT composite as the precursor for next generation carbon fiber. Highly entangled DWNTs were most difficult to disperse. All well dispersed nanotubes exhibit high orientation in the drawn composite fiber, while the entangled DWNT globules were unoriented. In the case of PAN/DWNT, poor nanotube

dispersion resulted in limited property improvements. While, even the relatively cheaper VGCNF result in useful property gains, the most improvements in properties come from highly dispersed small diameter tubes of long lengths. While the synthesis control can lead to longer nanotubes, they have to be preserved in unentangled state to achieve good dispersion with minimum or no sonication. Achieving ultrahigh nanotube orientation (orientation factor above 0.98) is critical for obtaining high modulus composite fibers containing MWNTs or large diameter SWNT bundles.

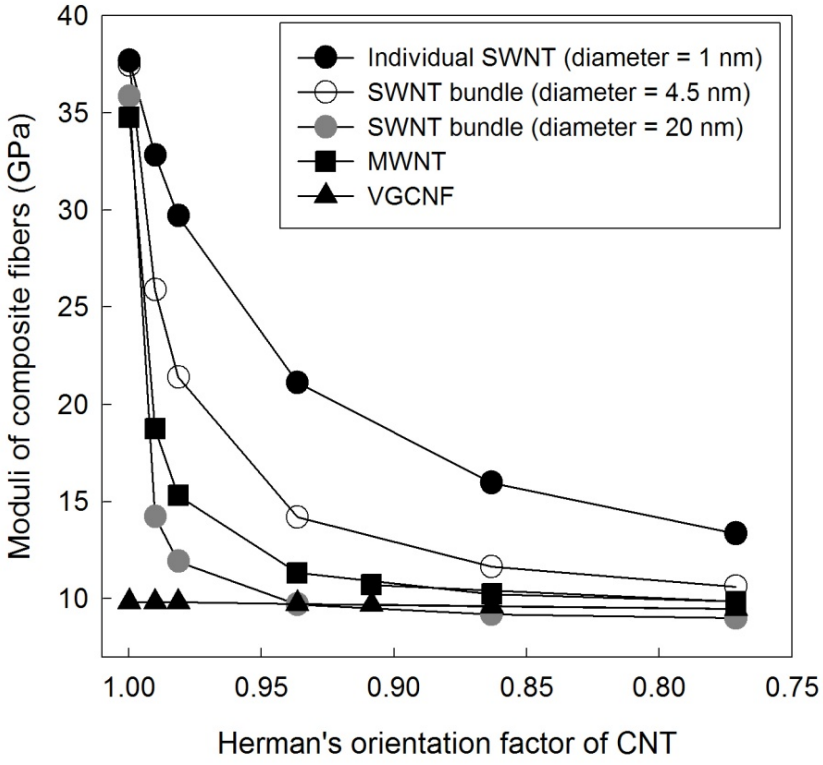


Figure 2.14 The calculated tensile modulus of composite fibers containing 5 wt% carbon nanotubes, as a function of carbon nanotube orientation factor, assuming that PAN orientation in the composite fiber is the same as given in the representative composite fibers in Table 2.1. Points are calculated values, and lines are interpolations.

# CHAPTER 3

# GEL SPINNING OF PAN/SWNT COMPOSITE FIBERS

## 3.1 Introduction

Numerous polymer/CNT composite systems have been processed with significantly improved properties, but SWNT exfoliation and orientation in polymer matrices remains a challenge. The orientation requirement for achieving high modulus in CNT based fibers is similar to that for achieving high modulus in polymeric and carbon fibers as discussed in Chapter 2. Ultra high orientation and hence high modulus in polymeric fibers such as Kevlar™, Zylon™, and pitch based carbon fibers[185] is achieved by spinning from liquid crystalline media. Modulus value as high as 931 GPa (>88% of the theoretical value for graphite) has been achieved in commercial pitch based carbon fiber (K1100). Ultra high orientation in polymers can also be achieved by gel spinning. Gel spun polyethylene fiber was commercialized in 1980s[186, 187]. Gel spinning has also been demonstrated on poly(vinyl alcohol) (PVA)[188, 189] and PAN[190-195]. Figure 3.1 shows the structural schematics of various types of fibers[196]. With decreasing disorder and defect density, the fiber strength and modulus increases. The typical commodity textile fibers contain amorphous and crystalline regions, as well as voids, chain ends, foreign particle, and chain entanglement, whose tensile strength is in the range of 0.5 GPa. Upon gel spinning of PE and PVA, and spinning of liquid crystalline polymer, one can produce high performance fiber whose tensile strength is about 5 GPa. The ideal fiber structure will be similar to the right panel in Figure 3.1. The theoretical calculation shows the tensile strength of these fibers will be about 70 GPa, assuming the density of 1 g/cm$^3$. In

this study, PAN/SWNT composite fiber was gel spun, demonstrating good SWNT orientation and exfoliation. Structure and properties of the fiber have been studied and compared to the properties of the control gel spun PAN fiber.

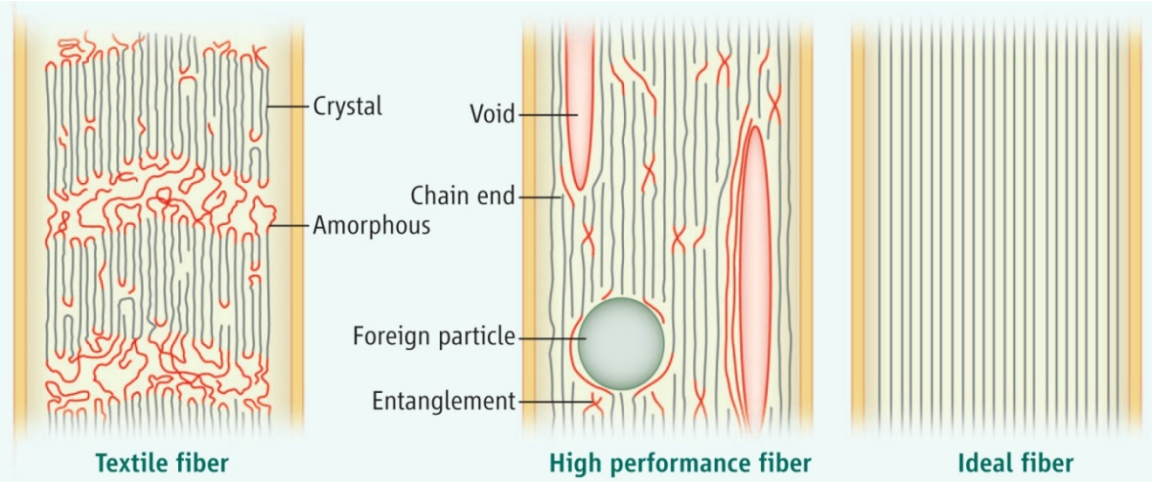


Figure 3.1 The schematic structures of various fibers[196].

## 3.2 Experimental

### 3.2.1 Materials

PAN (viscosity average molecular weight = $2.5\times10^5$ g/mol) was obtained from Exlan, Co. (Japan). PAN polymer was also containing methylacrylate co-monomer (~6.7 mol%) characterized by $^1$H and $^{13}$C NMR (Varian Co., Palo Alto, CA). Purified SWNTs were obtained from Carbon Nanotechnologies, Inc. (Houston, TX). Based on thermogravimetric analysis (TGA) in air, SWNTs used in this study contain less than 1 wt% metallic impurity. The bright field transmission electron micrograph (Figure 3.2) shows SWNT bundle diameter as large as 100 nm.

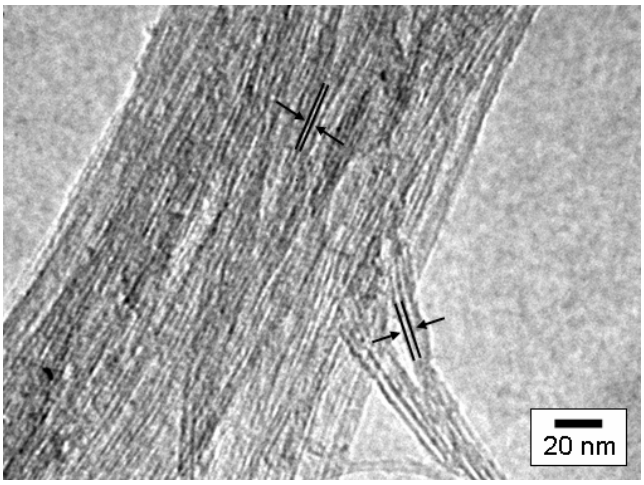


Figure 3.2 Bright field TEM image of SWNT used in this study.

### 3.2.2 Solution Preparation

Dimethyl formamide (DMF) from Sigma-Aldrich, Co. was used as received. SWNTs were dispersed in DMF at a concentration of 40 mg/L using 24 hr bath sonication (Branson 3510R-MT, 100 W, 42 kHz) at room temperature. PAN (15 g) was dried in vacuum at 100 °C and dissolved in DMF (100 mL) at 80 °C. Optically homogeneous SWNT/DMF dispersion was added to the PAN/DMF solution. The excess amount of solvent was evaporated by vacuum distillation at 80 °C, while stirring, to obtain the desired solution concentration (15 g solids (PAN+SWNT)/100 mL solvent). Similarly other solutions were prepared to yield SWNT concentration with respect to the polymer of 0, 0.5, and 1 wt%. The PAN/DMF.

Sonication is the most common method to disperse and exfoliate CNTs in dispersion medium such as organic solvent. However, the prolonged sonication would cause the shortening of CNT length as well. Therefore, one needs to find the optimum sonication time for processing. UV-vis-NIR spectroscopy can trace the CNT exfoliation. For CNT bundles, van Hove transitions would not be observed or would be merged

together due to the similarity of electronic structure to graphite sheet. Figure 3.3 exhibits the UV-vis-NIR spectra of SWNT/DMAc solution as a function of sonication time. As can be seen, van Hove transitions are getting resolved with increasing sonication time. It should also be noticed that the overall absorbance increases with increasing sonication time. The more resolved peaks (van Hove transitions) and increase in overall absorbance imply that SWNTs are debundling and the population of exfoliated SWNT increases with increasing sonication time, respectively. In addition, the spectra of 19hr and 36 hr sonication samples are very comparable each other, suggesting that the exfoliation is saturated and the more sonication will reduce the SWNT length, rather than having more exfoliation. Therefore, the sonication time was set to be about 24 hr to fully utilize SWNT exfoliation for this batch of nanotube. It should be noted that the concentration of SWNT studied in Figure 3.3 was about 5 mg/L. Since the solubility of CNT is different in different solvent, the optimum sonication will depend on the CNT concentration, type of solvent, and a particular CNT batch.

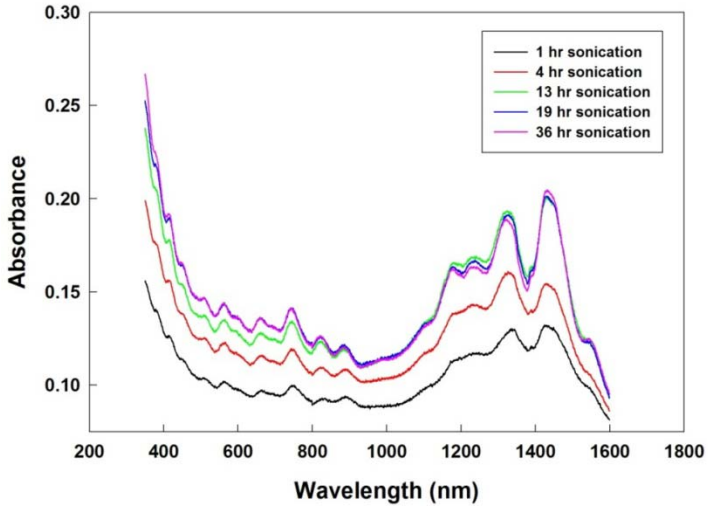


Figure 3.3 UV-vis-NIR spectra of SWNT/DMAc solution as a function of sonication time.

### 3.2.3 Fiber Spinning

PAN/SWNT/DMF solutions were spun at 31.4 m/min using 500 μm diameter single hole spinneret at 110 °C into a methanol bath maintained at -50 °C. The air gap between spinneret and the methanol bath was about 2 cm. The as-spun fibers were taken up at 100 m/min and were kept immersed in methanol bath (maintained between -20 to -40 °C) for 1 week, to ensure gelation. As a result, the as spun fiber draw ratio was 3.2. The gel fiber was further drawn (draw ratio in the range of 7 to 16) at 160 °C in glycerol bath followed by washing in ethanol and vacuum drying at 40 °C for 3 days. The total draw ratio, determined by multiplying spin draw ratio with post draw ratio, was as high as 51. Figure 3.4 shows the schematics of solution preparation, gel fiber spinning, and drawing procedure.

### 3.2.3 Fiber Characterization

Optical microscopy was carried out using a Leitz polarizing microscope. UV-vis spectra on solution and various fibers were obtained using SEE 1100 microspectrometer. Single filament tensile properties were determined using RSA III solids analyzer (Rheometric Scientific, Co.) at a gauge length of 25 mm and the crosshead speed of 0.25 mm/s. For each sample, 15 filaments were tested. Dynamic mechanical tests were also conducted using RSA III at 0.1, 1, and 10 Hz at a heating rate of 1 °C/min on a bundle of 10 filaments, also using a gauge length of 25 mm. Raman spectra were collected in the back scattering geometry using Holoprobe Research 785 Raman Microscope made by Kaiser Optical System using 785 nm excitation laser with polarizer and analyzer parallel to each other (vv mode). Spectra were obtained with the fiber axis at 0, 5, 10, 20, 30, 40,

50, 60, 70, 80, 85, and 90° from the polarization direction. The SWNT orientation in the composite fiber was determined from the peak intensity of the tangential band (ca. 1590 $cm^{-1}$) at various polarization angles. WAXD patterns were obtained on multifilament bundles on Rigaku Micromax-007 (operated at 50 kV, 100 mA, λ=1.5418 Å) using Rigaku R-axis IV++ detection system. The diffraction patterns were analyzed using AreaMax V. 1.00 and MDI Jade 6.1. From the azimuthal scans of the diffraction peak at 2θ~17°, PAN molecular orientation was determined. The crystallinity was determined using the integrated scans and the areas of the deconvoluted peaks. For baseline subtraction, linear line was drawn between 2θ = 10 and 50°. The PAN crystal size was also determined from the equatorial peak at 2θ~17° using Scherrer equation (K = 0.9). Fiber tensile fracture surfaces were observed on the gold coated samples by scanning electron microscopy (LEO 1530 SEM operated at 18 kV). Transmission electron microscopy study was conducted using Hitachi HF-2000 (operated at 200 kV). For TEM specimen preparation, the PAN/SWNT composite fiber (draw ratio 51) containing 1 wt% SWNT was heated in DMF at 150 °C for 30 min. The disintegrated fibrils were collected on lacey carbon TEM grids. TEM beam alignment and stigmation corrections were performed using evaporated aluminum standard (cat# 80044, EMS, Co.).

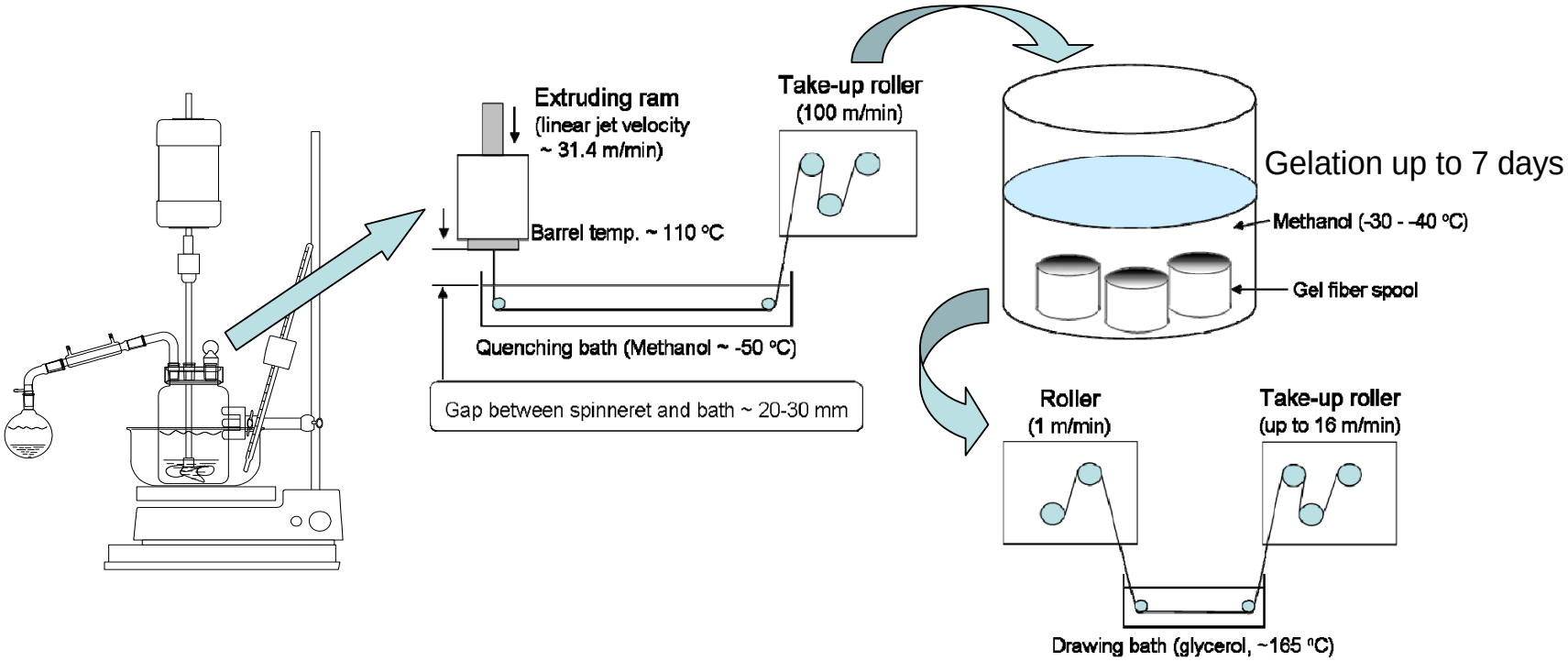


Figure 3.4. The schematics of solution preparation, gel spinning, and gel fiber drawing.

## 3.3. Results and Discussion

### 3.3.1 Structural Analysis of Gel Spun PAN/SWNT Composite Fibers

Crystal structure of PAN is reported to be either hexagonal or pseudo-hexagonal with two dimensional order[197, 198], or orthorhombic with three dimensional order[199, 200]. In a review of PAN crystal structure, Bashir[201] reported that the orthorhombic crystal form is due to the co-crystallization of PAN with polar solvents such as propylene carbonate and ethylene carbonate, and that hexagonal crystal can be formed upon removing these solvent molecules. WAXD photographs, as well as integrated and equatorial 2θ scans for PAN and PAN/SWNT (1 wt%) fibers are given in Figure 3.5. Various structural parameters determined from the X-ray study for the control PAN fiber at several draw ratios and for the fully drawn composite fibers are listed in Table 3.1.

The equatorial peaks at 2θ~17 and 30° shift to higher angles with increasing draw ratio (Figure 3.6a), resulting in closer packing as the transverse dimension of the PAN molecules decreases with stretching. The equatorial *d*-spacing of the fully drawn fiber further decreased with the incorporation of SWNT (Figure 3.6b). The ratio of these two equatorial *d*-spacings (Figure 3.6a) for the as spun PAN sample (1.705) is significantly less than the value for hexagonal packing, which is $\sqrt{3} = 1.732$. On drawing, this ratio approaches the hexagonal packing value of 1.732, both in the control PAN as well as in PAN/SWNT composite. The decrease in *d*-spacing for the control gel spun PAN as a function of draw ratio is consistent with the literature reports[193, 201, 202].

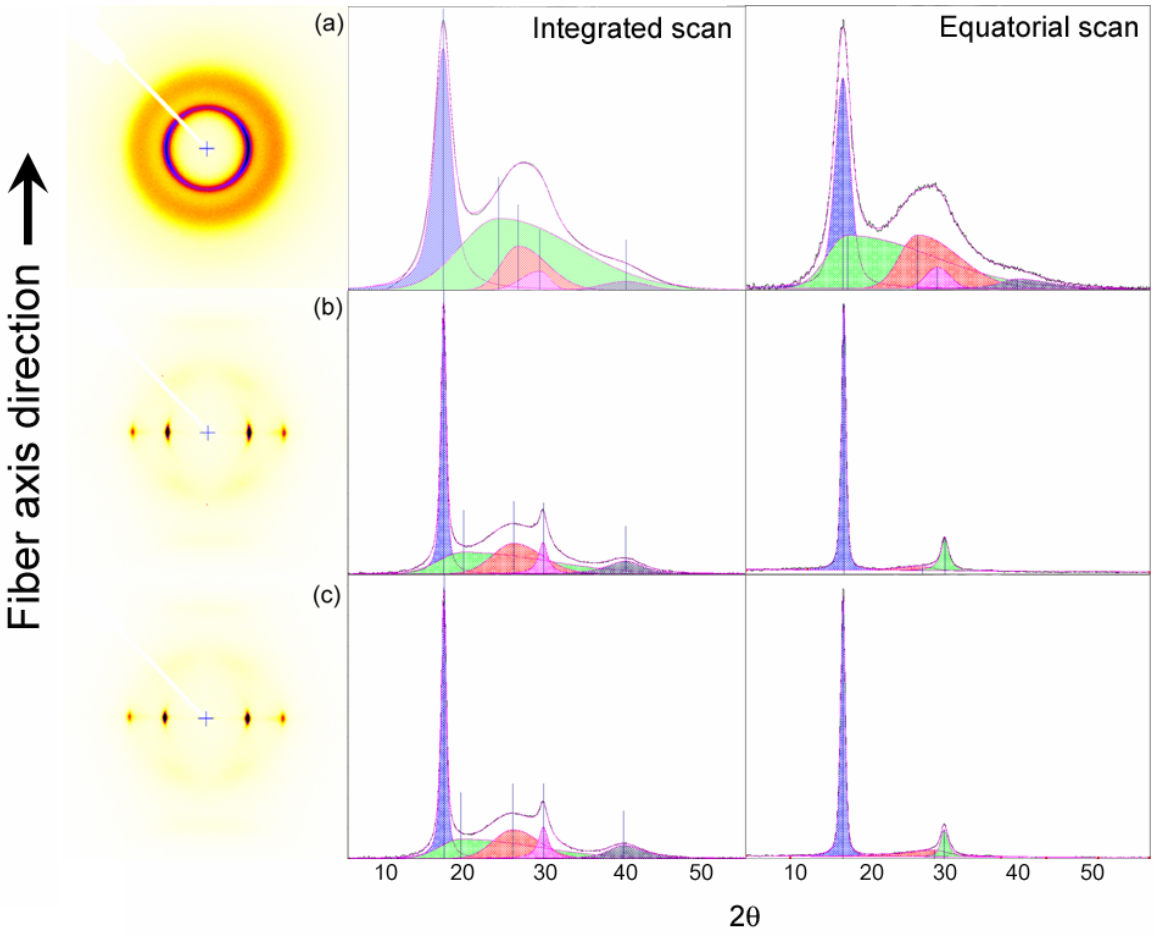


Figure 3.5 WAXD photographs and deconvoluted integrated and equatorial scans. (a) PAN draw ratio 3.2, (b) PAN draw ratio 51, and (c) PAN/SWNT (1 wt%) draw ratio 51.

Table 3.1 WAXD results for gel-spun PAN and PAN/SWNT composite fibers.

| | Control PAN (draw ratio) | | | | PAN/SWNT (0.5 wt%, DR=51) | PAN/SWNT (1 wt%, DR=51) |
|---|---|---|---|---|---|---|
| | 3.2 | 22 | 32 | 51 | | |
| Crystallinity (%) | 47 | 59 | 64 | 65 | 68 | 69 |
| $f$ * | 0.13 | 0.82 | 0.84 | 0.87 | 0.87 | 0.87 |
| Crystallite size (2θ~17°) (nm) | 3.2 | 10.4 | 11.3 | 11.7 | 11.2 | 11.5 |
| Meridional peak position (2θ, degrees)‡ | 40.2 | 39.9 | 39.9 | 39.7 | 39.5 | 39.4 |

* $f$ = Herman's orientation factor, DR = draw ratio
‡Chain axis order is the crystal formation from the planar zigzag or helical sequences along the fiber axis.

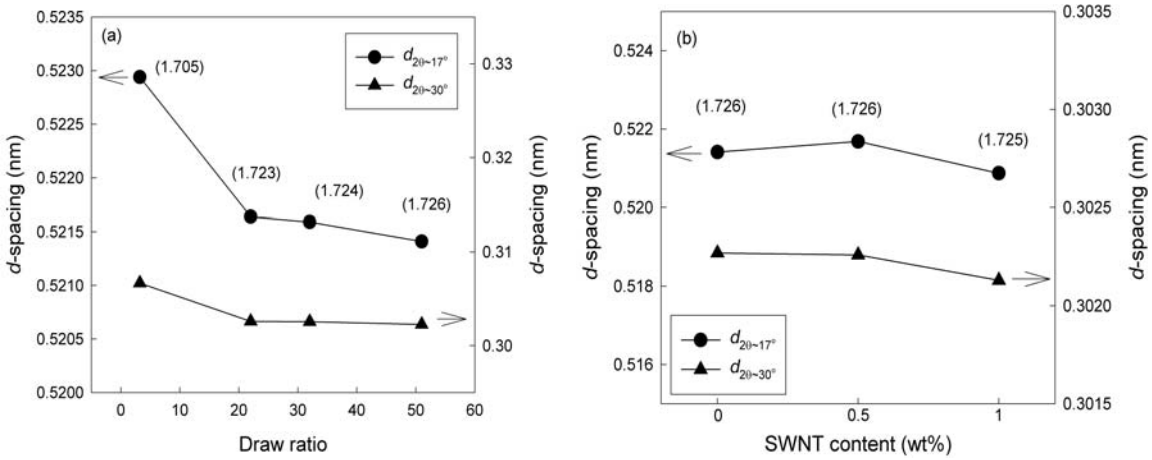


Figure 3.6 Change in equatorial PAN *d*-spacings (for 2θ~17 and 30° diffraction peaks). (a) PAN as a function of draw ratio and (b) PAN/ SWNT composite as a function of SWNT content. The values in parenthesis are the ratios of the two *d*-spacings.

With increasing draw ratio, planar zigzag sequences are likely to increase while the helical sequences in the crystal will be decreased. This conformational difference can be seen from the meridional peak. Generally PAN meridional peak can be deconvoluted into two peaks at 2θ~36 and 40° resulting from the planar zigzag and helical sequences, respectively[193]. The control PAN and the PAN/SWNT composite in this study do not reveal two peaks (Figure 3.7). However, the peak position is shifted to lower angle with increasing draw ratio as well as with the incorporation of SWNT (Table 3.1), suggesting tendency for increasing planar zigzag sequences. Crystallinity, orientation, and crystal size increase with increasing draw ratio. Composite fibers exhibited slightly higher crystallinity, polymer orientation, and somewhat lower crystal size when compared to the control fiber of the same draw ratio (draw ratio 51).

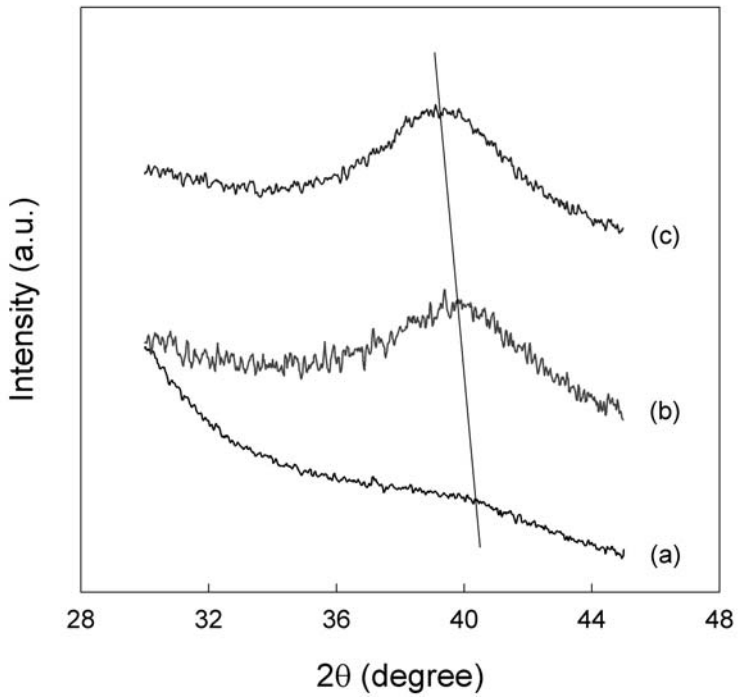


Figure 3.7 WAXD meridional scans. (a) PAN draw ratio 3.2, (b) PAN draw ratio 51, and (c) PAN/SWNT (1 wt% SWNT) darw ratio 51.

### 3.3.2 Morphological Studies of Gel Spun PAN/SWNT Composite Fibers

Scanning electron micrographs of the tensile fractured fiber surfaces show that both the control and composite fibers exhibit fibrillar structure. Pulled out nanotubes can also be seen in the composite fiber (Figure 3.8). Bright field high resolution transmission electron micrographs of PAN/SWNT (1 wt%) fiber show aligned and exfoliated SWNTs (Figure 3.9a and b). PAN crystal lattice (0.52 nm spacing) can also be observed in the SWNT vicinity (Figure 3.9c). Pulled out SWNTs observed in Figure 3.8b are in fact thought to be PAN covered SWNTs as seen in HRTEM image in Figure 3.9b. It is noted that the PAN/SWNT composites are highly resistant to the electron beam providing ample opportunity for high resolution TEM imaging. By comparison, control PAN fiber was significantly more radiation sensitive and could not be lattice imaged under the comparable imaging conditions. During TEM imaging, PVA/SWNT was also observed to

exhibit much higher electron beam resistance than the control PVA[203]. These observations suggest that polymer/SWNT crystals may in general be easier to image in the electron beam than the polymer alone.

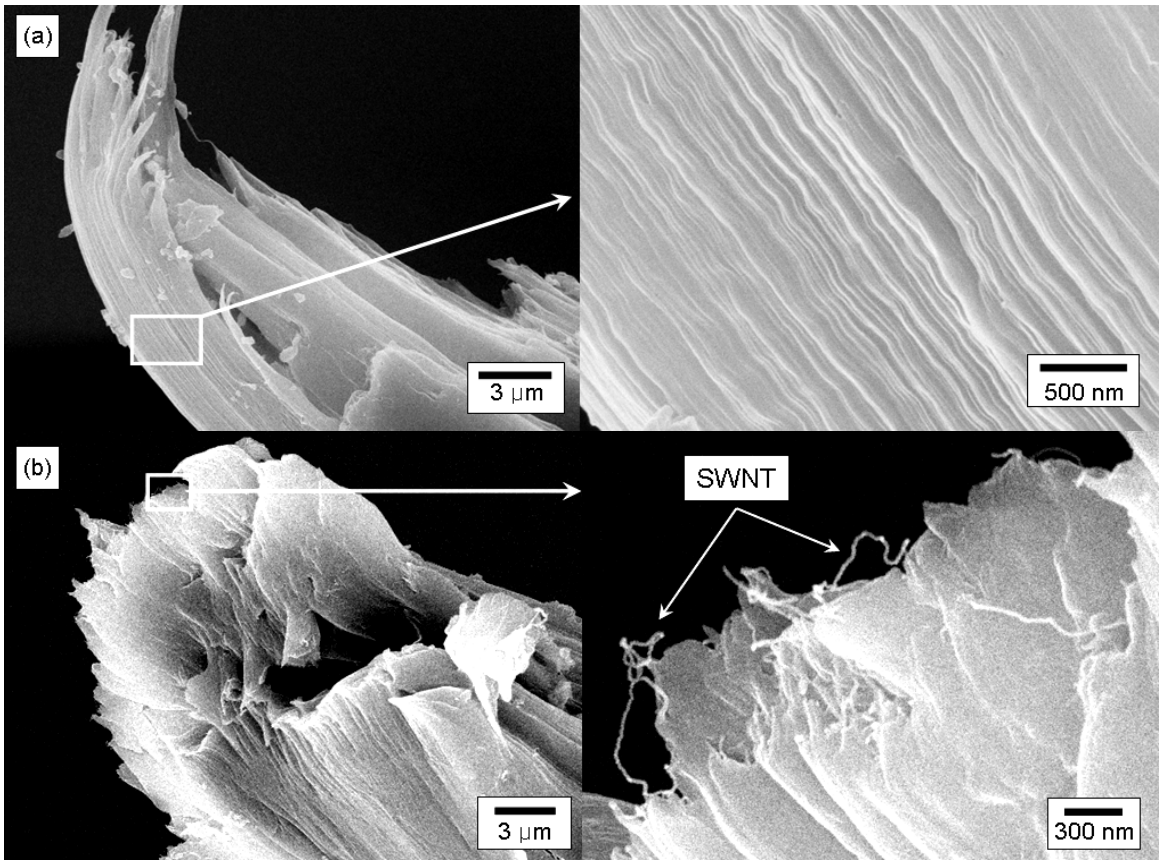


Figure 3.8 SEM micrographs for the fracture surface of (a) PAN fiber and (b) PAN/SWNT (1 wt%) fiber. Draw ratio of both fibers is 51.

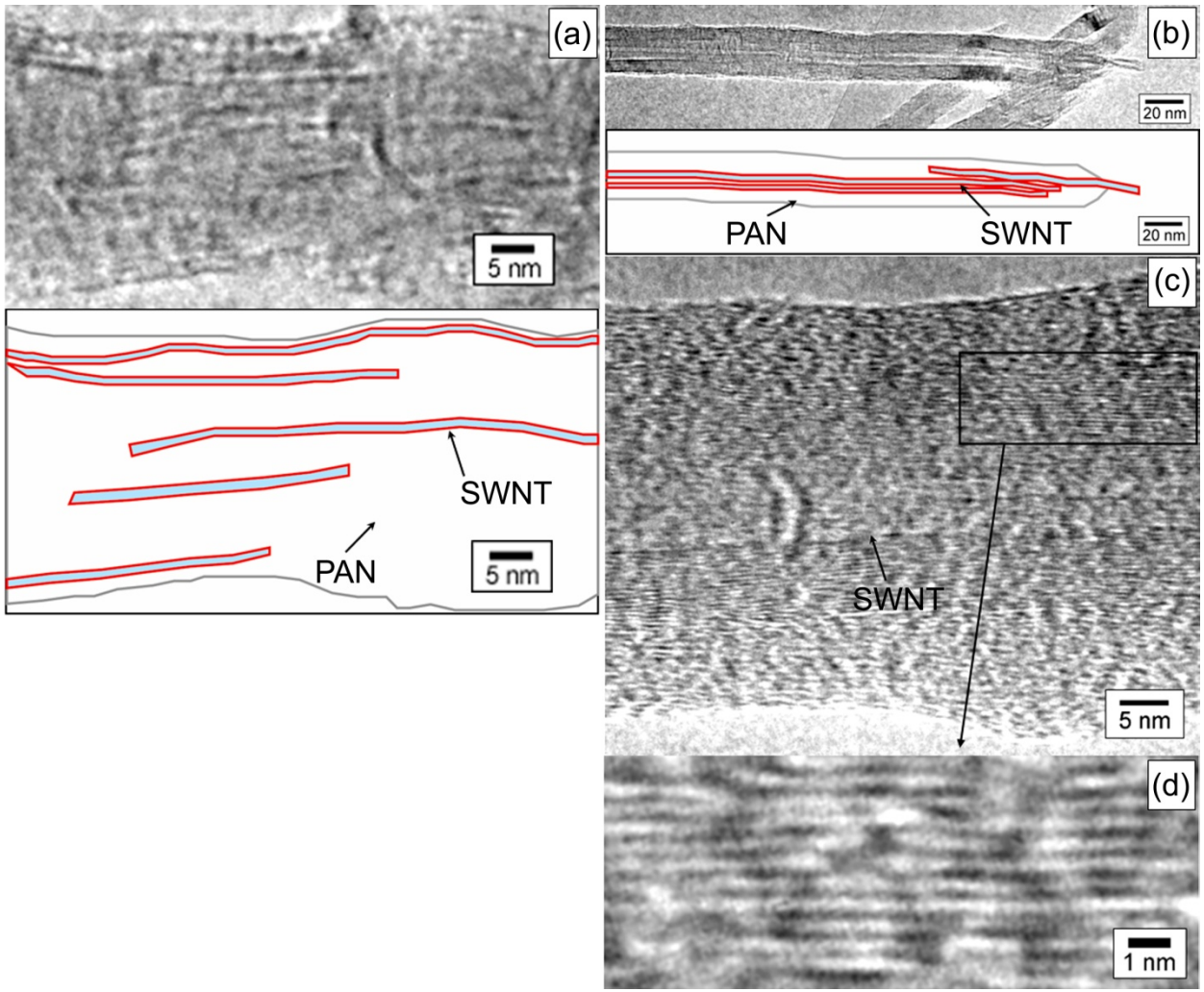


Figure 3.9 (a) and (b) HRTEM images and their schematics of PAN/SWNT (1 wt%) fiber of draw ratio 51 (c) and (d) HRTEM lattice images of the same fiber.

### 3.3.3 Effect of Drawing on UV-vis Specta of PAN/SWNT Composite Fibers

Exfoliated SWNTs exhibit van Hove transitions, while these transitions are suppressed in SWNT bundles. The transitions are also not observed in SWNTs doped with electron donor or acceptor. The dilute PAN/SWNT/DMF solution before DMF evaporation showed van Hove transitions, suggesting SWNT exfoliation in solution (Figure 3.10). However, the as spun gel fiber did not exhibit van Hove transitions (Figure 3.11a), suggesting SWNT re-aggregation during processing. The composite fiber with the intermediate draw ratio of 32 also did not exhibit these transitions. However, the fully drawn composite fiber (draw ratio 51) exhibited van Hove transitions, suggesting that SWNT exfoliation occurred during drawing (Figure 3.11c). The schematic of the SWNT exfoliation process is also shown in Figure 3.11.

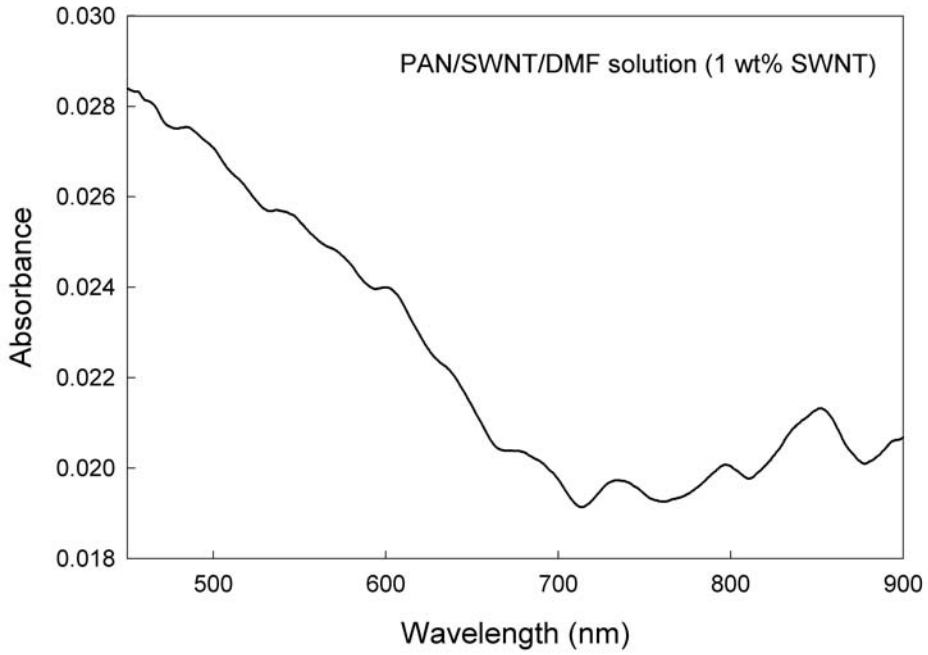


Figure 3.10 UV-vis spectrum for PAN/SWNTs/DMF solution (SWNT content is 1 wt% with respect to the polymer).

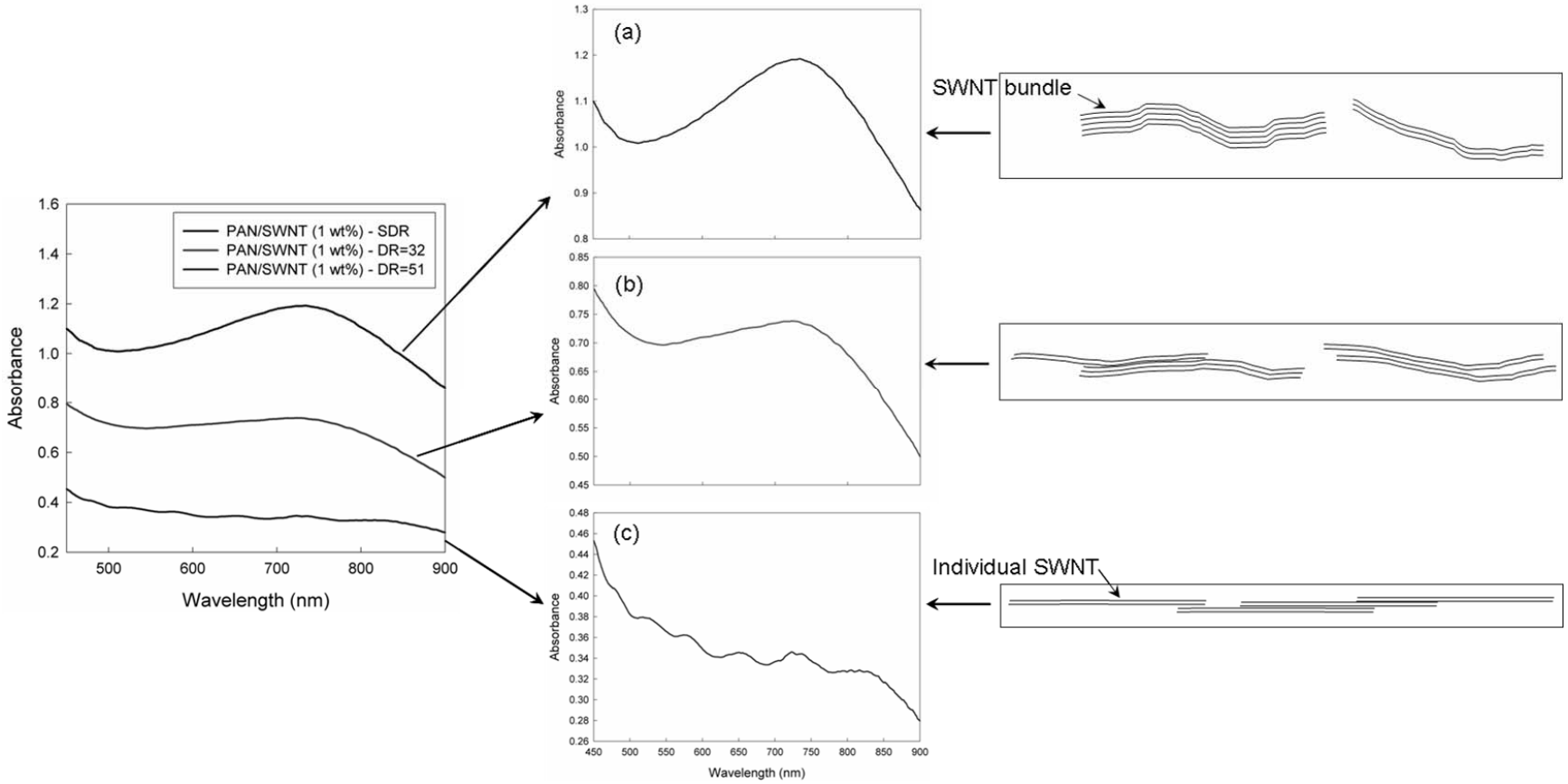


Figure 3.11 UV-vis spectra and the schematics of carbon nanotubes in PAN/SWNT (1 wt%) fiber at various draw ratios as follows: (a) 3.2, (b) 32, and (c) 51.

### 3.3.4 Effect of Gel Drawing on SWNT Orientation

The G-band intensity ratio, with polarization parallel and perpendicular to the fiber axis, at about 1592 $cm^{-1}$ is taken as a measure of SWNT orientation in composite[204, 205] and in SWNT fibers[46]. The full width at half maximum intensity (FWHM) from WAXD azimuthal scan of SWNT (1,0) plane has also been used to measure the SWNT orientation in fibers[46, 110, 206-209]. Figure 3.12a shows the G-band Raman spectra when the angle between polarizer and fiber axis are 0 and 90°, and gives the Raman G-band ratio for the PAN/SWNTs composite fiber (1 wt% SWNT, draw ratio 51) of 42. For comparison, the Raman G-band ratio for the SWNT fiber processed from liquid crystalline SWNT/$H_2SO_4$ solution was 20[46].

The relationship between Raman intensity and SWNT orientation are given elsewhere[52, 210]. The second order orientation parameter, $\langle P_2(\cos\theta)\rangle$, is the Herman's orientation factor, *f*. From the experimental Raman intensity data plotted in Figure 12(b), SWNT Herman's orientation factor, *f,* was calculated to be 0.915, while the fourth order orientation parameter, $\langle P_4(\cos\theta)\rangle$, was calculated to be 0.96 for the fully drawn PAN/SWNT (1 wt%) fiber using the least square fit of the above equation. These orientation values were determined without assuming any particular peak shape for the Raman intensity distribution as a function of polarization angle. For comparison it should be noted that PAN/SWNT fibers spun by conventional solution spinning reported in Chapter 2, SWNT Herman's orientation factor was calculated to be 0.98 assuming Gaussian Raman intensity distribution. Re-examination of the raw data from this study showed that, when no particular peak shape was assumed (a method used in the current study), an orientation factor of 0.90 was obtained for the conventional spun PAN/SWNT

fiber. Raman intensity ratio for the beam polarized parallel and perpendicular to the fiber axis was 38 for this conventional spun sample as compared to 42 for the gel spun sample. Thus the SWNT orientation (0.915) in the gel spun fiber is only slightly higher (Figure 3.12b) than in the conventional spun fiber (0.90). However, the SWNT orientation in the PAN/SWNT gel spun fiber is less than polymer orientation achieved in fibers such as Kevlar™, Zylon™, and Spectra™, where typical orientation factor value is ~0.99.

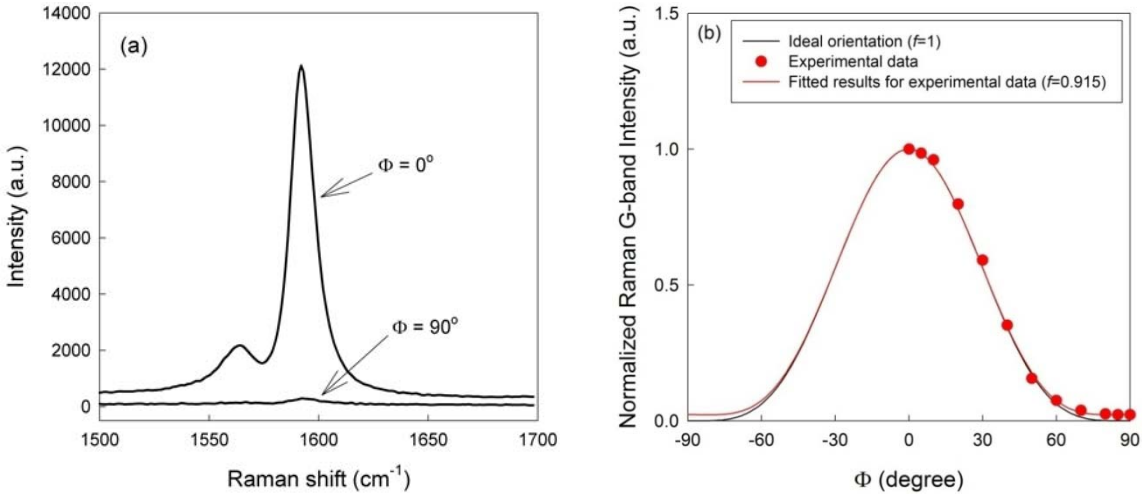


Figure 3.12 (a) G-band Raman spectra for PAN/SWNT (1 wt%) fiber of draw ratio 51.The angle between polarizer and the fiber axis are 0 and 90°. (b) The normalized Raman G-band intensity distribution as a function of angle between polarizer and the fiber axis. Circles represent the experimental data for PAN/SWNT (1wt%) fiber of draw ratio 51.

### 3.3.5 Solubility of PAN/SWNT Composite Fibers

It was previously reported that the PAN fiber processed by conventional solution spinning was soluble in DMF at room temperature, while PAN/SWNT fiber containing 10% SWNTs was not soluble[47]. In the current study, we observed that fully drawn gel spun PAN fiber as well as PAN/SWNT (1 wt%) are both insoluble in DMF at room temperature. Drawn gel spun PAN did dissolve when boiled in DMF, while the drawn

PAN/SWNT (1 wt%) only broke into fragments after boiling in DMF for 30 minutes. These fragments when observed in HRTEM, showed highly crystalline PAN well adhered to SWNTs (Figure 3.9c). To show the solubility difference, PAN and PAN/SWNT fibers were heated in DMF at 60 °C for 6 hrs. Under these conditions, control gel spun PAN fiber begins to disintegrate into fibrils, while the 1 wt% SWNT containing composite fiber did not (Figure 3.13). TEM observation that PAN crystals are well adhered to SWNTs, and X-ray result showing that in the composite fiber PAN lattice spacings are slightly smaller than their value in the control gel spun PAN, may explain the reduced PAN/SWNT solubility.

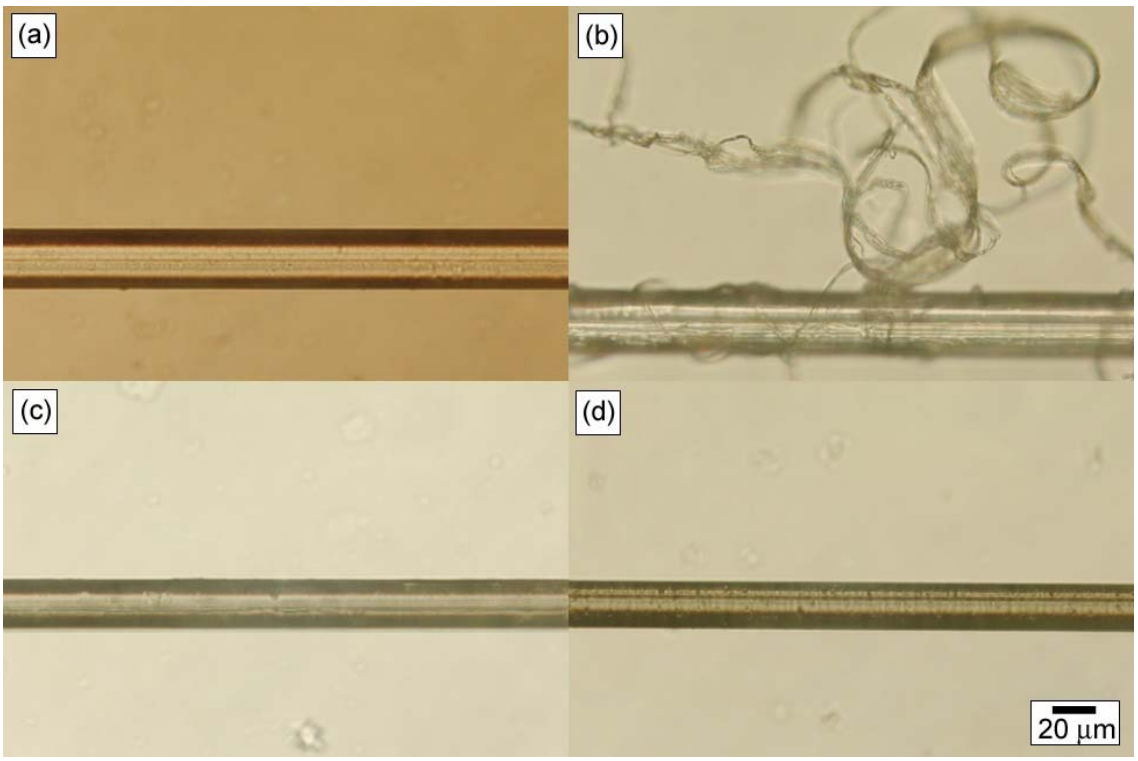


Figure 3.13 Optical micrographs of (a) PAN fiber (draw ratio 51) and (c) PAN/SWNT (1 wt%, draw ratio 51), (b) and (d) are the respective fibers after treatment in DMF at 60 $^{o}$C for 6 hr.

### 3.3.6 Mechanical Properties of Gel Spun PAN/SWNT Composite Fibers

The stress-strain curve of the highly drawn control PAN fiber shows a yield point at about 25% of the ultimate stress and frequent sudden stress reduction at various strain levels (Figure 3.14). These sudden stress reductions were a result of fibril breakage in the highly drawn control PAN fiber and not due to fiber slippage from the grips. The stress-strain curves in Figure 3.14 also show that such stress reduction and hence fibril breakage did not occur in the composite fibers. The tensile modulus and strength of the gel spun PAN fiber increased almost linearly up to a draw ratio of about 40, and above this value, draw ratio only had moderate effect on tensile properties (Table 3.2, Figure 3.15a). Draw ratio of 51, as well as tensile strength and tensile modulus (Figure 3.15b) of fully drawn fiber obtained in this study, are consistent with the literature report[194].

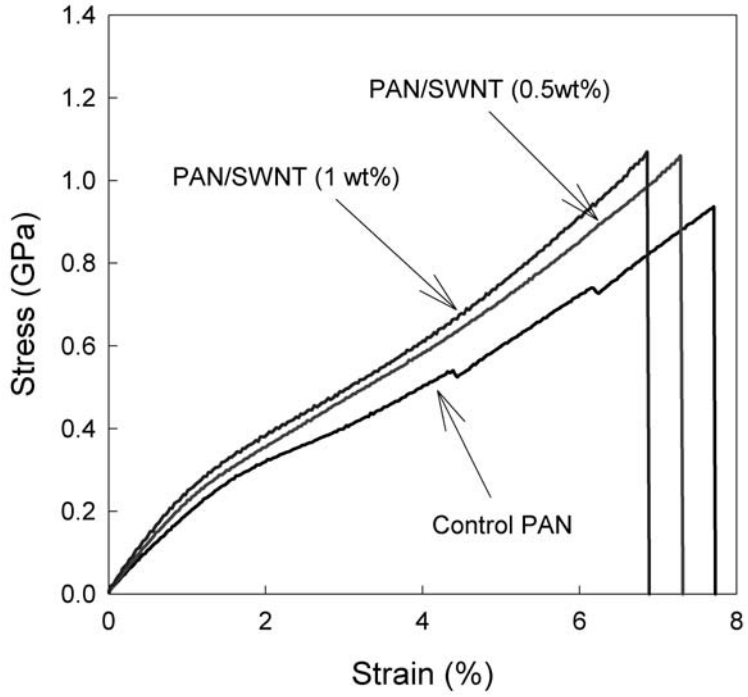


Figure 3.14 Typical stress-strain curves for PAN and PAN/SWNT composite fibers.

Table 3.2 Mechanical properties of gel-spun PAN fiber at various draw ratios.

| | Draw ratio* | | | | |
|---|---|---|---|---|---|
| | 22 | 32 | 38 | 45 | 51 |
| Diameter (μm) | 32.4±0.4 | 27.2±0.4 | 23.6±0.2 | 22.1±0.3 | 20.8±0.2 |
| Tensile Modulus (GPa) | 14.5±1.3 | 17.8±1.2 | 21.0±2.2 | 21.2±2.5 | 22.1±1.2 |
| Tensile Strength (GPa) | 0.58±0.05 | 0.76±0.08 | 0.85±0.14 | 0.88±0.10 | 0.90±0.18 |
| Strain to failure (%) | 8.4±0.9 | 8.1±1.0 | 7.9±1.2 | 7.8±0.8 | 7.4±0.8 |
| Work of rupture (MPa) | 26±5 | 32±6 | 35±9 | 35±7 | 35±9 |

Composite fiber tensile properties are listed in Table 3.3. With the addition of 1 wt% SWNT, room temperature modulus increased by 6.6 GPa (from 22.1 to 28.7 GPa). Assuming that the PAN modulus in the composite fiber is the same as in the control gel spun PAN, the modulus of the PAN/SWNT composite with fully exfoliated SWNT with an orientation factor of 0.915 calculated using previously published method is plotted in Figure 3.16. The composite fiber modulus calculated assuming ideal SWNT orientation, and the observed moduli values are also plotted in this Figure. Observed composite fiber modulus is same as predicted assuming ideal SWNT orientation. However, when the observed SWNT orientation is taken into consideration, then one can see that experimental modulus is higher than the predicted value. This suggests a change in the PAN matrix modulus with the incorporation of SWNTs. This is consistent with the slightly higher PAN crystallinity and orientation in the composite fiber.

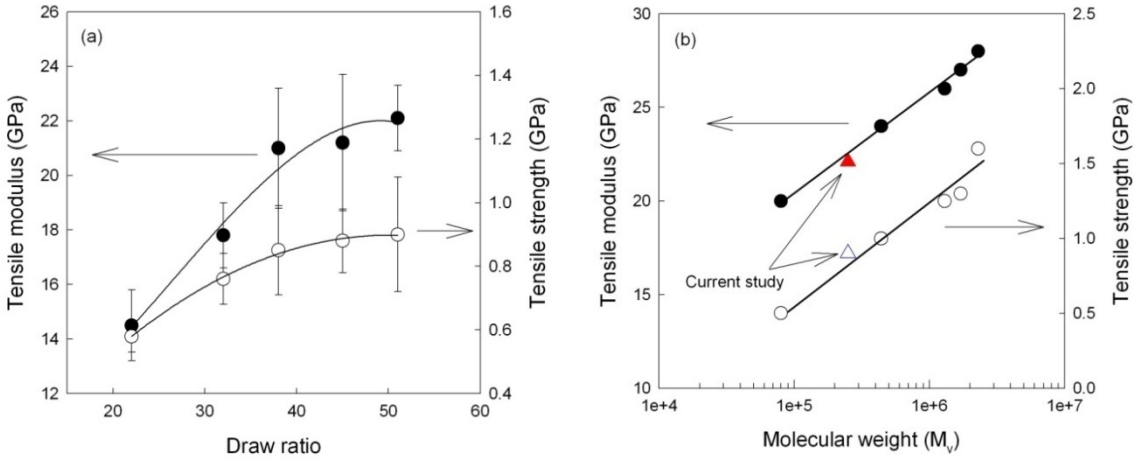


Figure 3.15 (a) The tensile modulus and strength of gel-spun PAN fibers as a function of draw ratio, and (b) Tensile modulus and strength of fully drawn atactic-PAN fiber or film as a function of molecular weight. The circles represent the data from reference[194] and the triangles are the experimental data from the current study.

Table 3.3 Mechanical properties of the gel-spun PAN and PAN/SWNT composite fibers (draw ratio = 51).

| | Diameter (μm) | Tensile Modulus (GPa) | Tensile Strength (GPa) | Strain to failure (%) | Work of rupture (MPa) |
|---|---|---|---|---|---|
| PAN | 20.8 ± 0.2 | 22.1 ± 1.2 | 0.90 ± 0.18 | 7.4 ± 0.8 | 35 ± 9 |
| PAN/SWNT (0.5 wt%) | 19.6 ± 0.3 | 25.5 ± 0.8 | 1.06 ± 0.14 | 7.2 ± 0.6 | 41 ± 8 |
| PAN/SWNT (1 wt%) | 18.7 ± 0.2 | 28.7 ± 2.7 | 1.07 ± 0.14 | 6.8 ± 0.8 | 39 ± 8 |

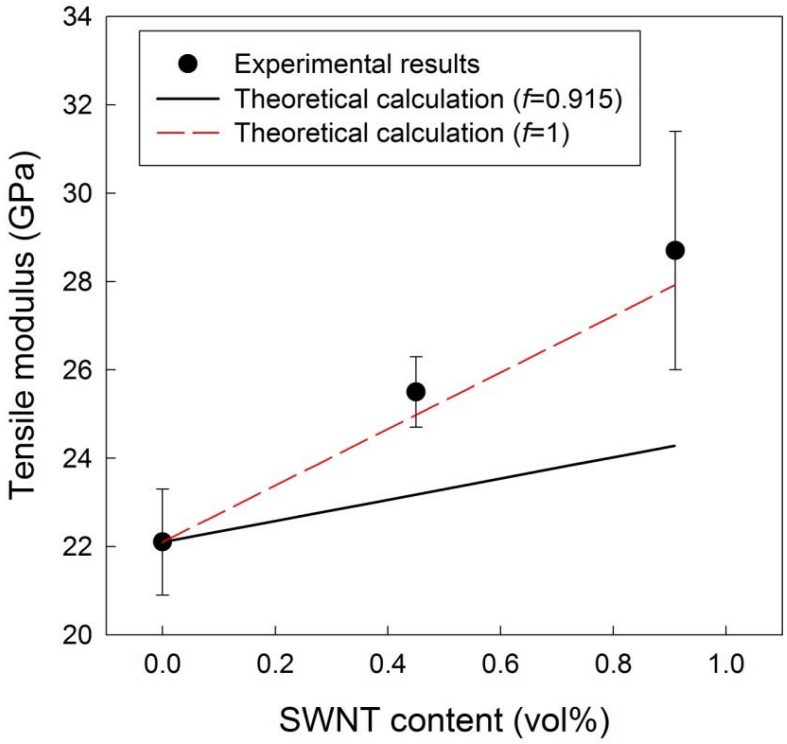


Figure 3.16. Tensile modulus of PAN/SWNT fibers (draw ratio 51) as a function of SWNT content. Solid line is the calculated value based on rule of mixtures assuming PAN modulus in the composite is the same as for the control PAN fiber and that the SWNT modulus is 640 GPa. Circles represent the experimental data.

Tan δ as a function of temperature at a frequency of 10 Hz shows relaxations at ~140, 75, and 25 $^{o}$C (Figure 3.17a). These transitions are generally termed as α (and $\alpha_c$), $\beta_c$, and γ, respectively. Despite higher frequency (10 Hz), these transition temperature values are lower than the literature reported values[192] of 150, 100, and 25 $^{o}$C at 3.5 Hz, respectively. However, it is noted that the molecular weight in this literature reported study is an order of magnitude higher ($2.3\times10^6$ g/mol) than the molecular weight used in the current study ($2.5\times10^5$ g/mol). The α relaxation was attributed to the micro-Brownian motion in the amorphous phase, which can vanish upon annealing or drawing, and $\alpha_c$ relaxation is likely associated with the molecular motion in syndiotactic or short isotactic sequences. $\beta_c$ relaxation was reported to exist in both iso- and atactic-PAN, and was

attributed to the molecular motion from helical sequences in the paracrystalline regions. The γ relaxation was attributed to the local motion in the syndiotactic or short isotactic sequences (the planar zigzag conformation), and the long tail of γ relaxation down to -150 $^{o}$C is ascribed to the various local motions for conformationally disordered regions. $\beta_c$ transition in the composite fiber were of reduced magnitude, broader, and shifted to higher temperature as compared to the control PAN fiber. Since $\beta_c$ relaxation is strongly dependent on the helical sequences in PAN crystal, this suggests increased planar zigzag sequences in the composite fiber, consistent with the WAXD data, as discussed earlier. The γ transition and its tail down to -100 °C for the composite fiber was nearly identical to the transition for the control PAN fiber, while the magnitude for the α or $\alpha_c$ transition increased with the incorporation of SWNT and slightly shifted to higher temperature. Tan δ magnitude of PAN/SWNTs (1 wt%) composite $\beta_c$ peak decreased and all three transition temperatures increased with increasing frequency (Figure 3.17b). The activation energy calculated using Arrhenius equation and the $\beta_c$ peak temperatures at various frequencies (Table 3.4) show significantly higher energy for the composite fiber as compared to that of the control PAN fiber. This suggests that the presence of SWNTs act as a barrier for this motion.

The storage moduli of composite fibers are higher than that of the control PAN fiber in the entire temperature range (Figure 3.18a). The difference between the storage moduli of fully drawn PAN/SWNT (1 wt%) and PAN fibers at various frequencies plotted in Figure 3.18b show that nanotube contribution to the storage modulus is decreasing with increasing temperature and increasing with increasing frequency. At -75 °C (198 K), 1 wt% nanotubes contribute ~13.9 GPa to the storage modulus, while this

contribution is reduced to 6.6 GPa at 25 °C (298 K), and ~0.2 GPa at 150 °C (423 K) at 1 Hz. Theoretical calculations show that SWNT modulus at 423 K (150 °C) is more than 96% of its value at 0 K[211, 212]. Thus, in this temperature range, SWNT modulus is not very sensitive to temperature. Therefore, the strong temperature dependence of the storage modulus contribution arising from SWNT in the gel spun PAN/SWNT composite fiber is unusual and may suggest that load transfer ability and hence interfacial strength is increasing almost monotonically with decreasing temperature, even below the γ transition temperature (~25 °C). Part of the modulus increase may be attributed to the changes in PAN structure and morphology resulting from the presence of SWNT.

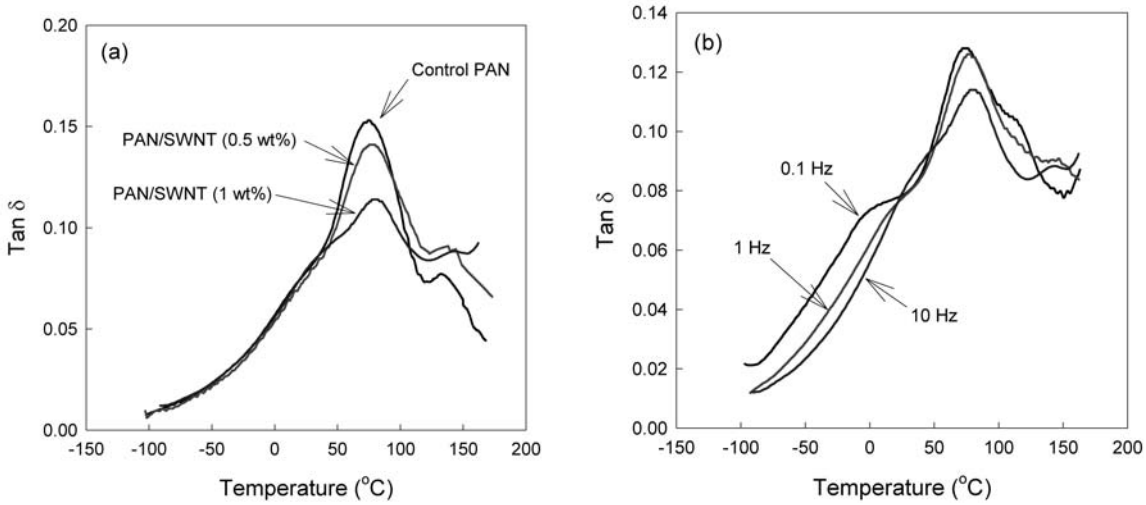


Figure 3.17 Tan δ behavior of (a) PAN and PAN/SWNT fibers as a function of temperature at 10 Hz, and (b)PAN/SWNT (1 wt%) fiber at various frequencies. All the specimens were drawn to a draw ratio of 51.

Table 3.4 Dynamic mechanical analysis results for gel spun PAN and PAN/SWNT composite fibers.

| | $\beta_c$ transition temperature (°C) at various frequencies | | | |
|---|---|---|---|---|
| | 0.1 Hz | 1 Hz | 10 Hz | $E_A^*$ (kJ/mole) |
| Control PAN | 66.7 | 71.1 | 75 | 544 |
| PAN/SWNT (0.5 wt%) | 71.7 | 75.1 | 78 | 717 |
| PAN/SWNT (1 wt%) | 74.6 | 77.2 | 80.4 | 809 |

- The transition temperatures are the tan δ peak temperatures.

* $E_A$ is activation energy calculated using Arrhenius equation ( $f = A\exp\left(-\frac{E_A}{RT}\right)$ ), where *f*, R, and T are frequency, gas constant, and absolute temperature, respectively.

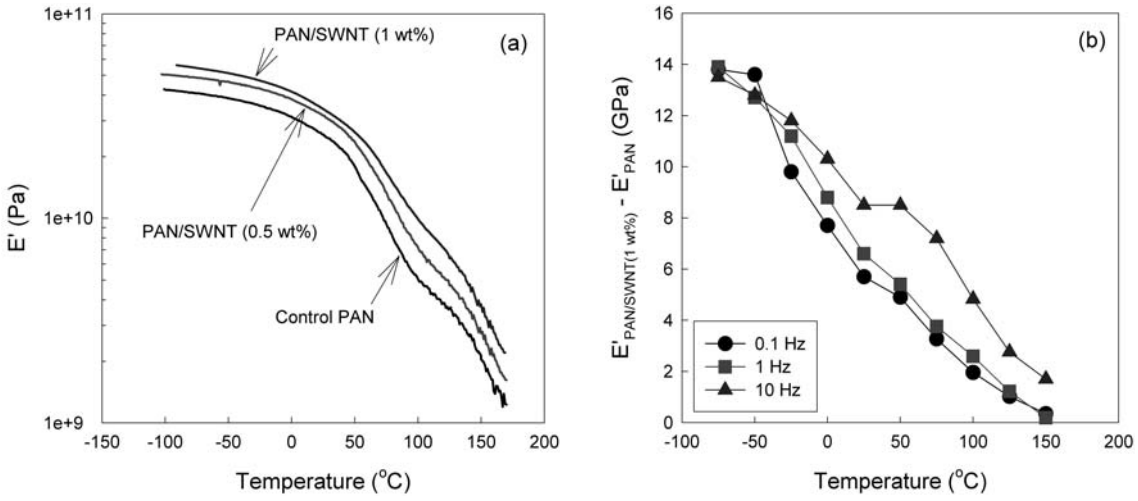


Figure 3.18 (a) Storage modulus of PAN and PAN/SWNT fibers as a function of temperature at 10 Hz, and (b) storage modulus difference between control PAN and PAN/SWNT fibers (1 wt% SWNT) as a function of temperature at various frequencies. All the specimens were drawn to a draw ratio of 51.

### 3.4 Conclusions

PAN/SWNT fibers were gel spun at 0, 0.5, and 1 wt% SWNT content to a draw ratio of 51. Structure, morphology, and mechanical and dynamic mechanical properties of these fibers have been studied. Raman spectroscopy showed high SWNT orientation, with a Herman's orientation factor of 0.91. PAN/SWNT composite exhibited much

higher electron beam radiation resistance than PAN. As a result, PAN lattice images could be easily observed in the composite fiber. The PAN/SWNT composite fiber also exhibited higher solvent resistance than the control PAN fiber. UV-vis spectroscopy of highly drawn fiber exhibited van Hove transitions, suggesting SWNT exfoliation upon drawing. SWNT exfoliation was also confirmed by high resolution transmission electron microscopy (HRTEM). At 1 wt% SWNT, fiber modulus increased by 6.6 GPa at room temperature, suggesting ideal reinforcement efficiency. However, at 1 wt% SWNT loading, storage modulus of the PAN fiber (at 1 Hz) increased by 13.9, 6.6, and 0.2 GPa at -75, 25, and 150 °C, respectively. This suggests that the load transfer ability and hence interfacial strength is increasing with decreasing temperature, even below the $\gamma$ transition temperature.

# CHAPTER 4

# STABILIZATION AND CARBONIZATION STUDIES OF GEL SPUN PAN/SWNT COMPOSITE FIBERS

## 4.1 Introduction

Among various types of polymers, PAN has been shown to have strong interaction with CNT. In the previous Chapters, it was shown that CNT incorporation into PAN fiber leads to higher PAN molecular orientation and closer chain packing crystal structure, resulting in improved mechanical properties, electron beam radiation resistance, reduction in thermal shrinkage, and enhanced solvent resistance. The overall quality of the precursor fiber ultimately translates into enhanced property the carbon fiber. Since PAN/CNT fibers have shown significantly improved properties as compared to PAN fibers, there is great potential to obtain novel grade of carbon fiber from PAN/CNT composite fibers. It has been shown that the stabilization and carbonization of PAN/ VGCNF and PAN/MWNT composite films processed by gel drawing can produce carbon films with the improved mechanical properties and electrical conductivity[167, 213, 214]. However, these studies were not able to produce mechanically meaningful carbon films (about 30 GPa of modulus). In this Chapter, the structure and property development of the stabilized and carbonized PAN and PAN/SWNT fibers are presented and analyzed.

## 4.2 Experimental

### 4.2.1 Preparation of Precursor Fibers

Control PAN and PAN/SWNT composite fibers were prepared by gel spinning as described in Chapter 3. PAN used in this study was poly(acrylonitrile-co-methylacrylate) containing 6.7 mol% methylacrylate characterized by $^{1}$H NMR (Varian Co., Palo Alto, CA). Polymer was supplied by Japan Exlan, Co. and the average molecular weight was 250,000 g/mol. SWNT (lot number XO1PPP) were obtained from Carbon Nanotechnologies, Inc. (Houston, TX) and the catalytic impurity was determined to be about 1 wt% by thermogravimetric analysis (TGA). Control PAN and PAN/SWNT fibers were processed using spinnerets of 500 and 250 μm diameters. All the fibers used in this study were drawn by 38 times.

### 4.2.2 Oxidative Stabilization and Carbonization

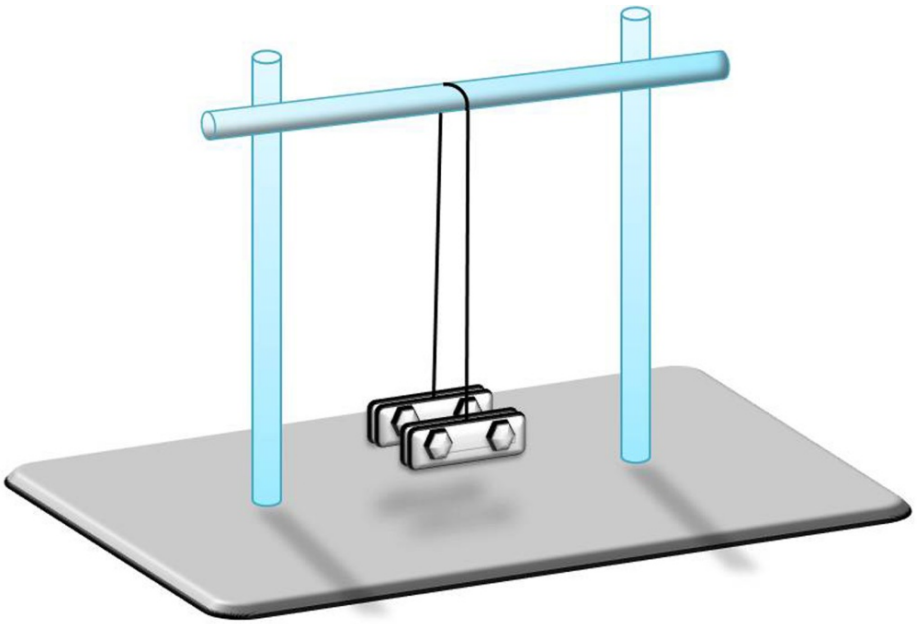

Figure 4.1 The schematic description of the experimental setup for stabilization and carbonization.

For stabilization, fibers were clamped between two carbon steel blocks and hung over a quartz rod (Figure 4.1), and stabilization was carried out in a box furnace (Lindberg, 51668-HR Box Furnace 1200C, Blue M Electric) in air at various stress levels (0.025, 0.017, 0.009, and 0.006 N/tex, stress is based on the linear density of the precursor fiber). Fibers were heated from room temperature to 285 $^{o}$C in air at a heating rate of 1 $^{o}$C/min and held at 285 $^{o}$C for 10 hr followed by heating up to 330 $^{o}$C at a heating rate of 1 $^{o}$C/min and held at 330 $^{o}$C for 3 hr. The stabilized fibers were cooled down to room temperature over a period of several hours. The stabilized PAN and PAN/SWNT fibers were subsequently carbonized in argon by heating from room temperature at a heating rate of 5 $^{o}$C/min, and by holding a 1100 $^{o}$C for 5 min at various stress levels (0.025, 0.017, 0.009, and 0.006 N/tex, stress is based on the linear density of the precursor fiber). In the initial study, the precursor fiber diameter was 20 - 23 μm, resulting in 12 - 13 μm diameter carbon fibers (also referred to as large diameter fibers). Since higher tensile strength can be obtained in smaller diameter fibers, PAN and PAN/SWNT (99/1) fibers were also gel spun with a diameter of about 12 μm (with a draw ratio of 38). These fibers resulted in about 6 μm diameter carbon fibers (also referred to as small diameter fibers). For stabilization of the small diameter fibers, fibers were heated from room temperature to 285 $^{o}$C in at a heating rate of 1 $^{o}$C/min and held at 285 $^{o}$C for 2 hr followed by heating up to 330 $^{o}$C at a heating rate of 1 $^{o}$C/min and held at 330 $^{o}$C for 1 hr. After being cooled down to room temperature, the carbonization was carried out using the same conditions as used for the large diameter fibers.

### 4.2.3 Characterization

Differential scanning calorimetry (DSC) was conducted to assess the degree of stabilization of the fibers. 1 – 1.5 mg of neat specimens was heated from 40 – 400 $^{o}$C at a heating rate of 1 $^{o}$C/min. After the 1$^{st}$ heating scan, the sample pan in the DSC furnace was quenched to 40 $^{o}$C at a rate of 100 $^{o}$C/min and the identical heating scan was conducted for 2$^{nd}$ and 3$^{rd}$ run. Fourier transformed-infrared (FT-IR) spectroscopy on the specimens stabilized in furnace was carried out. The fibers were placed under FT-IR equipped with optical microscope and the spectra were collected by 2048 accumulation at a resolution of 4 cm$^{-1}$ against air background. PeakFit (v4.11) was used to analyze the –C≡N stretching region in the FT-IR spectra. The peak positions for conjugated (~2210 cm$^{-1}$) and β-amino (~2190 cm$^{-1}$) nitrile groups have been discussed and established in literature[215-220], while neat nitrile band is around 2240 cm$^{-1}$. For the carbonized fibers, Raman spectra were collected in the back scattering geometry using Holoprobe Research 785 Raman Microscope made by Kaiser Optical System using 785 nm excitation laser with polarizer and analyzer parallel to each other (VV mode), and the fibers were placed parallel to the polarizer and analyzer. Wide angle X-ray diffraction (WAXD) patterns were obtained on multifilament bundles by Rigaku Micromax-002 (λ=1.5418 Å) using Rigaku R-axis IV++ detection system. The diffraction patterns were analyzed using AreaMax V. 1.00 and MDI Jade 6.1. Fiber tensile fracture surfaces were observed on the gold coated samples by scanning electron microscopy (LEO 1530 SEM operated at 10 kV). High resolution transmission electron microscopy (HRTEM) study was conducted using Hitachi HF-2000 (operated at 200 kV). For TEM specimen preparation, the stabilized and carbonized fibers were ground using pestle and mortar into very fine powder. The ground powder was collected on lacey carbon coated copper grid. All beam

alignment and stigmation corrections were first performed using evaporated aluminum standard on TEM grid (cat# 80044, EMS, Co.) before the sample was inserted and imaged in the bright field mode. Single filament tensile properties were determined using RSA III solids analyzer (Rheometric Scientific, Co.) at a gauge length of 25 mm and the crosshead speed of 0.25 mm/s. For each sample, a least 15 filaments were tested. For determining fiber diameter, the weight of the constant length of the stabilized and the carbonized fibers (about 3 – 4 m) was measured, and the diameter was calculated by assuming density of fibers as 1.5 and 1.8 g/cm$^3$, respectively. The neat fiber diameter was calculated by the same weighing method using 1.18 and 1.3 g/cm$^3$ as the density for PAN and SWNT, respectively (rule of mixtures for composite fiber was used for density calculation). The electrical conductivity of carbon fibers was measured using 4 probe method (Keithly 2400). For electrical conductivity measurement, fibers were placed on a glass slide and 4 different lead frame from fiber was made using silver paste (DuPont Co.) as shown in Figure 4.2. The applied current was in the range from 10 μA to 1 mA.

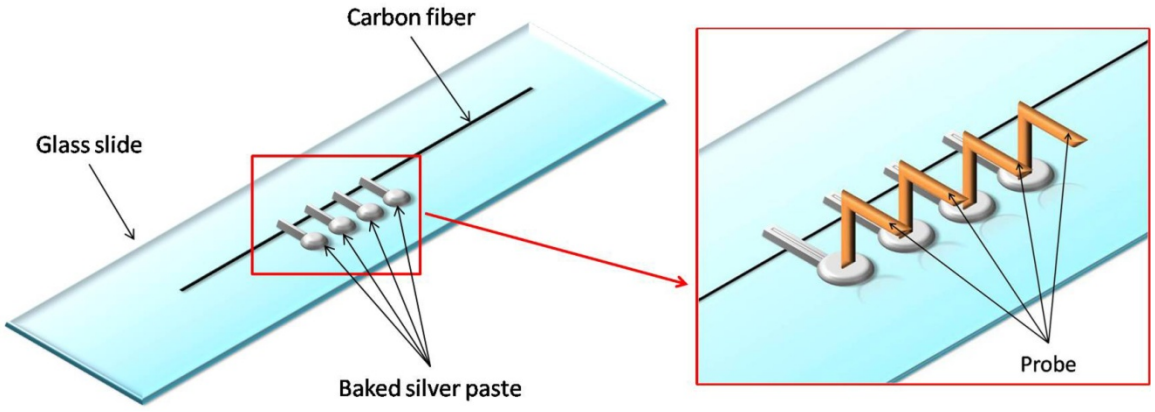


Figure 4.2 The schematics of electrical conductivity measurement for carbon fibers.

## 4.3 Results and Discussion

### 4.3.1 Properties of Precursor Fibers

The mechanical and structural properties of gel spun PAN and PAN/SWNT (1 wt%) fibers are listed in Table 4.1. From WAXD analysis, it is shown that the PAN/SWNT fibers exhibit higher crystal orientation and crystallinity with slightly smaller crystal size. SWNT orientation in composite fibers were determined to be 0.904 by Raman G-band intensity as described in Chapter 3. Stabilization is known to be a governing step to obtain highly graphitic carbon fiber, which results in high modulus. During stabilization, cyclization, dehydrogenation, and oxidation reactions occur. Stabilization reactions of PAN are exothermic. DSC thermograms of PAN and PAN/SWNT fibers under air environment (Figure 4.3) show that the composite fiber has almost 30% less heat evolution. As we mentioned previously, SWNT has strong interaction with PAN molecules therefore, the PAN/SWNT composite fibers and films show enhanced mechanical properties, solvent resistance and electron beam radiation resistance as well. In addition, this interaction may also lead to the improved thermal stability of polymer matrix. Based on DSC thermogram of PAN/SWNT fiber, one can interpret that 30% of PAN molecules in composite fiber are interacting with SWNT, which can only be stabilized with extensive heat treatment. Furthermore, the resultant fibers were heat treated repeatedly in DSC for $2^{nd}$ and $3^{rd}$ run. Control PAN fiber shows no more heat evolution during $3^{rd}$ run while PAN/SWNT fibers still show about 30 J/g of heat of stabilization reaction, indicating the unreacted PAN molecules during $1^{st}$ and $2^{nd}$ run remain intact. The calculated heat of stabilization is also listed in Table 4.2.

Tables 4.1 Various properties of neat gel spun PAN and PAN/SWNT (1 wt%) fibers used for preparing carbon fiber.

| | Control PAN | PAN/SWNT |
|---|---|---|
| Draw ratio | 38 | |
| Diameter (μm) | 23.6 ± 0.2 | 21.8 ± 0.1 |
| Tensile modulus (GPa) | 21.0 ± 2.2 | 26.6 ± 2.2 |
| Tensile strength (GPa) | 0.85 ± 0.14 | 1.05 ± 0.10 |
| Strain to failure (%) | 7.9 ± 1.2 | 8.2 ± 0.6 |
| Crystallinity (%)[1] | 65 | 68 |
| Crystallite size$_{2\theta\sim17^\circ}$ (nm)[2] | 11.3 | 10.8 |
| $f_{c,2\theta\sim17^\circ}$ | 0.916 | 0.927 |
| $f_{SWNT}$[3] | - | 0.904 |

[1] Calculated by deconvolution of integrated WAXD patterns
[2] Calculated by Sherrer's equation with constant K=0.9
[3] Calculated by fitting Raman G-band intensity variation

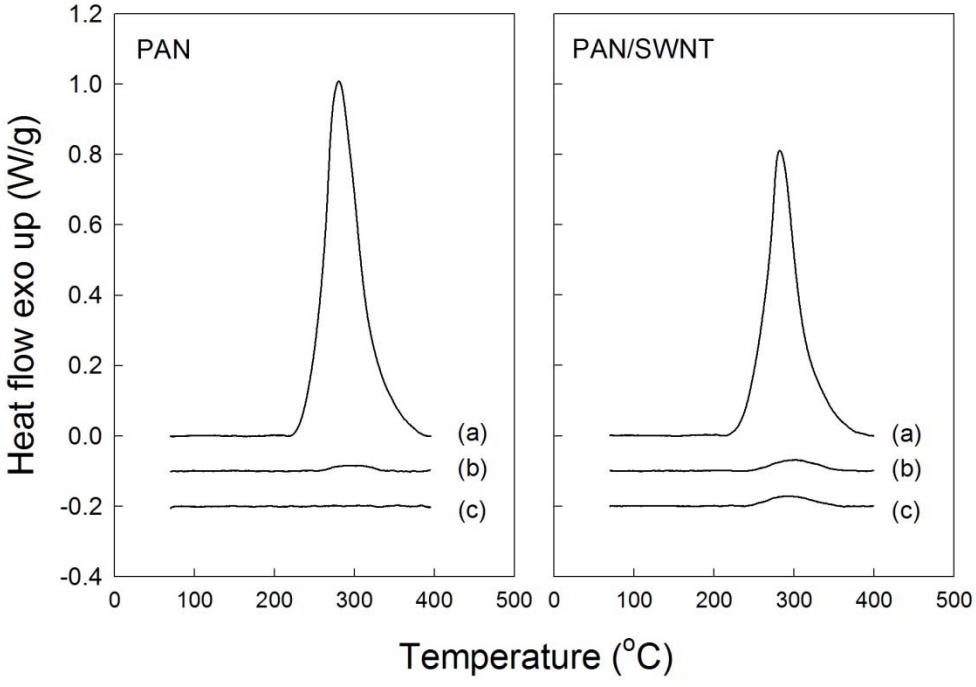


Figure 4.3 DSC thermograms of gel spun PAN and PAN/SWNT fibers: (a) 1st, (b) 2nd, and (c) 3rd run.

Table 4.2 Heat of stabilization for PAN and PAN/SWNT fibers.

| | $\Delta H_{stabilization}$ (kJ/g) | | |
|---|---|---|---|
| | 1st run | 2nd run | 3rd run |
| Control PAN | 3.4 | 0.02 | - |
| PAN/SWNT | 2.5 | 0.04 | 0.03 |

### 4.3.2 FT-IR Spectra Analysis of Stabilized Fibers

Infrared spectra of fibers stabilized with and without stress are shown in Figure 4.4. Stabilization without stress was carried out in air in a thermogravimetric analyzer (TGA) for 30 min. The chemical structures of various nitrile groups are shown in Figure 4.5. The conjugated nitrile group can be generated upon dehydrogenation of PAN and b-amino nitrile groups[221] can be formed due to the termination of cyclization reaction. The termination of cyclization is thought to take place every 4 - 5 PAN repeat units, as a result of its helical conformation[215, 222]. Therefore more planar zigzag conformation in the fiber is expected to increase the gap between cyclization terminations. Chain scission may occur during cyclization termination. Therefore, the fiber containing more planar zigzag conformations would result in less frequent chain scission, and hence result in lesser defects, thus ultimately affecting the tensile strength of the resulting carbon fiber. The PAN/SWNT gel fiber has more planar zigzag sequences than the PAN fiber as shown in Chapter 3. This difference may affect stabilization. Since the peak positions of different types of nitrile groups are known, the nitrile spectra was fitted without varying the peak position, and by allowing the peak width and intensity to vary (Figure 4.6), and the data is compared in Table 4.3. There are more unreacted nitrile groups in PAN/SWNT stabilized under stress than in the control PAN stabilized under the same conditions, and the quantity of unreacted groups increased with increasing stress as

judged by the relative areas of the FT-IR peaks. This confirms that the presence of SWNT as well as stress hinders stabilization reaction. AN/SWNT samples stabilized in furnace under stress, exhibited significantly higher conjugated nitrile and significantly lower b-amino nitrile than the control PAN stabilized under the same conditions. The stabilized structure in PAN/SWNT predominantly contains conjugated nitrile, while in PAN it is predominantly b-amino nitrile. This further suggests that SWNTs constrains PAN molecules and hence results in the higher degree of cyclization as discussed earlier. When stabilized in TGA, both PAN and PAN/SWNT fibers have very comparable amounts of different nitrile groups after 30 min of heat-treatment in air at 285 $^{o}$C. We think that during this short stabilization time, core of the fiber is mostly un-stabilized and hence the effect of the presence of SWNTs is not obvious.

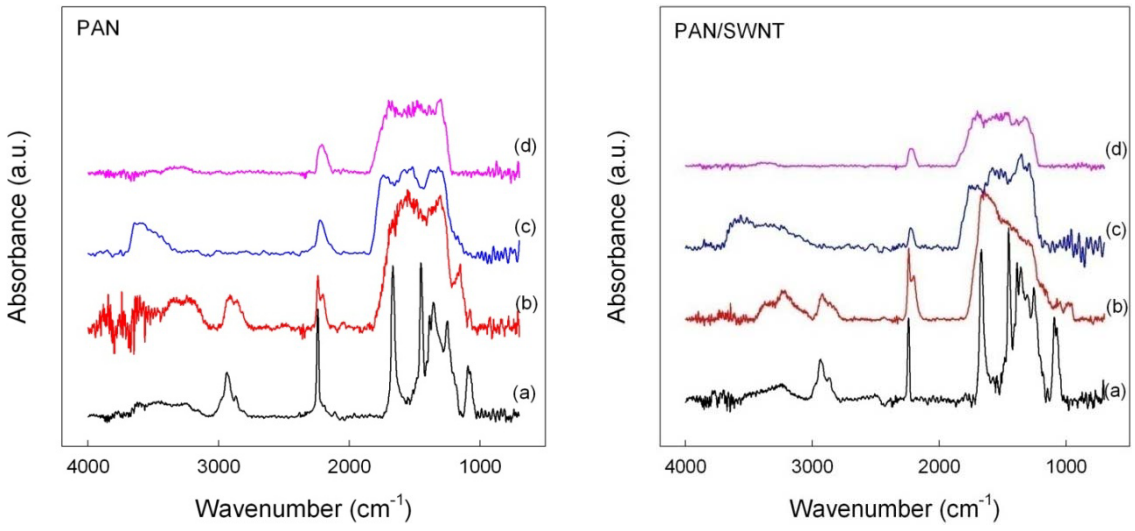


Figure 4.4 FT-IR spectra for PAN and PAN/SWNT fibers: (a) neat fibers, (b) stabilized under TGA for 30 min, (c) stabilized in furnace under 0.006 N/tex (7 MPa) stress, and (d) stabilized in furnace under 0.025 N/tex (30 MPa) stress.

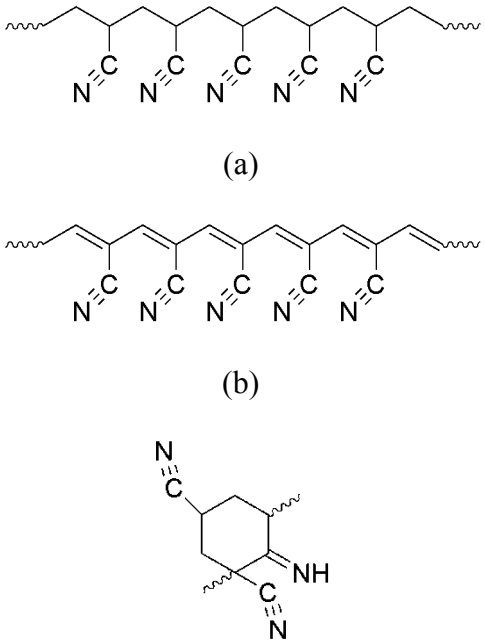


Figure 4.5 Chemical structure of three possible nitrile group during stabilization: (a) unreacted nitrile, (b) conjugated nitirle, and (c) β-amino nitrile groups.

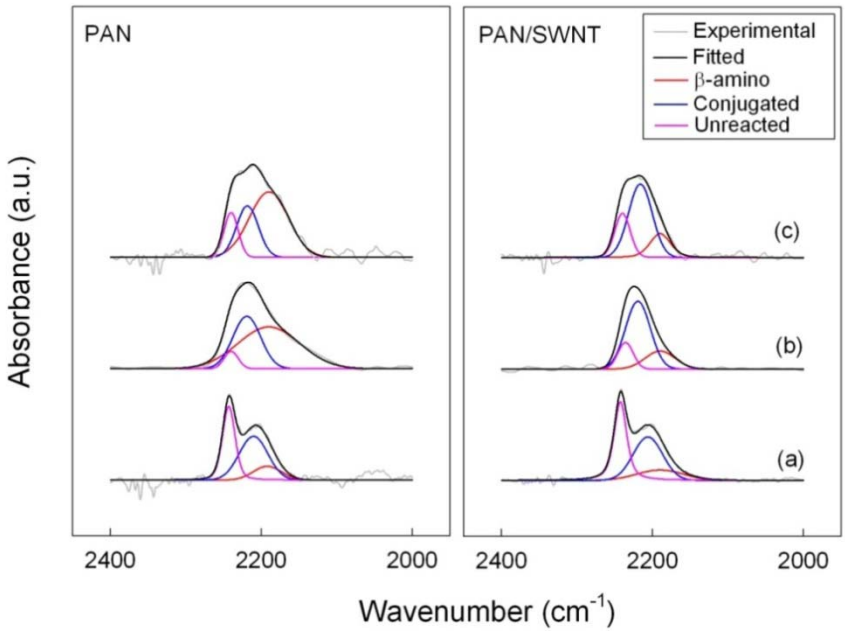


Figure 4.6 Nitirle band fitting results for PAN and PAN/SWNT fibers: (a) stabilized under TGA for 30 min, (b) stabilized in furnace under 0.006 N/tex stress, and (c) stabilized in furnace under 0.025 N/tex stress.

Table 4.3 Peak fitting results for FT-IR spectra of PAN and PAN/SWNT fiber stabilized in various conditions.

| | Precursor fiber | | HT-30 min at 285 °C (TGA) | | HT-furnace[2] (0.006 N/tex) | | HT-furnace[2] (0.025 N/tex) | |
|---|---|---|---|---|---|---|---|---|
| | PAN | PAN/SWNT | PAN | PAN/SWNT | PAN | PAN/SWNT | PAN | PAN/SWNT |
| Unreacted nitrile (%)[1] | 100 | 100 | 38.9 | 42.4 | 5.7 | 15.5 | 14.7 | 23.7 |
| Conjugated nitrile (%)[1] | - | - | 46.5 | 43.3 | 33.9 | 64.0 | 26.1 | 57.7 |
| β-amino nitrile (%)[1] | - | - | 14.6 | 15.3 | 60.4 | 20.5 | 59.2 | 18.6 |

[1] Area fraction by peak deconvolution
[2] Specimen for HT-furnace was stabilized fibers in furnace

### 4.3.3 Morphological Studies of Stabilized and Carbonized Fibers

PAN molecules in the interphase region have higher orientation than in the matrix as shown in Chapter 3. PAN/SWNT composite fibers show fibrillar structure even after stabilization and carbonization (Figure 4.7).

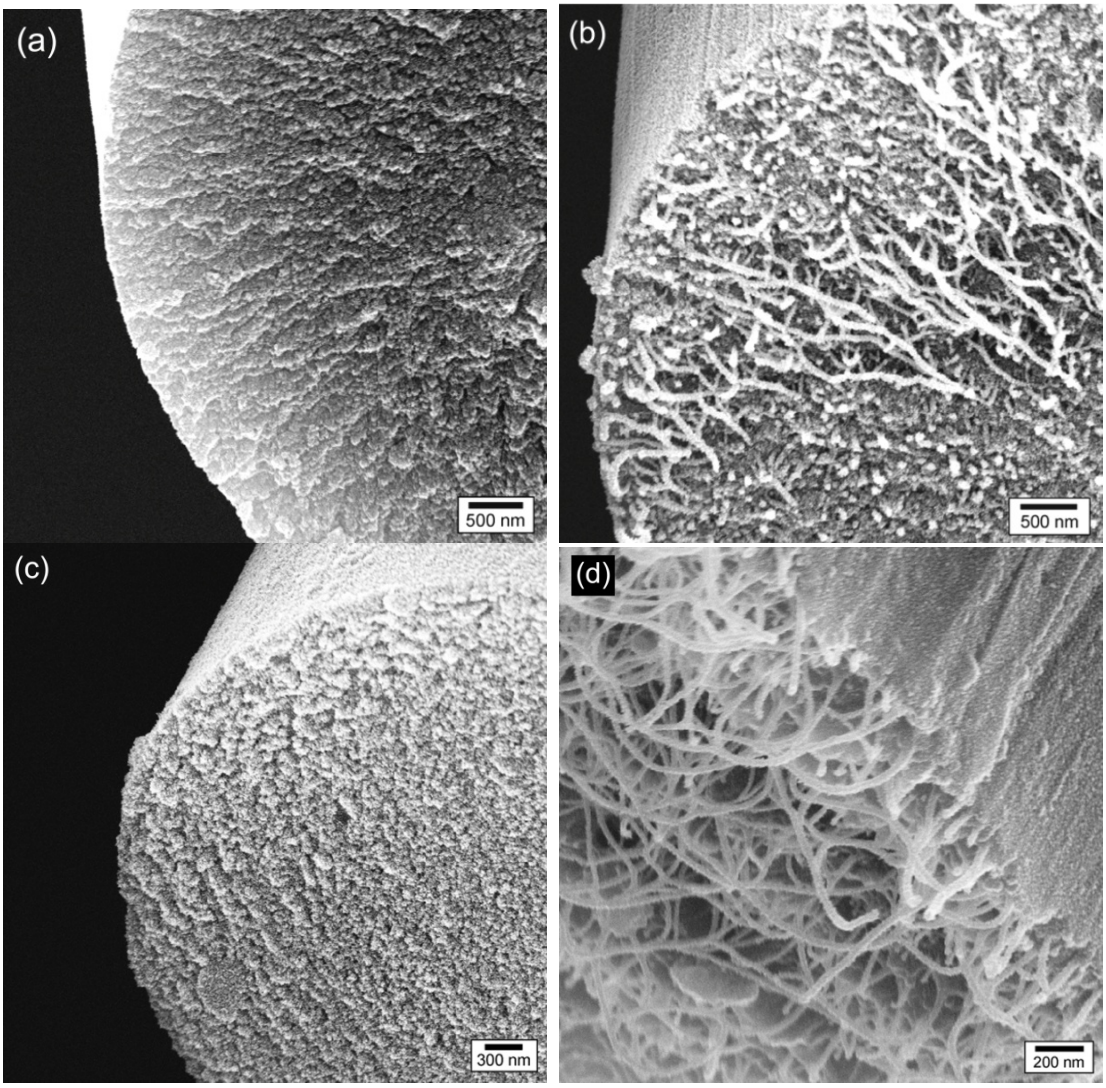


Figure 4.7. SEM micrographs for the stabilized (a) PAN and (b) PAN/SWNT fibers.

Figure 4.8 is the schematic model of the carbonized PAN/SWNT fiber combined with SEM and HR-TEM micrographs. The carbonized composite contains nanofibrils embedded in the brittle carbon matrix. Nanofibrils consists of SWNT surrounded by well developed graphitic structure (Figure 4.8d). PAN molecules in the interphase region when carbonized form well ordered graphite. Figure 4.8d shows HR-TEM image of the nanofibril, exhibiting that SWNTs are densely packed however, they do not exist as bundles instead they are separated by carbonized PAN. SWNTs are also aligned well along the carbon fiber axis. SAED pattern for this specimen shows well defined arcs associated with the graphite (002) plane. While the PAN molecules in the vicinity of SWNT form well-defined graphite, the carbonized PAN matrix shows relatively less ordered structure, which is mostly disordered or amorphous carbon (Figure 4.8e). In the absence of SWNT, it is generally reported that the turbostratic graphite structure would be obtained when the stabilized PAN fibers are carbonized under 1700 $^{o}$C. In order to increase the degree of graphitization, one must subsequently heat treat the carbonized fiber up to 3000 $^{o}$C under inert environment. Therefore, carbonization temperature, 1100 $^{o}$C, used in the current study is relatively low to obtain the graphitic structure as compared to the conventional carbon fiber processing.

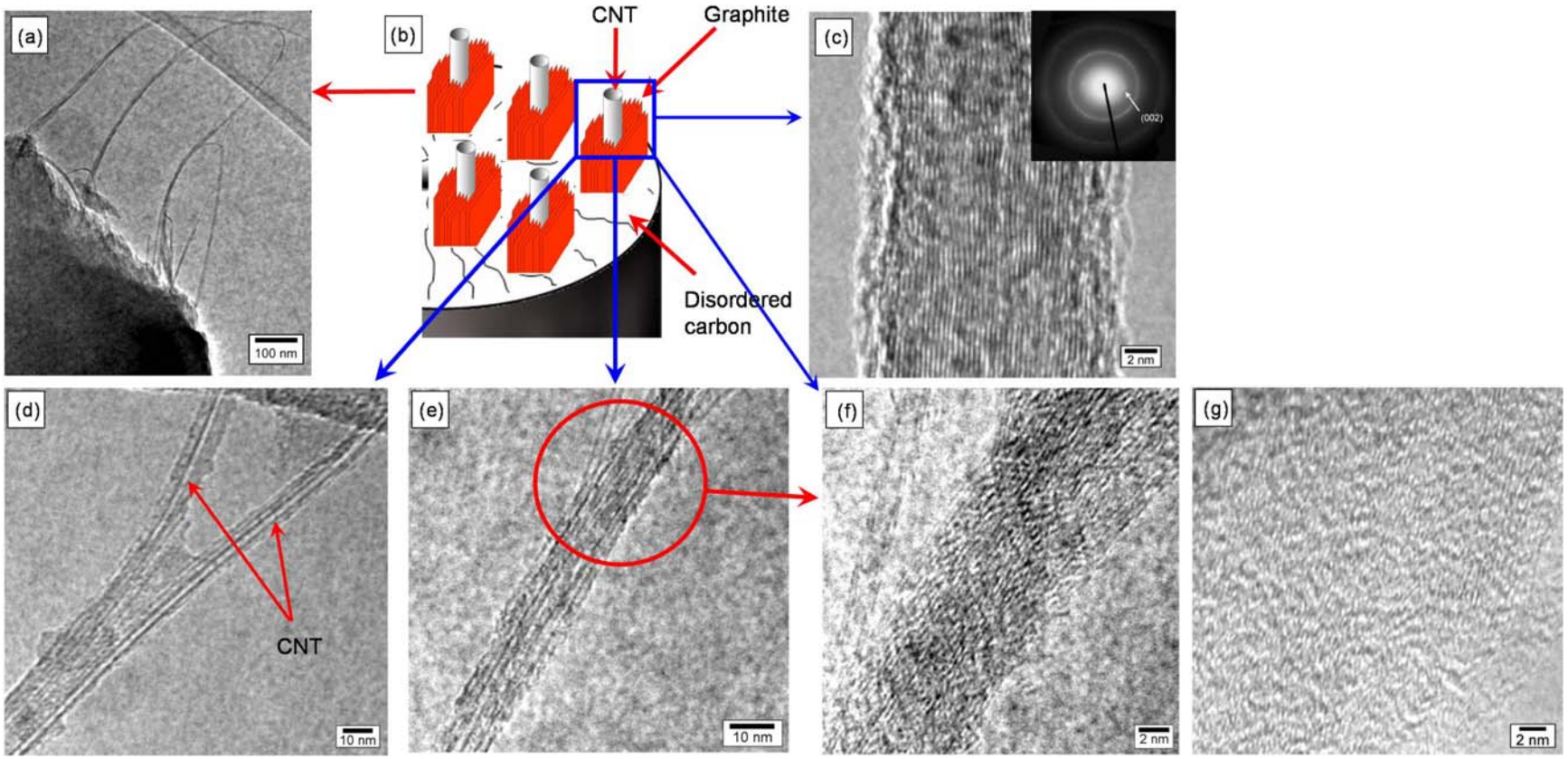


Figure 4.8 Schematic description of the structure development of the carbonized PAN/SWNT fiber: (a) low resolution TEM images showing nanofibrillar structure, (b) schematics, (c) HRTEM micrograph of nanofibril suggesting well-defined graphite structure development (inset represents selected area electron diffraction (SAED) pattern exhibiting highly graphitic (002) plane oriented along the nanofibril axis), and (d)-(f) HRTEM micrograph of carbonized PAN/SWNT fiber. (g) HRTEM micrograph of carbonized PAN fiber showing disordered carbon structure.

### 4.3.4 Raman Spectroscopy of Carbonized Fibers

The Raman spectra of carbonized PAN fibers show strong disorder band (at ~ 1300 cm-1) and begins to show a shoulder for the graphitic G-band (at ~ 1580 cm-1) when stress is increased during stabilization and carbonization (Figure 4.9A). On the other hand, carbonized PAN/SWNT fiber exhibits a distinct G-band even when stabilized and carbonized at a low stress (Figure 4.9B). The G-band intensity increases with increasing stress, confirming stress induced graphitization. The Raman observation is in agreement with high resolution transmission electron microscopy, showing less ordered carbon for carbonized PAN and well ordered carbon for carbonized PAN/SWNT. It also should be noted that the G-band in carbonized PAN/SWNT fibers in Figure 4.9B is not due to SWNT. Due to resonance, SWNT results in a very strong intensity G-band as can be seen in the PAN/SWNT precursor fiber (Figure 4.10). In the stabilized and carbonized fibers, laser is absorbed by the stabilized and carbonized products of PAN, quenching SWNT spectra.

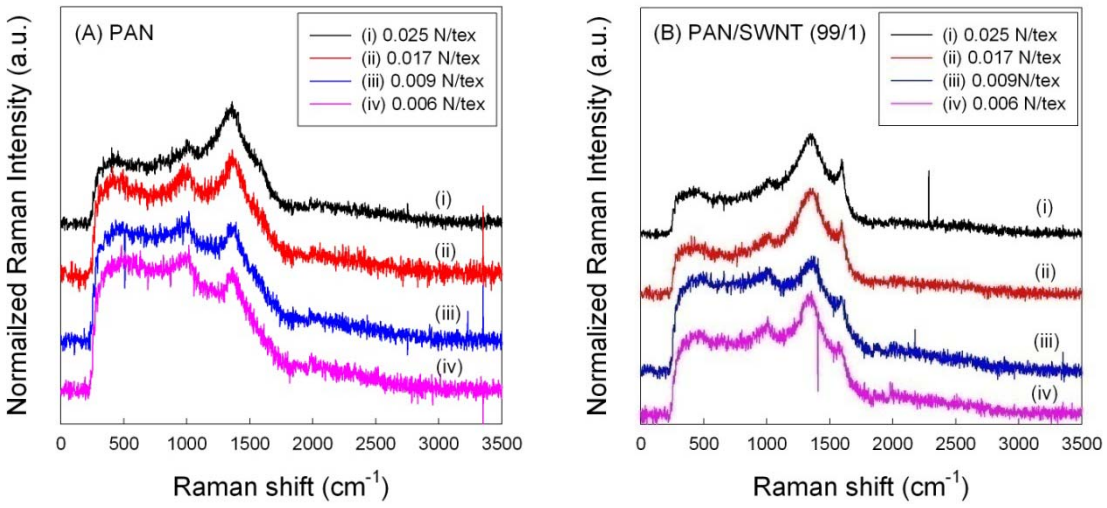


Figure 4.9. Raman spectra for the carbonized PAN and PAN/SWNT fibers as a function of initial stress.

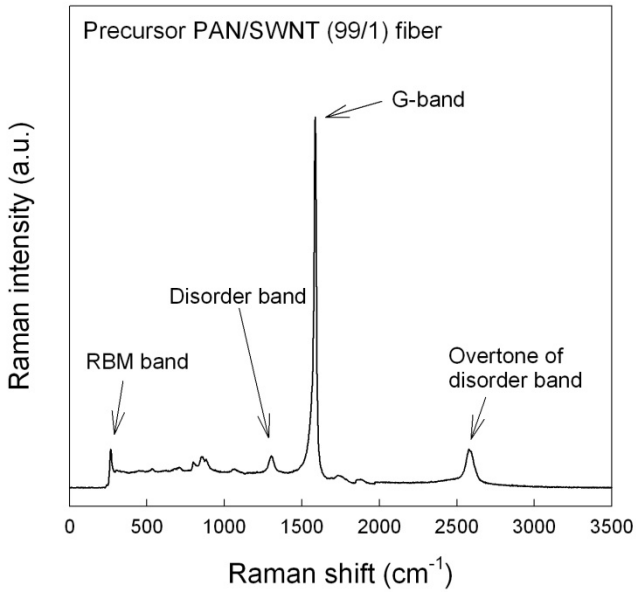


Figure 4.10 Raman spectrum of the precursor gel spun PAN/SWNT (99/1) fiber.

### 4.3.5 Structural Analysis of Stabilized and Carbonized Fibers

Figure 4.11 shows the 2D WAXD patterns and integrated scans for the neat, stabilized, and carbonized fibers. Upon stabilization, the crystalline structure of PAN is vanished for both PAN and PAN/SWNT fibers and new diffraction peaks are developed. These two peaks are expected to originate from the inter-spacing and axial order of the cyclized structure. The analysis on integrated scans exhibits that the higher crystalline phase orientation ($f_{(002)}$=0.432) and larger crystal size (1.19 nm) were observed for the stabilized PAN/SWNT fibers as compared to those (0.421 and 1.15 nm, respectively) of the stabilized PAN fibers. The crystal size along the fiber axis ((10) plane) of the cyclized structure in the stabilized PAN/SWNT fiber was also relatively larger (2.30 nm) than that of the stabilized PAN fiber (1.76 nm). This suggests that the SWNT incorporation facilitate the crystal growth of cyclized structure not only along the lateral direction but to the stabilized fiber axis direction as well. In addition, all the structural factors are

enhanced with increasing the applied stress during stabilization (Table 4.4), confirming stress induced cyclization as discussed in FT-IR analysis. WAXD data exhibit similar results for both the carbonized PAN and PAN/SWNT fibers. Unlike Raman spectroscopy, which is almost inactive to the turbostratic graphitic structure as well as HR-TEM which can only observe more localized area of the specimen, WAXD analysis takes an average throughout the specimens. WAXD from both the turbostratic as well as the more perfect graphitic structure are equally detectable. Therefore, WAXD data is more representative of the overall structure of the fibers. However, the graphitic structure of the carbonized PAN/SWNT fibers in the vicinity of SWNT compromise the overall structural similarity, thus results in significantly improved mechanical properties. As listed in Table 4.4 and Table 4.5, the orientation factor and crystal size along both fiber axis and lateral direction of the stabilized and carbonized PAN/SWNT fibers are slightly larger than those of the stabilized and carbonized PAN fibers.

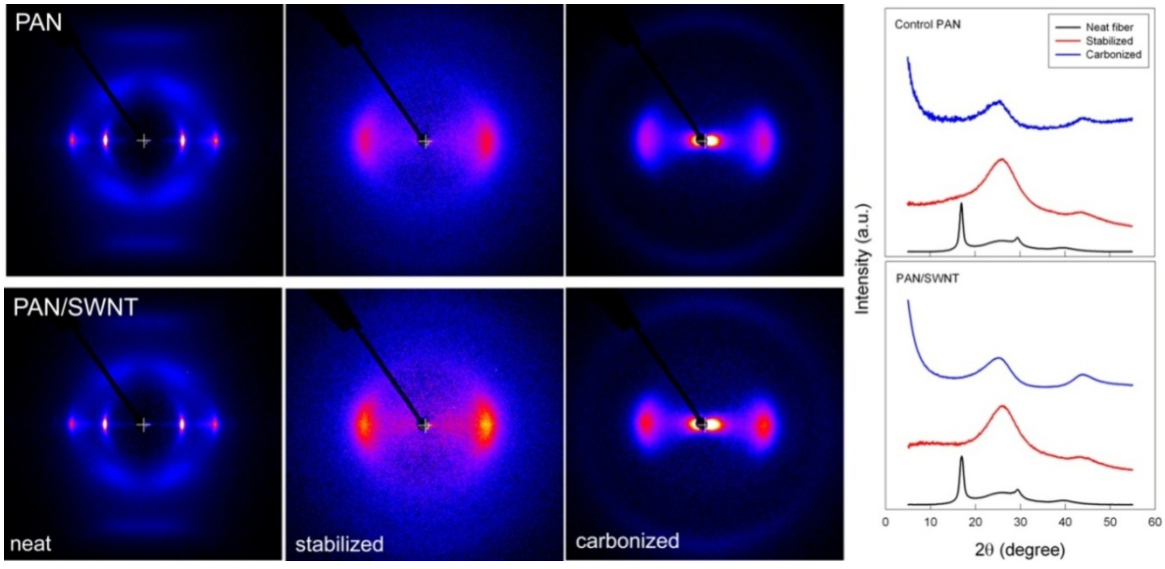


Figure 4.11 WAXD patterns and integrated scans of PAN and PAN/SWNT fibers.

Table 4.4 Structural parameters of large diameter stabilized PAN and PAN/SWNT fibers.

| Precursor | Applied stress(N/tex) | $f_{ladder}$ | $L_{(2\theta\sim26°)}$ (nm) | $L_{(2\theta\sim43°)}$ (nm) |
|---|---|---|---|---|
| Large diameter PAN | 0.025 | 0.421 | 1.2 | 1.8 |
| | 0.006 | 0.405 | 1.1 | 1.5 |
| Large diameter PAN/SWNT (99/1) | 0.025 | 0.432 | 1.2 | 2.3 |
| | 0.006 | 0.412 | 1.1 | 1.8 |

Table 4.5 Structural parameters of carbonized PAN and PAN/SWNT fibers.

| Precursor | | Applied stress (N/tex) | $f_c$ | $Z^1$ (degree) | $d$-spacing$_{(002)}$ (nm) | $L_{(002)}$ (nm) | $L_{(10)}$ (nm) |
|---|---|---|---|---|---|---|---|
| Large diameter PAN | | 0.025 | 0.763 | 33.9 | 0.349 | 1.2 | 1.7 |
| | | 0.006 | 0.742 | 35.8 | 0.351 | 1.1 | 1.6 |
| Large diameter PAN/SWNT (99/1) | | 0.025 | 0.798 | 31.2 | 0.344 | 1.3 | 1.8 |
| | | 0.006 | 0.750 | 34.4 | 0.350 | 1.2 | 1.7 |
| Small diameter PAN/SWNT (99/1) | | 0.025 | 0.795 | 31.4 | 0.345 | 1.3 | 2.1 |
| Commercial carbon fibers | P-25 | | - | 31.9 | 0.344 | 2.6 | 6 |
| | T-300 | | - | 35.1 | 0.342 | 1.5 | 4 |
| | IM8 | | - | - | 0.343 | 1.9 | 5 |

1 Full width at half maximum (FWHM) from azimuthal scans of (002) plane

### 4.3.6 Mechanical Properties of Stabilized and Carbonized Fibers

Tensile modulus of the stabilized PAN/SWNT fibers is about 26% higher than the stabilized PAN fibers while tensile strength and strain to failure of the two fibers were quite comparable (Table 4.6). Increased stress during stabilization resulted in higher modulus and tensile strength. Fiber Shrinkage decreases with increasing applied stress during stabilization (Figure 4.12). Also at a given stress, less shrinkage is observed in PAN/SWNT than in PAN. The shrinkage data is based on the fiber length measurement before and after stabilization.

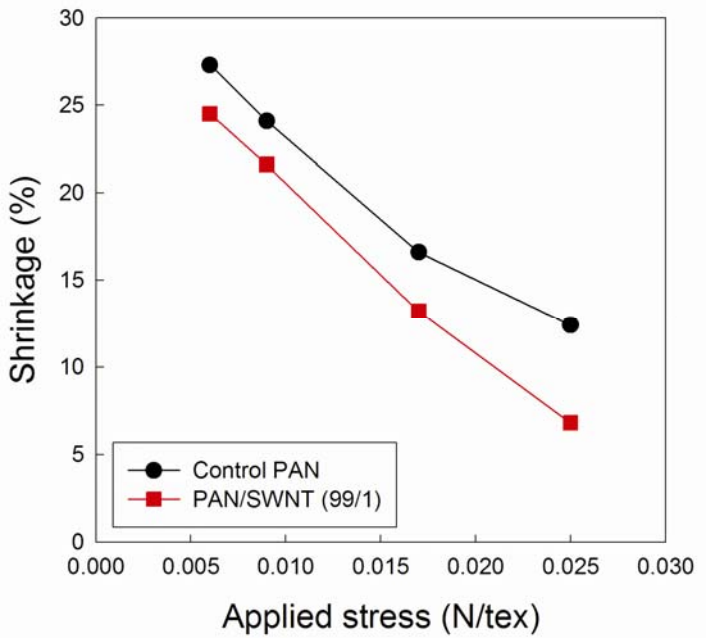


Figure 4.12 Fiber shrinkage behavior after stabilization as a function of applied stress.

Carbonized PAN/SWNT fiber exhibits higher tensile strength and modulus than the control PAN fiber processed under the same conditions (Table 4.7). The addition of 1 wt% SWNT resulted in 64% increase in tensile strength and 49% increase in modulus for

the small diameter carbon fiber. The substantially higher modulus in carbonized PAN/SWNT as compared to carbonized PAN is attributed to higher orientation and higher graphitic order. On the other hand tensile strength is a defect dependent property and is not as sensitive to orientation and graphitic order. The presence of nanotubes and the development of graphitic carbon in the vicinity (about 10 - 30 nm thick layer), most likely is a less defective structure than the surrounding glassy carbon. We think than these graphitic fibrils act as reinforcement, resulting in higher tensile strength fiber. For comparison, the tensile properties of the commercial carbon fibers are also listed in Table 4.7. As can be seen, the tensile modulus of the carbonized small diameter PAN/SWNT (99/1) fibers is higher than the PAN based T300 and IM9 fibers. Tensile strength and modulus of the experimental PAN/SWNT fibers can be further improved by process optimization.

Figure 4.13 shows the comparison of effective modulus of 1 wt% CNT in various polymer matrices by normalizing the CNT concentration in each composite. The theoretical and experimental modulus of CNTs is in the range from 640 GPa to 1060 GPa. Considering the SWNT modulus used in this study is 640 GPa, the reinforcement efficiency (~6.6 GPa) is outstanding for gel spun PAN/SWNT fiber, suggesting that the gel spinning of PAN/SWNT system is effective way to utilize the CNT property. Furthermore, 148 GPa enhancement in modulus of carbonized PAN/SWNT fiber indeed indicates that the SWNT incorporation facilitates the formation of well ordered graphite in the vicinity of SWNT.

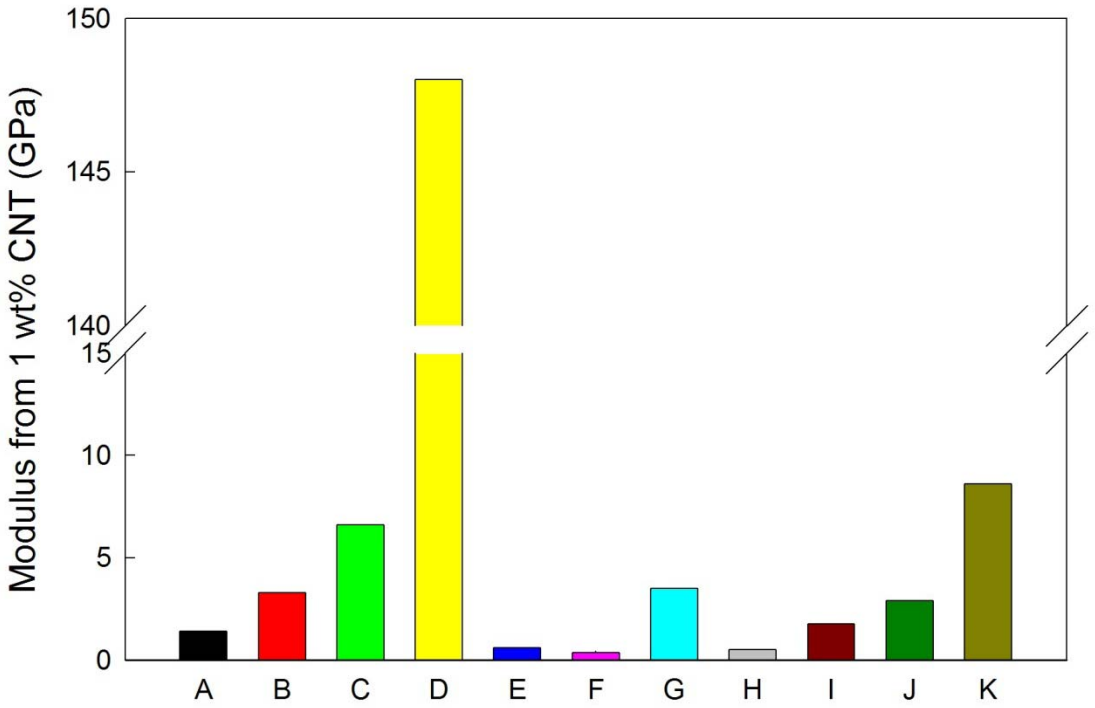


Figure 4.13 Effective modulus of CNTs in various polymer matrices. A. PAN/SWNT (5 wt% - Chapter 2), B. PVA/SWNT (3 wt%)[120], C. PAN/SWNT (1 wt% - Chapter 3), D. Carbonized PAN/SWNT (1 wt% - this chapter), E. PP/SWNT (1 wt%)[223], F. PMMA/SWNT (8 wt%)[224], G. PP/SWNT (1 wt%)[225], H. Nylon 6/SWNT (1.5 wt%)[69], I. PANI/SWNT (2 wt%)[226], J. PBO/SWNT (10 wt%)[81], K. Carbonized pitch/SWNT (5 wt%)[227].

### 4.3.7 Electrical conductivity of carbonized fibers

The electrical conductivity of carbonized PAN/SWNT (99/1) was about $3.7\times10^4$ S/m, while that of carbonized PAN was $2.3\times10^4$ S/m. By incorporating 1 wt% SWNT, the electrical conductivity of resulting carbon fiber can be enhanced by at least 50%. This indicates that not only the addition of SWNT can increase the conductivity by itself but also the more graphitic region in the vicinity of SWNT can attribute to the improvement of electrical conductivity.

Table 4.6 Mechanical properties of stabilized large diameter PAN and PAN/SWNT fibers.

| Precursor | Applied stress(N/tex) | Linear density (tex) | Tensile modulus (N/tex) | Tensile strength (N/tex) | Strain to failure (%) |
|---|---|---|---|---|---|
| Large diameter PAN | 0.025 | 0.58 | 12.7 ± 1.3 | 0.26 ± 0.05 | 4.7 ± 0.5 |
| | 0.006 | 0.77 | 8.7 ± 0.7 | 0.19 ± 0.03 | 5.2 ± 0.3 |
| Large diameter PAN/SWNT (99/1) | 0.025 | 0.41 | 16.0 ± 0.7 | 0.29 ± 0.02 | 4.5 ± 0.6 |
| | 0.006 | 0.64 | 11.3 ± 1.3 | 0.22 ± 0.03 | 4.6 ± 0.9 |

Table 4.7 Mechanical properties of carbonized PAN and PAN/SWNT fibers.

| Precursor | | Applied stress (N/tex) | Linear density (tex) | Tensile modulus (N/tex) | Tensile strength (N/tex) | Strain to failure (%) |
|---|---|---|---|---|---|---|
| Large diameter PAN | | 0.025 | 0.27 | 147 ± 13 | 1.1 ± 0.1 | 0.63 ± 0.08 |
| Large diameter PAN/SWNT (99.5/0.5) | | 0.025 | 0.25 | 184 ± 8 | 1.2 ± 0.2 | 0.65 ± 0.02 |
| Large diameter PAN/SWNT (99/1) | | 0.025 | 0.22 | 190 ± 9 | 1.4 ± 0.1 | 0.75 ± 0.04 |
| Small diameter PAN | | 0.025 | 0.064 | 168 ± 18 | 1.1 ± 0.2 | 0.68 ± 0.04 |
| Small diameter PAN/SWNT (99/1) | | 0.025 | 0.044 | 250 ± 27 | 1.8 ± 0.2 | 0.72 ± 0.05 |
| Commercial carbon fibers | P-25 | | 0.179 | 84 | 0.7 | 0.9 |
| | T-300 | | 0.067 | 129 | 1.8 | 1.5 |
| | IM8 | | 0.037 | 179 | 2.9 | 1.9 |

## 4.4 Conclusions

Gel spun PAN and PAN/SWNT composite fibers were stabilizaed and carbonized with varying stress. DSC showed significantly lower heat evolution in PAN/SWNT fibers under oxidative stabilization than in PAN, suggesting that the presence of SWNT hinders PAN reactivity. Infrared spectroscopy showed that even after prolonged stabilization under stress, PAN/SWNT fiber contained more unreacted nitrile than comparably stabilized PAN. The structure in stabilized PAN/SWNT appeared to be predominantly composed of conjugated nitrile, while in stabilized PAN it appeared to be composed of predominantly β-amino nitriel. Fibrillar structure was observed in the stabilized and carbonized PAN/SWNT, while the corresponding PAN fibers exhibited brittle fracture. Carbonized PAN/SWNT fibers exhibit higher orientation, smaller graphite *d*-spacing and larger crystal size, than PAN carbonized under similar conditions. PAN/SWNT carbonized at 1100 oC under stress shows the development of graphitic structure (as evidenced by Raman and high resolution transmission electron microscopy), while carbonized PAN showed only the presence of disordered carbon. Small diameter carbonized PAN/SWNT fibers containing 1 wt% SWNT exhibited 64% higher tensile strength and 49% higher tensile modulus than the corresponding carbonized PAN. In addition, the electrical conductivity of carbonized PAN/SWNT is 50% higher than that of carbonized PAN.

# CHAPTER 5

# SMALL DIAMETER CARBON FIBER FROM PAN/CNT COMPOSITE FIBERS SPUN BY BI-COMPONENT GEL SPINNING

## 5.1 Introduction

Development of high strength carbon fibers began in 1960s, and after nearly half a century of development, technology now seems mature. Carbon fiber market is now growing at the annual rate of approximately 15%. High strength carbon fibers are increasingly being used in significant quantity in civilian applications. For example, approximately 50% weight of the Boeing 787 is composed of composites utilizing carbon fibers. While commercial continuous carbon fibers are now available with nearly 90% of the theoretical modulus, tensile strength achieved in today's commercial carbon fiber is only a small fraction of the theoretical value. Efforts are underway to narrow the gap between the theory and practice. However the problem is not trivial. Since their discovery in 1991, carbon nanotubes have been expected to result in improved tensile strength materials. After more than 15 years of development, significant breakthroughs are now being reported in developing high strength wholly carbon nanotube fibers[46, 110, 111, 228-230], as well as carbon nanotube reinforced materials[47, 81, 118, 206, 208].

While there are several precursor materials for carbon fiber production such as polyacrylonitrile (PAN), pitch, and cellulose[231-233], PAN fiber is most widely used precursor due to its high carbon yield, as well as high tensile and compressive strength of the resulting carbon fiber[38]. There is significant research activity for reinforcing PAN with carbon nanotube [47, 141, 144, 163-167, 234-237]. Chapter 4 shows that the addition of 1 wt%

carbon nanotubes can increase the tensile strength and tensile modulus of PAN based carbon fibers by 64%, and 49%, respectively. Currently commercial carbon fibers are processed using conventional solution spinning, where polymer solution is extruded directly into a coagulation bath. However, by using gel spinning, higher modulus and strength PAN precursor fiber can be prepared than can be obtained by conventional solution spinning. The higher mechanical properties of the gel spun fiber results in higher mechanical property carbon fibers than can be obtained by solution spun fibers. Gel spinning invented at DSM (Netherlands) around 1980 is currently commercially practiced only for polyethylene to process high performance fibers such as Spectra™ and Dyneema™. There is significant research and patent literature on gel spinning of polymers such as poly(vinyl alcohol) (PVA) and PAN. The third component of the technology for producing high strength carbon fiber is to process a small diameter carbon fiber. Diameter of current commercial carbon fibers is in the range of 5 to 10 μm. Smaller diameter fibers exhibit higher tensile strength. It is difficult to spin continuous fiber with diameters below 10 μm, resulting in a carbon fiber of about 5 μm diameter. Smaller diameter PAN fibers (10 nm to 1 μm diameter) can be processed by electrospinning[165, 238-243]. However, two problems are encountered in this approach for making high strength carbon fibers. First, the molecular orientation and hence tensile modulus achieved in electrospinning is rather low. Secondly, processing continuous fiber by electrospinning has been challenging.

Bi-component spinning has been used since 1960s to make small diameter fibers for fine textiles, and is typically practiced for melt processing[244-250]. In this chapter, core-shell and islands-in-a-sea bi-component geometry along with gel spinning is used to

process effectively small diameter PAN and PAN/CNT fibers to make carbon fibers with diameters less than one micrometer. Small diameter fiber results in high strength, gel spinning leads to high draw ratio and hence high orientation and modulus. Fibers are further reinforced by carbon nanotubes.

## 5.2 Experimental

### 5.2.1 Materials and Solution Preparation

Poly(acrylonitrile-co-methylacrylate) containing 6.7 mol% methylacrylate, with average molecular weight of about 250,000 g/mol, was obtained from Japan Exlan, Co. Carbon nanotubes (lot number XO021UA) were obtained from Unidym, Inc. (Houston, TX) and the catalytic impurity was determined to be about 1.6 wt% by thermogravimetric analysis (TGA). TEM and Raman spectra of the nanotubes are given in Figure 5.1 and Figure 5.2, respectively. In Figure 5.1, most of the nanotubes are large diameter (2 - 5nm) DWNT and triple wall nanotube (TWNT) can be found frequently. Since there are no SWNT observed by TEM, it can be expected that Raman spectra of this CNT will not show any RBM peaks as shown in Figure 5.2. Poly(methyl metharcrylate) (PMMA), molecular weight in the 85,000 – 150,000 g/mol, obtained from Cyro Industries (Orange, CT) was used as the sacrificial "shell" and "sea" component. Dimethyl formamide (DMF) was obtained from Sigma-Aldrich, Co. CNTs were dispersed in DMF at a concentration of 40 mg/L using 24 hr bath sonication (Branson 3510R-MT, 100 W, 42 kHz) at room temperature, and PAN (14.85 g) was dissolved in DMF (100 mL) at 80 $^{o}$C. Optically homogeneous CNT/DMF dispersion was added to the PAN/DMF solution. The excess amount of solvent was evaporated by vacuum distillation at 80 °C, while stirring,

to obtain the desired solution concentration (15 g solid/100 mL solvent). The solution for shell or sea component was prepared by dissolving 55 g PMMA in 100 mL DMF at 150 $^{o}$C.

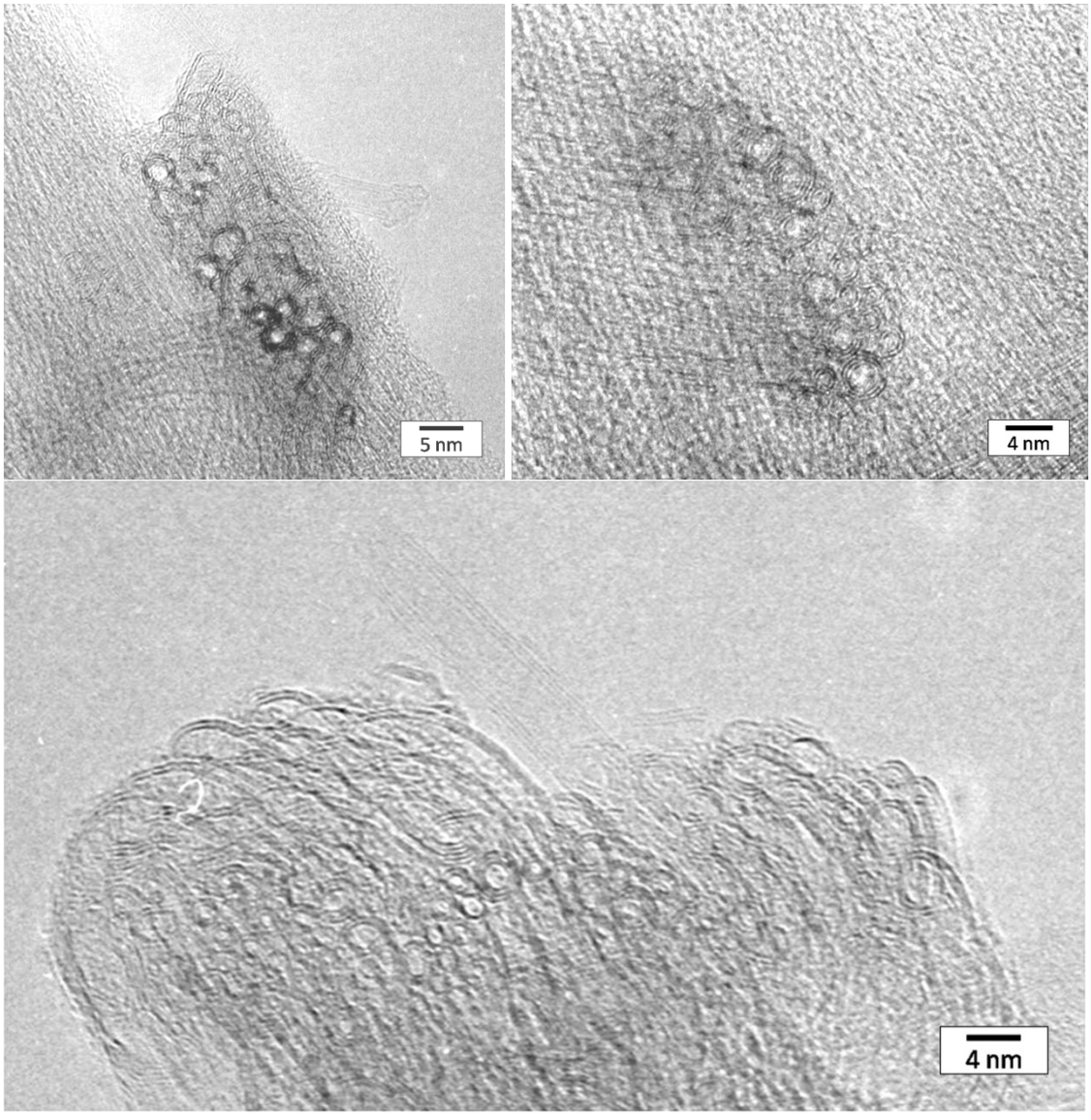


Figure 5.1 HRTEM micrographs of pristine CNT used in this study showing that majority of CNTs are DWNT and some of them are TWNT.

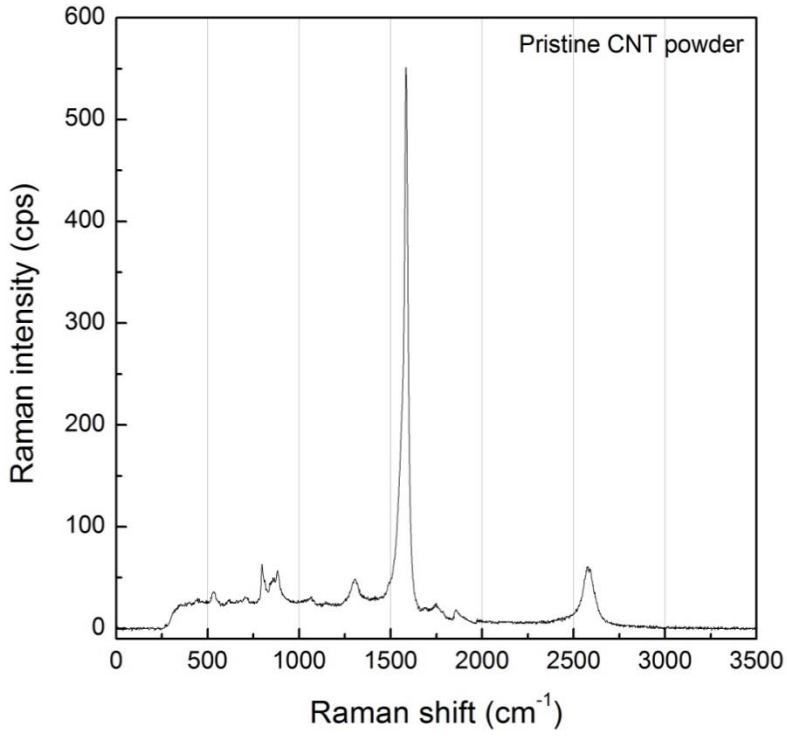


Figure 5.2 Raman spectrum of pristine CNT.

### 5.2.2 Bi-Component Fiber Spinning

Both the core-shell and the islands-in-a-sea fibers were processed using spinneret of 250 μm diameter. The schematic of the bi-component spinning set up and of the core-shell and islands-in-a-sea geometries are given in Figure 5.3. The temperature of both the solution reservoirs (core and islands – PAN or PAN/CNT; shell and sea – PMMA) was maintained at 120 $^{o}$C, while the spinneret was maintained at 140 $^{o}$C. For core-shell fiber spinning, the volumetric flow rate of core and shell component were set to be 0.5 $cm^3$/min and 1.5 $cm^3$/min, respectively. The linear jet speed of core-shell as-spun fiber was about 40 m/min. In islands-in-a-sea geometry, the volumetric flow rates of both the sea and island components were 1.5 $cm^3$/min, which is equivalent to the linear jet speed of 61 m/min based on the spinneret diameter. The solution was spun into a methanol bath

maintained at -50 $^{o}$C. The air gap between the spinneret and the methanol bath was kept at about 5 cm. The as-spun fibers were taken up at 200 m/min and kept immersed in methanol bath at about -50 $^{o}$C for several days. The gel bi-component fiber was drawn in several stages at 110, 150, and 170 °C, using in line heater. The total draw ratio of the PAN and PAN/CNT gel fiber with the PMMA "shell" component was about 16 (this does not include the 3.3 draw ratio in the methanol bath during spinning while the draw ratio of islands-in-a-sea fibers was about 10. The drawn fibers were subsequently vacuum dried at 70 $^{o}$C for 3 days. Figure 5.4 show the SEM micrographs of core-shell with shell component and islands-in-a-sea bicomponent fibers with/without sea component. Sacrificial component, PMMA, was removed by dissolution in nitromethane.

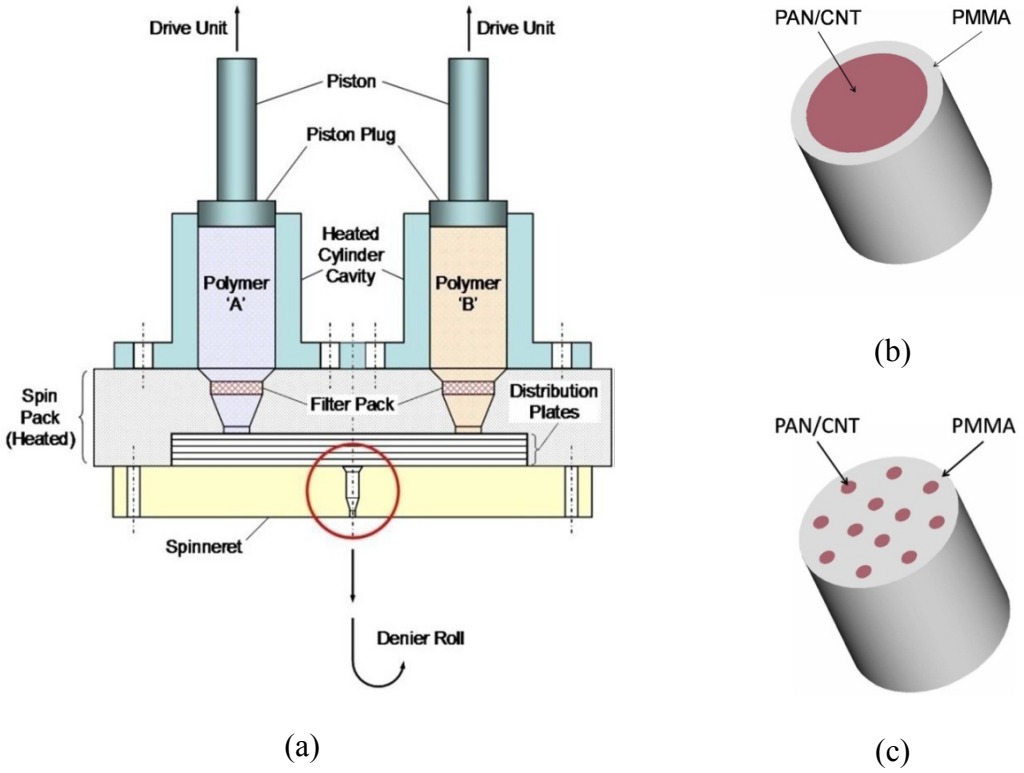


Figure 5.3 The schematics of (a) bi-component spinning apparatus, (b) core-shell, and (c) islands-in-a-sea geometry bi-component fiber.

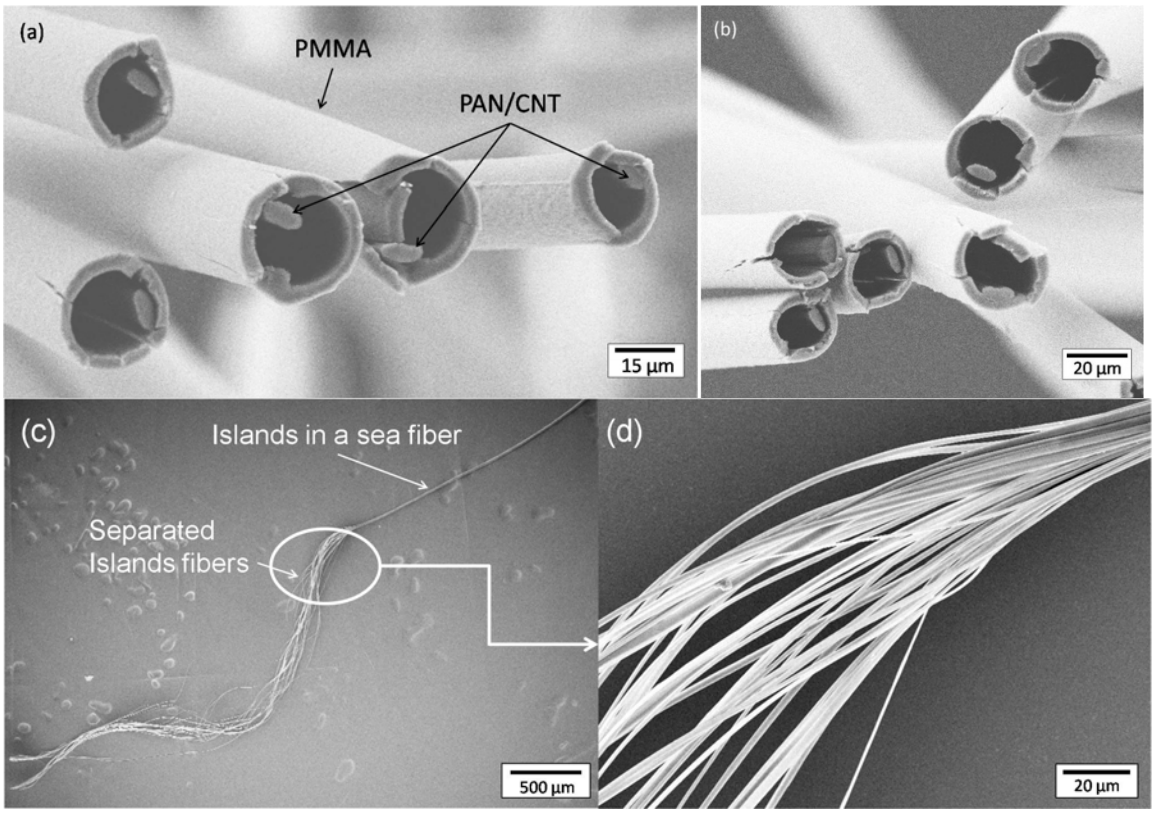


Figure 5.4 SEM micrographs of gel spun bi-component fiber. (a) and (b) cross sectional view of core-shell fiber, (c) low magnification image showing separation of islands fibers (PAN/CNT) from islands-in-a-sea fiber after removing sea component (PMMA), and (d) high magnification image of circled region from left image showing clear separation of individual islands fiber.

### 5.2.3 Stabilization and Carbonization of Bi-Component Fibers

The dried core-shell and islands-in-a-sea precursor fibers (without removing the sea component PMMA) were stabilized in a box furnace (Lindberg, 51668-HR Box Furnace 1200C, Blue M Electric) in air by hanging over a quartz rod using two clamping steel blocks as illustrated in Chapter 4. Based on the precursor fiber cross-sectional area (PAN or PAN/CNT), 20 MPa (0.017 N/tex) and 10 MPa (0.009 N/tex) of initial stress was applied to core-shell and islands-in-a-sea fibers, respectively. Fibers were heated from room temperature to 285 $^{o}$C in air at a heating rate of 1 $^{o}$C/min and held at 285 $^{o}$C

for 4 hr followed by heating up to 330 $^{o}$C at a heating rate of 1 $^{o}$C/min and held at 330 $^{o}$C for 2 hr. The stabilized fibers were cooled down to room temperature over a period of several hours. During stabilization, sea component (PMMA) was completely burned out, which is confirmed by TGA (Figure 5.5). The stabilized island PAN and PAN/CNT fibers were subsequently carbonized in argon by heating from room temperature at a rate of 5 $^{o}$C/min, and by holding at 1200 $^{o}$C for 5 minutes.

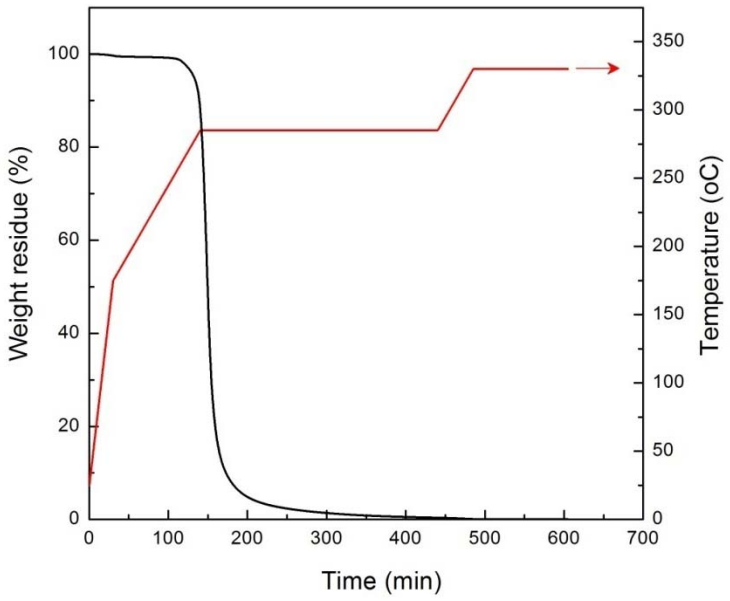


Figure 5.5 TGA curve of PMMA in air. Heating profile is the same as used in stabilizing the islands-in-a-sea fiber.

### 5.2.4 Characterization of Carbonized Bi-Component Fibers

For islands fibers, tensile test was conducted on multi-filament specimen due to the difficulty in preparing single filament sample, while single filament test was conducted on core fibers. In multifilament test, specimens typically containing 4 – 6 filaments were prepared and tested using RSA III solids analyzer (Rheometric Scientific, Co.) at a gauge length of 6 mm and the cross head speed of 0.006 mm/s (0.1%/s). The

tensile fractured specimen were sputtered coated with gold and examined by scanning electron microscopy (SEM, LEO 1530 operated at 10 kV) to determine the effective cross-sectional area. Care was taken to ensure that imaging was done perpendicular to the fiber axis. To further ensure accurate cross-sectional area determination, SEM was calibrated by standard sample (301BE, EMS, Co., Hatfield, PA). The cross-sectional area of the fiber was determined using image analysis software (UTHSCSA Image Tool version 3.0, University of Texas Health Science Center, San Antonio, TX). The obtained cross-sectional area was used to calculate the tensile properties of each specimen. Wide angle X-ray diffraction (WAXD) patterns were obtained on multifilament bundles on Rigaku Micromax-002 (X-ray wavelength, $\lambda = 0.15418$ nm) using Rigaku R-axis IV++ detection system. The diffraction patterns were analyzed using AreaMax V. 1.00 and MDI Jade 6.1. Orientation ($f_{002}$) and crystal size ($L_{002}$ and $L_{10}$) of the carbonized graphitic structure were determined. Raman spectra of the carbonized fibers were collected in the back scattering geometry using Holoprobe Research 785 Raman Microscope made by Kaiser Optical System using 785 nm excitation laser with polarizer and analyzer parallel to each other (vv mode), and the fibers were placed parallel to the polarizer and analyzer.

## 5.3 Results and Discussion

### 5.3.1 Mechanical Properties of Carbonized Bi-Component Fibers

Tensile properties of the carbonized core and island fibers are listed in Table 5.1. For comparison, the tensile properties of the larger diameter carbon fibers processed from gel spun PAN and PAN/CNT based fibers reported previously are also listed in Table 5.1. Figure 5.6 shows the typical and best stress-strain curves for the carbonized PAN and

PAN/CNT island fibers. Tensile strength of different cross-sectional area PAN and PAN/CNT based carbon fibers show a definite increase in strength with reduction in cross-sectional area (Figure 5.7a). This data confirms two points: (a) At a given cross-sectional area, tensile strength of PAN/CNT based carbon fibers containing 1wt% CNT in the precursor can be 30 to 60% higher than the corresponding PAN based carbon fiber. (b) Tensile strength, as expected, increases with decreasing cross-sectional area. Limited data presented in Figure 5.7a also suggests that carbon nanotube reinforcement efficiency is higher at lower cross-sectional area. When analysis similar to the analysis of Peijs et al[251] is conducted on our samples, it results in effective stress on carbon nanotube of 67, 95, 61, and 28 GPa. These numbers are well within the range of theoretical[19, 20] tensile strength of the individual carbon nanotubes. They can also be compared to the effective carbon nanotube stress of 88 GPa, achieved in PVA/CNT film[251]. However the structure of the PAN/CNT based carbon fibers is not simply carbon nanotubes added in the carbonized PAN. Rather, the presence of carbon nanotubes effects the carbonization of PAN. Polyacrylonitrile in the immediate vicinity of carbon nanotubes stabilizes and carbonizes differently than the PAN farther away from nanotubes.

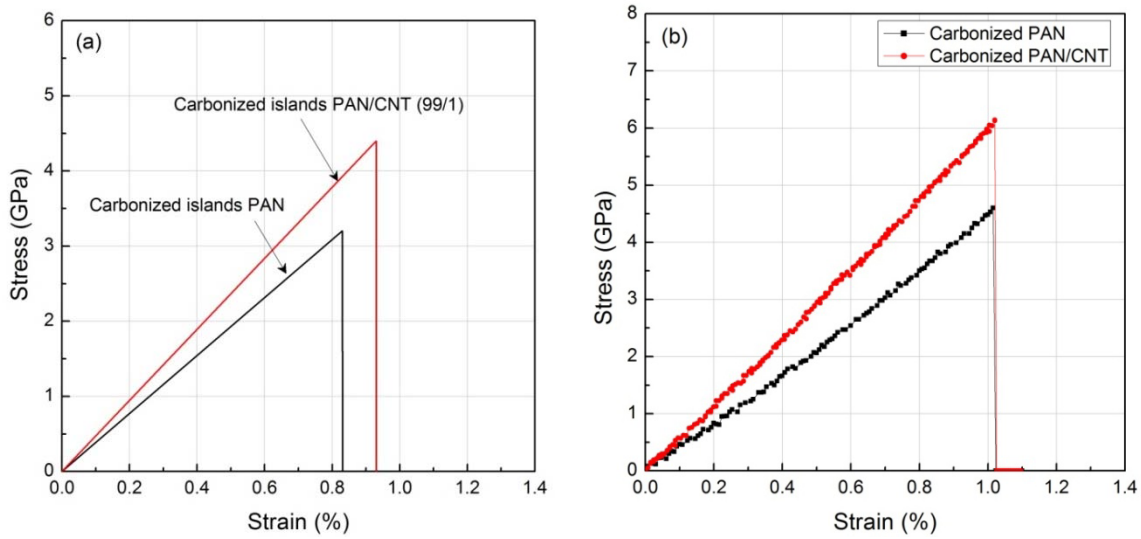


Figure 5.6 (a) Typical stress-strain curves for carbonized islands PAN and PAN/CNT (99/1), and (b) stress-strain curves for the best carbon fibers to date.

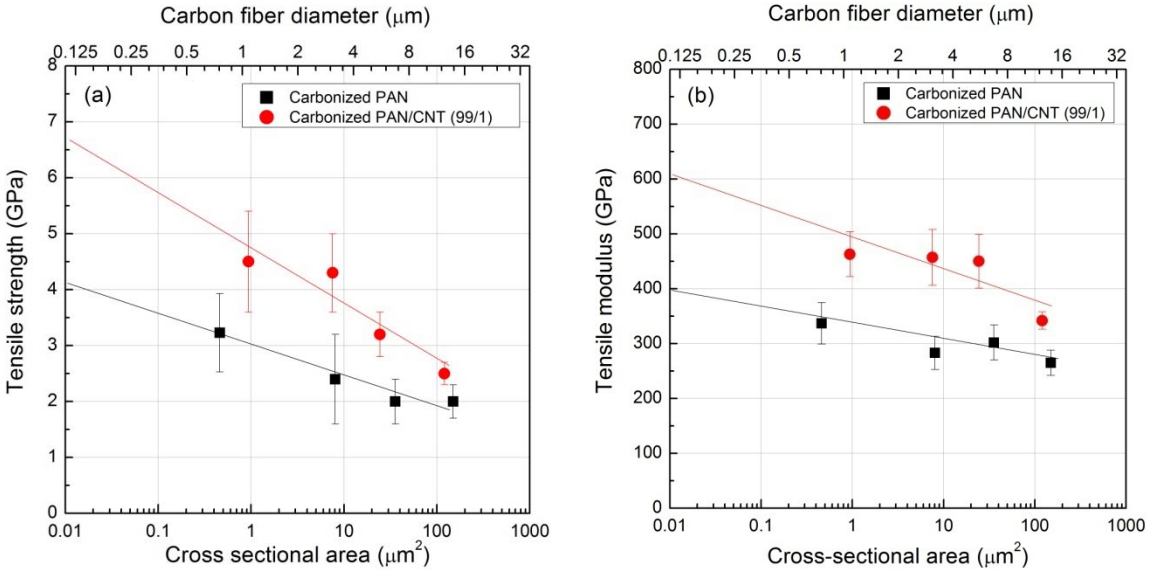


Figure 5.7 (a) Tensile strength and (b) tensile modulus of carbonized PAN and PAN/CNT fibers as a function of cross-sectional area. Data for two large diameter cross-sectional area fibers are from Chapter 4.

Table 5.1 Mechanical properties of carbonized islands, core, and large diameter PAN and PAN/CNT (99/1) fibers.

| | | Carbonized islands fibers | | Carbonized core fibers | | Carbonized gel drawn fibers(Chapter 4) | |
|---|---|---|---|---|---|---|---|
| | | PAN | PAN/CNT (99/1) | PAN | PAN/CNT (99/1) | PAN | PAN/CNT (99/1) |
| Linear density (tex) | | $8.3 \times 10^{-4}$ | $1.7 \times 10^{-3}$ | $1.5 \times 10^{-2}$ | $1.4 \times 10^{-2}$ | $6.4 \times 10^{-2}$ | $4.4 \times 10^{-2}$ |
| Cross-sectional area ($\mu m^2$) | | 0.46 | 0.94 | 8.04 | 7.55 | 35.6 | 24.4 |
| Tensile strength | (GPa) | 3.2 ± 0.7 | 4.5 ± 0.9 | 2.4 ± 0.8 | 4.3 ± 0.7 | 2.0 ± 0.4 | 3.2 ± 0.4 |
| | (N/tex) | 1.78 ± 0.39 | 2.5 ± 0.5 | 1.33 ± 0.44 | 2.39 ± 0.39 | 1.1 ± 0.2 | 1.8 ± 0.2 |
| Tensile modulus | (GPa) | 337 ± 38 | 463 ± 41 | 283 ± 30 | 457 ± 51 | 302 ± 32 | 450 ± 49 |
| | (N/tex) | 187 ± 21 | 257 ± 23 | 157 ± 17 | 254 ± 28 | 168 ± 18 | 250 ± 27 |
| Strain to failure (%) | | 0.85 ± 0.13 | 0.96 ± 0.23 | 0.83 ± 0.18 | 0.93 ± 0.07 | 0.68 ± 0.04 | 0.72 ± 0.05 |

Tensile modulus of PAN based carbon fibers increases monotonically with carbonization temperature while tensile strength reaches a maximum value at about 1500 °C. Modulus of the small diameter carbonized gel spun PAN is higher than that for the commercial fiber carbonized at the same temperature, and that for the corresponding PAN/CNT based carbon fiber it is substantially higher (Figure 5.8a). This represents contributions coming from gel spinning, carbon nanotubes, as well as from small cross-sectional area. Tensile strength of the small diameter PAN based carbon fiber is lower than the commercial fiber carbonized at the same temperature. On the other hand, PAN/CNT based carbon fiber exhibit average tensile strength comparable to the commercial carbon fiber carbonized at the same temperature, while the best data obtained to date (6.14 GPa) is significantly higher than the commercial value (Figure 5.8b). It is noted that commercial fiber has gone through many years of material and process optimization. The fact that PAN/CNT based carbon fiber without optimization shows substantially higher properties over the commercial fiber produced with many years of optimization, suggests the commercialization potential of small diameter PAN/CNT based carbon fiber.

The advantage of PAN based carbon fibers over pitch based carbon fiber or over wholly carbon nanotube carbon fibers is in compressive strength. PAN based carbon fibers are strong in tension as well as in compression and therefore, these are the only carbon fibers used in those structural composites where compressive strength is also a requirement. What is the compressive strength of the small diameter gel spun PAN/CNT based carbon fiber? Compressive strength is measured on the composites, which requires significantly larger quantity of samples, than have been made so far. However, the recoil

test can give an indirect measure of the compressive strength of the elastic fibers[252, 253]. When an elastic fiber fails in tension, it will also fail in compression if its tensile strength is higher than its compressive strength. The tensile stress wave propagates through the fiber to the clamp and recoils as a compressive stress wave. If there are no energy losses in the fiber, then the magnitude of the compressive stress wave is the same as that of the tensile stress. About 50% of the small diameter carbon fiber processed from gel spun PAN/CNT fibers did not fail in compression when failed in tension. An examples of such a fiber is shown in Figure 5.9. The fiber length on fiber template was more than 3 mm (It should be noted that the initial length for tensile testing was 6 mm). High magnification image also reveal there is no buckling behavior throughout the fiber. These observations suggest that the carbon fiber made from the small diameter gel spun PAN/CNT has a compressive strength comparable to or higher than its tensile strength.

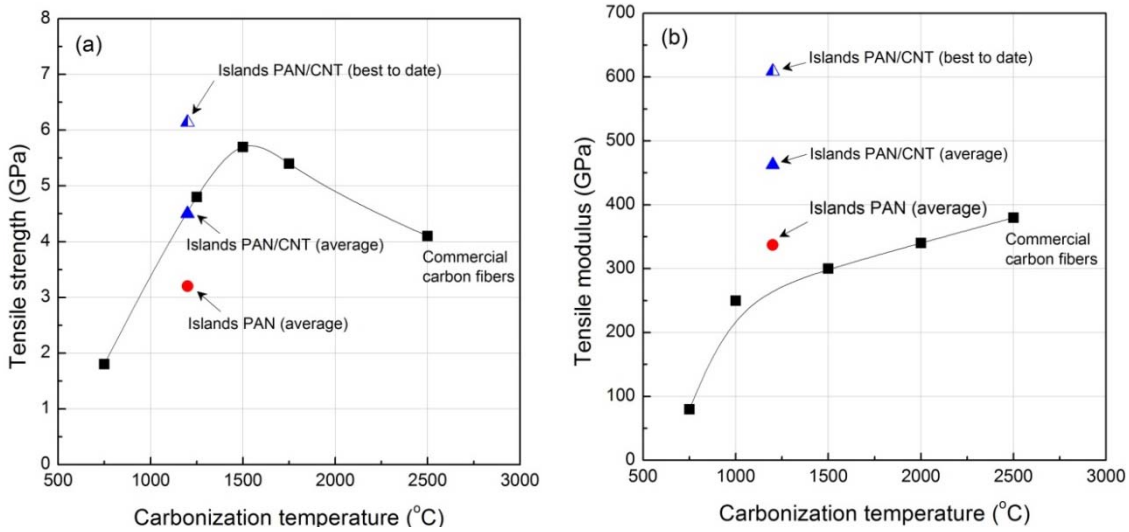


Figure 5.8 (a) Tensile strength and (b) tensile modulus of carbonized PAN and PAN/CNT fibers. Black square points represent the data from commercial carbon fibers for comparison.

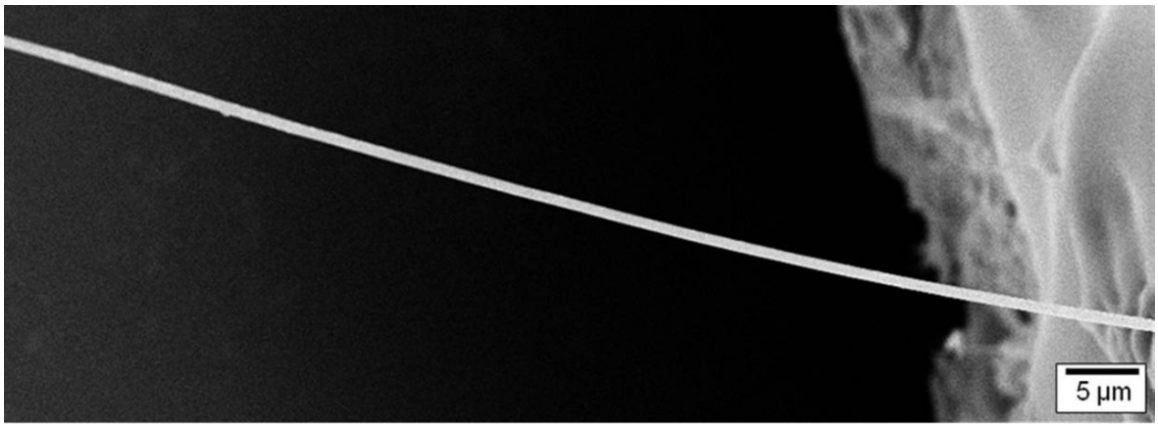


Figure 5.9 SEM micrographs of residual carbon fiber (from PAN/CNT (99/1)) on tensile test template.

### 5.3.2 Raman Spectroscopy of Carbonized Bi-Component Fibers

When carbonized at 1200 $^{o}$C, gel spun PAN does not develop a graphitic structure. However, when carbonized at this temperature and at the same stress, gel spun PAN/CNT containing 1 wt% CNTs show significant graphitic peak in the Raman spectra (Figure 5.10). It has previously been discussed that this graphitic peak is not due to the presence of CNT, but a result of PAN conversion to a graphitic structure in the presence of CNT. Therefore, we conclude that the increase in tensile strength of the PAN/CNT based carbon fiber over PAN based carbon fiber is a combined effect of reinforcement from CNT as well as due to the presence of graphitic layer surrounding CNT. The graphitic layer in PAN/CNT fiber at 1200 $^{o}$C is a result of carbon nanotubes ability to template polymer orientation and crystallization. Highly oriented PAN in the vicinity of carbon nanotube graphitizes at a relatively low temperature of 1200 $^{o}$C, where PAN is not normally know to develop a graphitic structure.

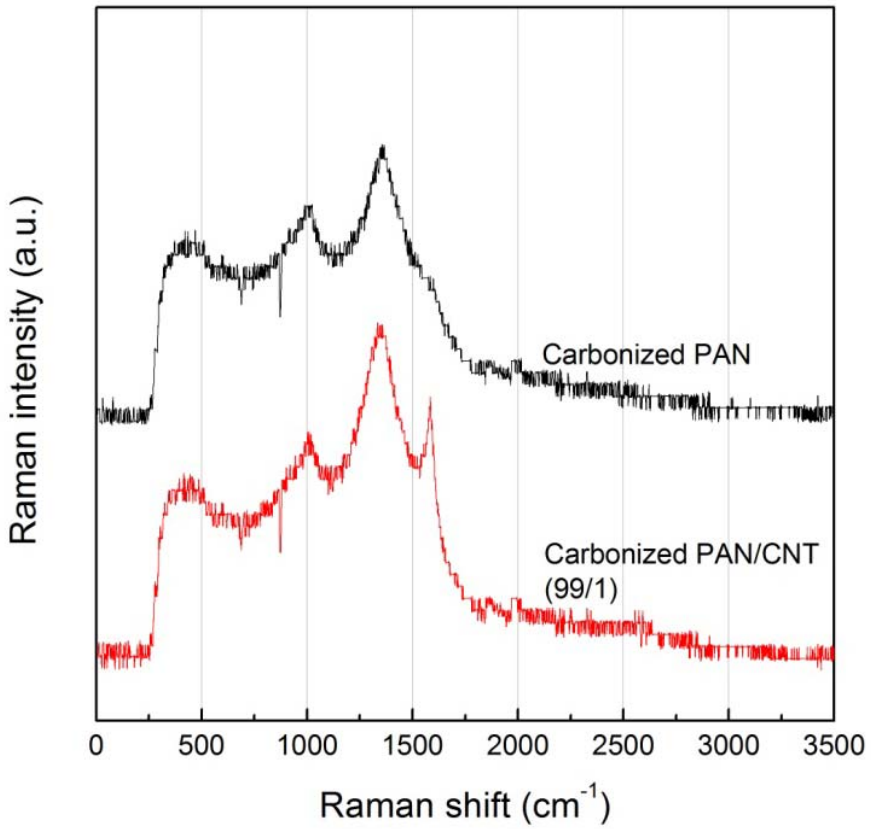


Figure 5.10 Raman spectra of carbonized islands PAN and PAN/CNT (99/1) fibers.

### 5.3.3 Structural and Morphological Studies of Carbonized Bi-Component Fibers

CNT containing carbon fiber has marginally higher orientation, smaller *d*-spacing, and larger crystal size along the fiber axis (Table 5.2 and Figure 5.11). Fracture surfaces of the PAN/CNT based carbon fiber show fibrils with 20 to 50 nm diameter (Figure 5.12). These fibrils represent PAN that has been graphitized around carbon nanotube. The fracture behavior of the small diameter gel spun PAN is typical of the PAN based carbon fibers (Figure 5.13). Additional SEM micrographs of carbonized bi-component fibers are also given in Appendix E.

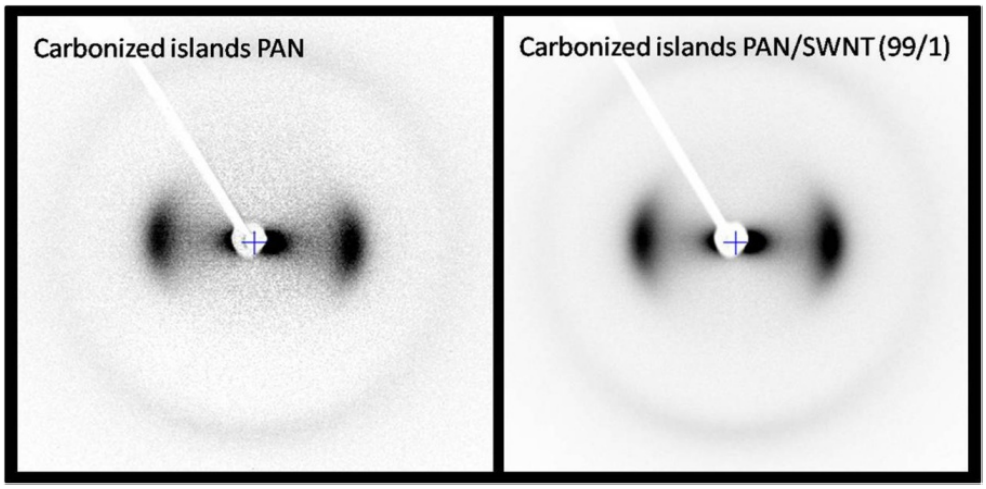


Figure 5.11 WAXD 2D patterns of carbonized islands PAN and PAN/CNT (99/1) fibers.

Table 5.2 Structural papameters of carbonized islands fibers.

| | Carbonized islands PAN | Carbonized islands PAN/SWNT (99/1) |
|---|---|---|
| $f_{002}$ | 0.73 | 0.74 |
| $Z^a$ (degree) | 37.3 | 37.2 |
| $d$-spacing$_{(002)}$ (nm) | 0.357 | 0.356 |
| $L_{(002)}{}^b$ (nm) | 1.3 | 1.3 |
| $L_{(10)}{}^c$ (nm) | 1.8 | 2.1 |

a Full width at half maximum from azimuthal scans of (002) plane
b Crystal size from equatorial scan
c Crystal size from meridional scan

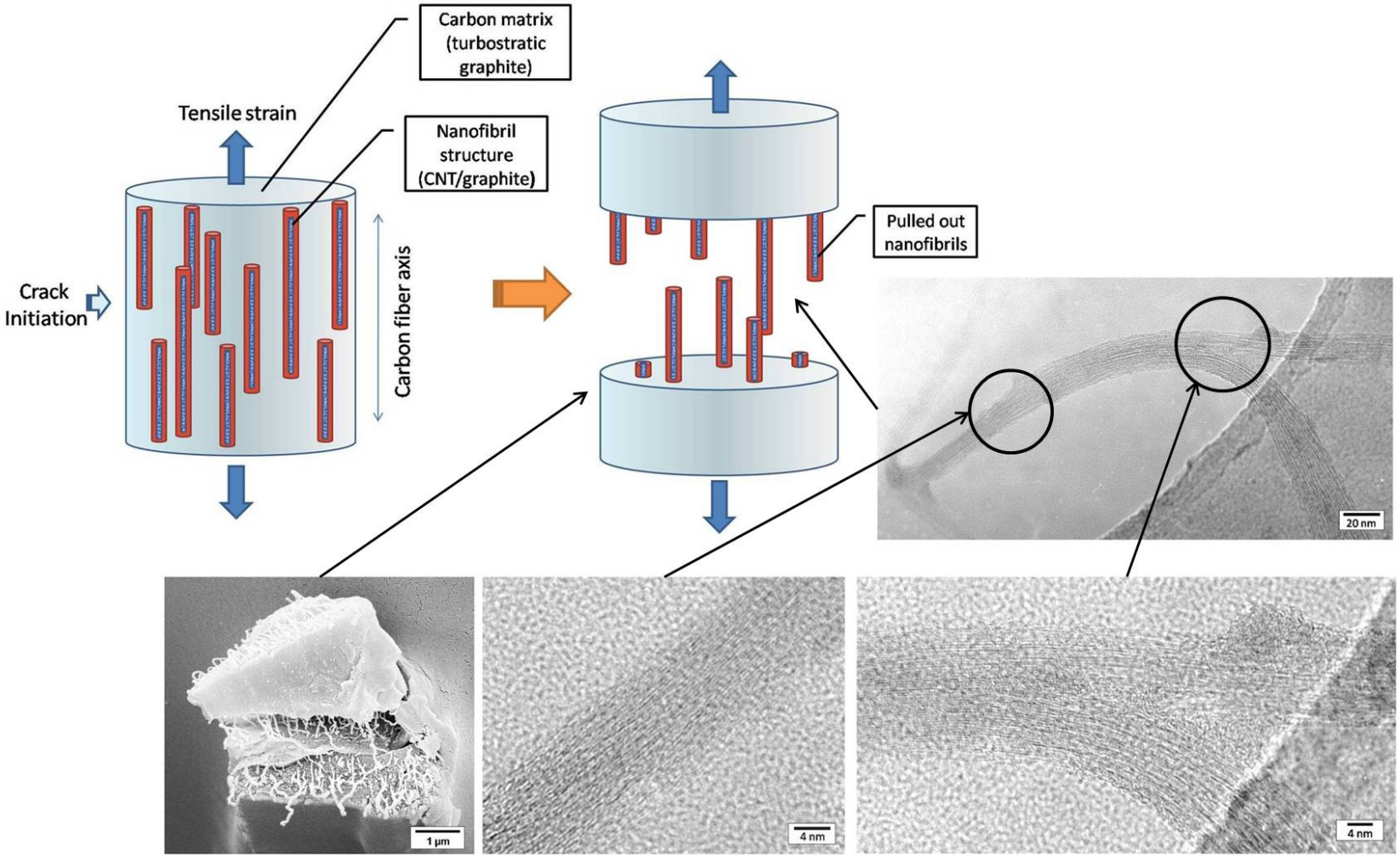


Figure 5.12 The schematics of fracture behavior of carbonized PAN/CNT, and SEM and TEM micrographs of carbonized islands PAN/CNT fibers.

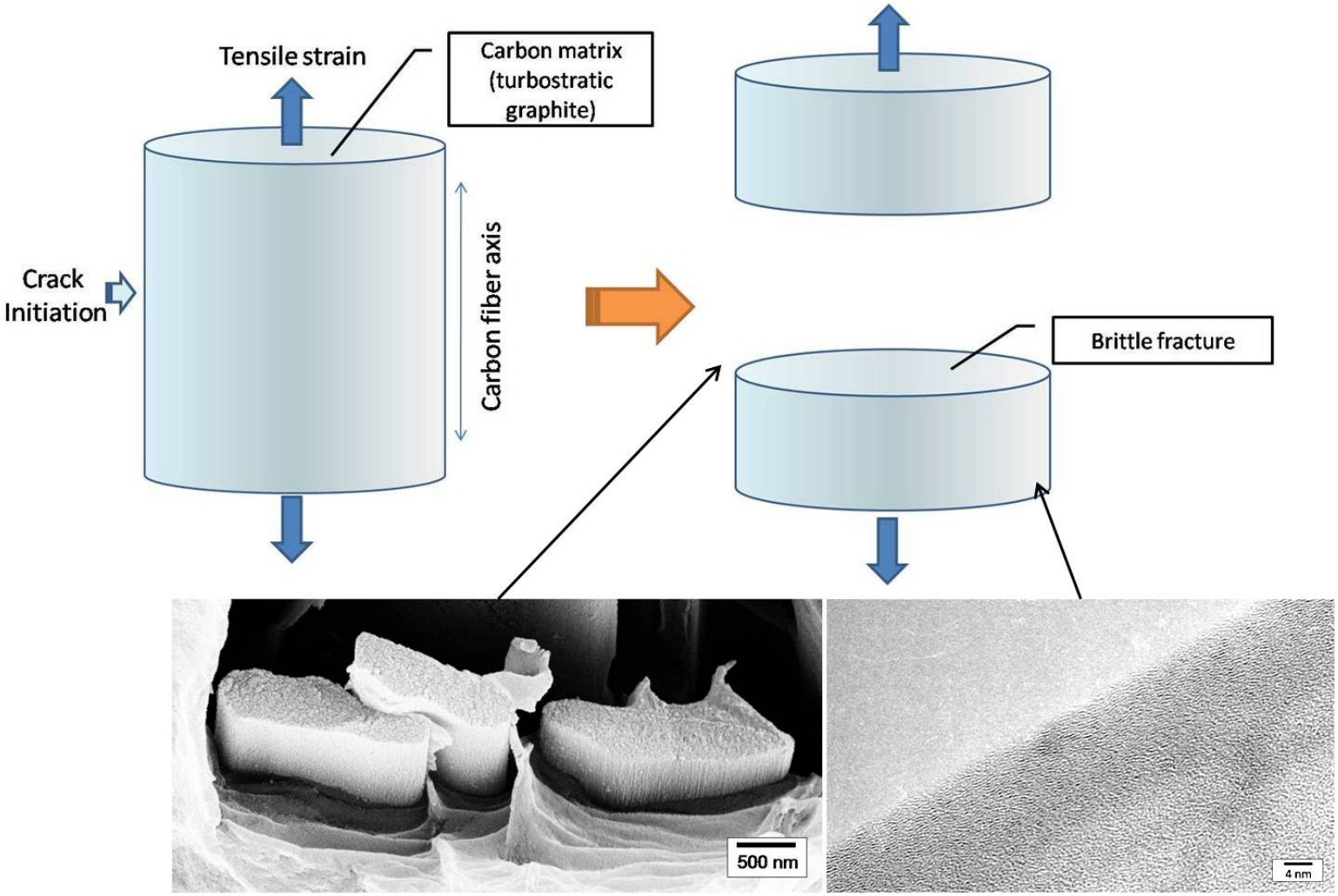


Figure 5.13 The schematics of fracture behavior of carbonized PAN, and SEM and TEM micrographs of carbonized islands PAN fibers.

## 5.4 Conclusions

Small diameter continuous PAN/CNT precursor fibers are processed by bi-component and gel spinning. The subsequent stabilization and carbonization result in carbon fibers whose diameters were about 1 μm. CNT containing precursor fiber produced the carbon fiber with the tensile strength of 2.5 N/tex (4.5 GPa) and tensile modulus of 257 N/tex (463 GPa). The best tensile strength obtained to date was 3.4 N/tex (6.14 GPa) for CNT containing carbon fiber.

# CHAPTER 6

# CONCLUSIONS AND RECOMMENDATIONS

## 6.1 Conclusions

The reinforcement efficiencies of various types of CNTs was investigated by correlating the physical properties with interfacial area between PAN matrix and CNT, and CNT length. Due to the larger interfacial area, the effect of SWNT was the most in improving the low strain properties such as modulus and shrinkage. The enhancement in high strain properties such as tensile strength and work of rupture by MWNT was attributed to the longer length of MWNT. The increased polymer orientation and crystal size point to the potential of PAN/CNT composite as the precursor for next generation carbon fiber. Achieving ultrahigh nanotube orientation (orientation factor above 0.98) is critical for obtaining high modulus composite fibers containing MWNTs or large diameter SWNT bundles.

In order to obtain high orientation of both PAN matrix and CNT, gel spinning was conducted on PAN/SWNT solution. Although the orientation factor of PAN and SWNT was 0.93 and 0.92, which is not as high to obtain ultimate reinforcement based on the simple rule of mixtures, the mechanical properties exhibited that the composite fiber behaved like almost ideally reinforced fiber. The structural and morphological analysis revealed the well ordered PAN crystal in the vicinity of SWNT, while the farther region from SWNT showed relatively less ordered structure. Therefore, one can conclude that the incorporation of SWNT not only reinforce the PAN matrix but also modify the PAN matrix order such as crystallinity, crystal size, and orientation.

The gel spun fibers were stabilized and carbonized to obtain carbon fiber. DSC and FT-IR results showed that the SWNT incorporation affects the PAN reactivity, resulting in different chemical structure as compared to the control PAN fiber. The HRTEM and Raman spectroscopy evidenced the graphitic structure formation in the vicinity of SWNT, which was shown as the highly ordered region in gel spinning results. The tensile properties of the carbonized PAN/SWNT are at least 50% higher than those of the carbonized control PAN fiber. In addition, the analysis of SWNT reinforcement in carbon fiber showed that the modulus from just 1 wt% SWNT was almost 150 GPa. This indicates indeed the change of PAN matrix and resulting graphitic structure formation by addition of SWNT.

Bi-component spinning reduced the effective precursor fiber diameter by 5-10 times. The resulting carbon fiber exhibited higher tensile strength than that of general gel spun fibers, which is strongly dependent on the defect of fiber such as micro-voids, foreign particles, and entanglement. The analysis showed that the further reduction in fiber diameter will enhance the tensile strength as high as 7 GPa at about 100 nm fiber diameter. However, this can be obtained without any processing optimization such as spinning condition, co-polymer content, the type of co-monomer, stabilization temperature, time, tension during stabilization and carbonization, and carbonization temperature. Therefore, further optimization of bi-component gel spun PAN fibers combined with the addition of CNT will lead to the next generation carbon fiber.

## 6.3 Recommendations

1. For fiber spinning, rheological properties of poymer/CNT solution play an important role. The preliminary experimental data on the rheological properties of PAN/CNT (5 wt%)/DMAc solutions prepared in Chapter 2 are given in Appendix A. The viscosity values of composite solution containing 5 wt% SWNT and MWNT at low shear rate are higher than that for the control PAN solution. PAN/MWNT and PAN/SWNT solution behaves similar to Bingham body at low shear rate region, suggesting that there is strong network structure. On the other hand, the viscosity values at high shear rate are slightly lower than that of the control PAN solution. This indicates that the shear induces alignment of PAN molecules along with CNT alignment. We expect that further investigation of the rheological properties of PAN/CNT solution will lead to a better understanding of PAN-CNT molecular interaction and aid in developing better processing conditions for fiber spinning.

2. Gelation and crystallization conditions are important to produce a fiber with optimum structure and minimum defects. Although the gel drawn fiber has good properties (Chapter 3), the processing conditions have not been optimized. Fiber properties as a function of gelation time are shown in Appendix B. These results are limited to a particular solid concentration and gelation temperature. Property optimization will include effect of polymer concentration, spinning temperature, gelation temperature and time, and drawing temperature.

3. In Chapter 3, dynamic mechanical analysis showed that the difference between storage moduli of PAN and PAN/SWNT fibers exhibit significant temperature dependence. The detailed dynamic mechanical property data for the experiments reported in Chapter 3, are given in Appendix C. Further analysis of these results is needed.

4. Appendix D shows some of the DSC results for indentifying the stabilization conditions of PAN and PAN/CNT composite fibers. The stabilization process is very important for determining the resulting carbon fiber properties. Over-stabilization or under-stabilization should be strictly avoided. Determination of optimum stabilization conditions will be critical for producing the next generation carbon fiber.

5. Small diameter fibers obtained in Chapter 5 exhibited large fiber diameter distribution (1 - 3 μm). For practical applications, this diameter distribution must be narrowed to a much smaller range. For this purpose, spinning conditions need further investigation.

# APPENDIX A

# RHEOLOGICAL PROPERTIES OF PAN/CNT SOLUTIONS

PAN/CNT/DMAc solutions containing 5 wt% SWNT and MWNT were prepared as described in Chapter 2. For viscosity measurement, ARES (advanced rheometric expansion system, TA Instruments Co.) was used with parallel plate geometry (25 mm diameter). The gap between plates was set to be 1 mm.

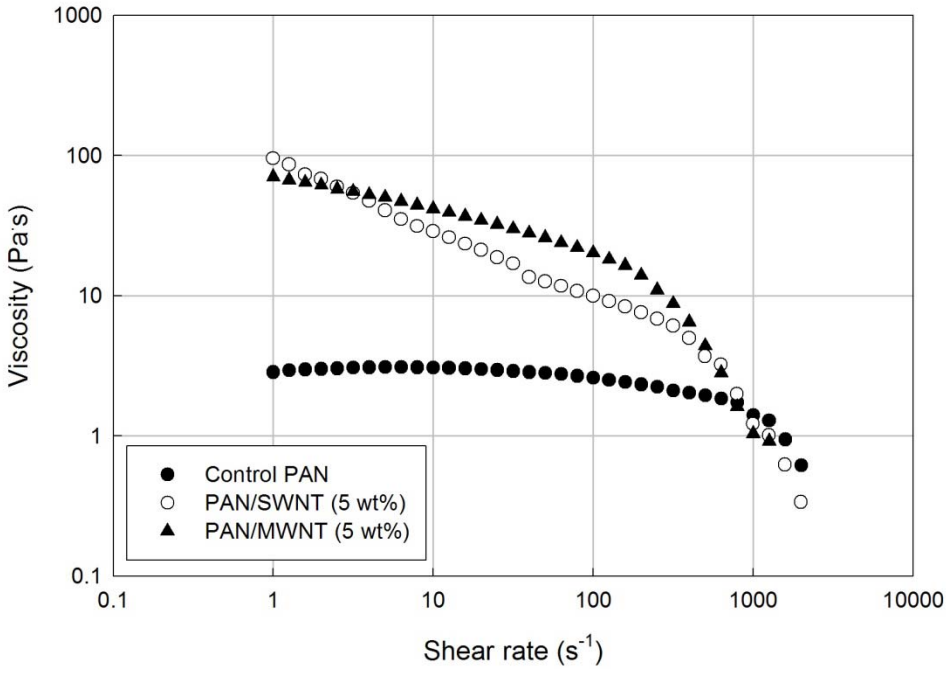


Figure A.1 Steady shear viscosity of PAN, PAN/SWNT, and PAN/MWNT solutions as a function of shear rate. Viscosity was determined at room temperature.

# APPENDIX B

# MECHANICAL PROPERTIES OF GEL SPUN PAN/SWNT FIBERS AS A FUNCTION OF GELATION TIME

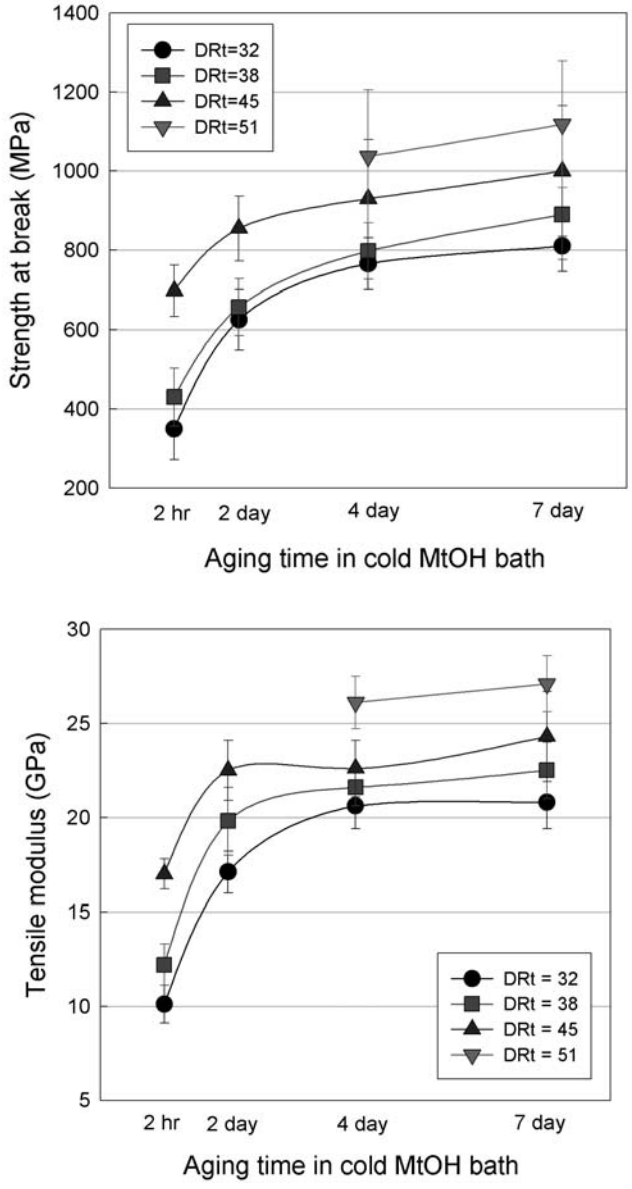


Figure B.1 Tensile strength and modulus of PAN/SWNT (1 wt%) fibers as a function of gelation time and draw ratio.

# APPENDIX C

# DYNAMIC MECHANICAL PROPERTIES OF GEL SPUN PAN AND PAN/SWNT FIBERS - TEMPERATURE DEPENDENCE OF INTERPHASE INTERACTION

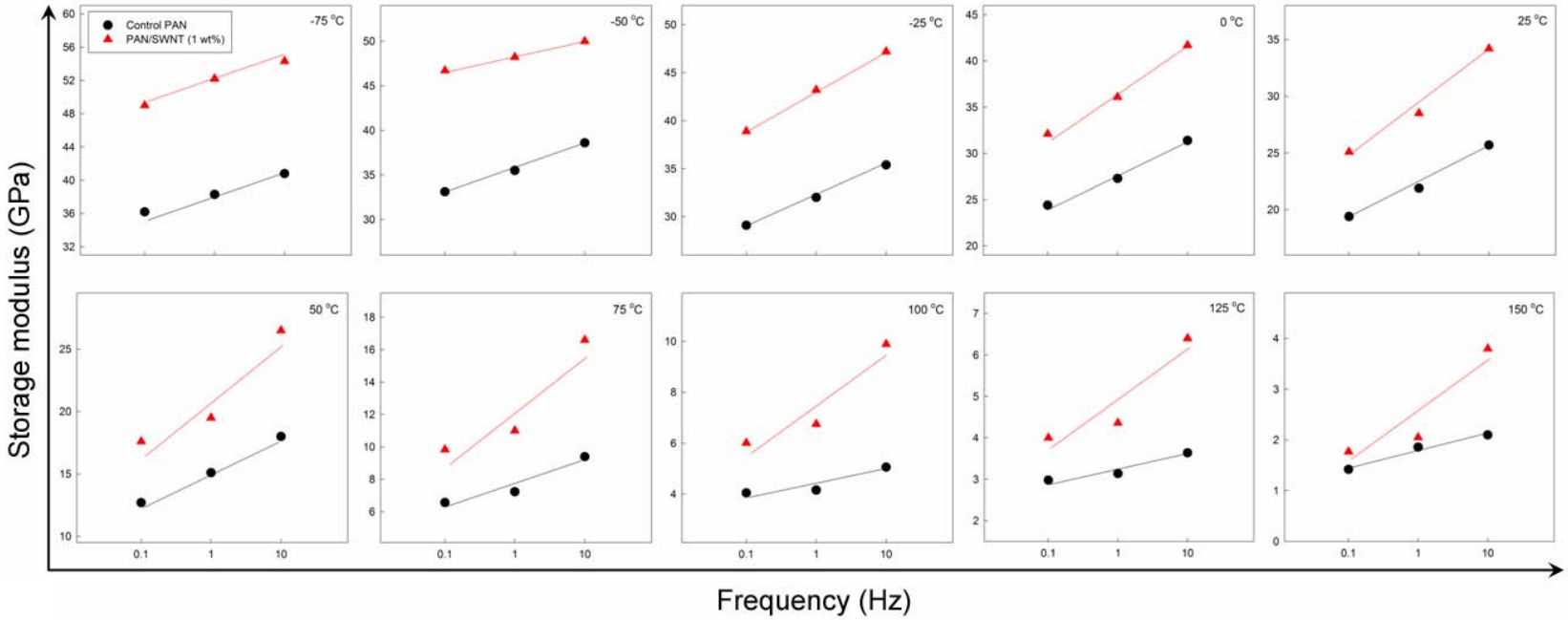


Figure C.1 Storage modulus of gel spun PAN and PAN/SWNT (1 wt%) fibers as a function of frequency at various temperatures.

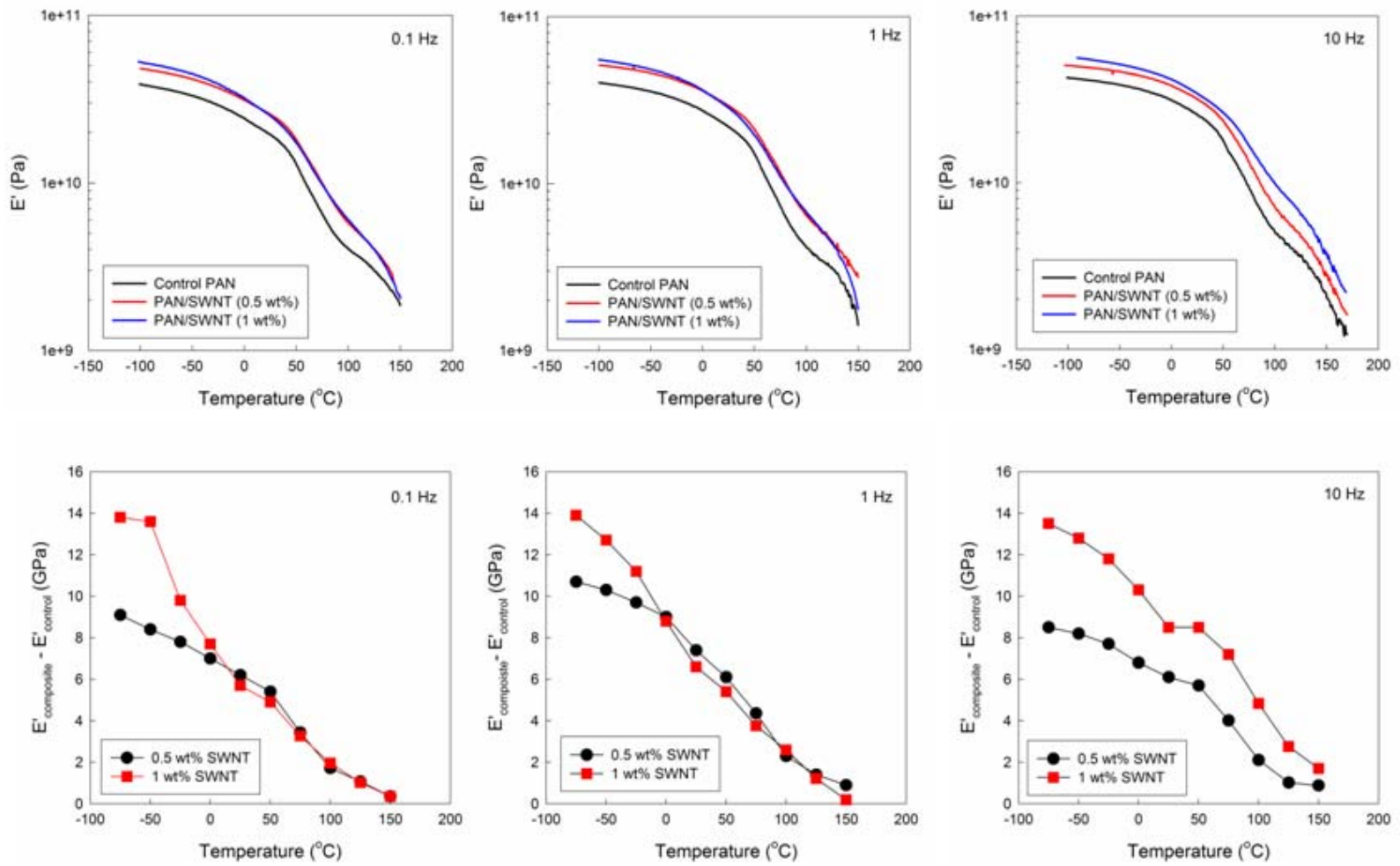


Figure C.2 Storage modulus of gel spun PAN and PAN/SWNT (0.5 wt% and 1 wt%) fibers as a function of temperature (upper column). Storage modulus difference between control PAN and composite fibers as a function of temperature, showing frequency dependence (lower column).

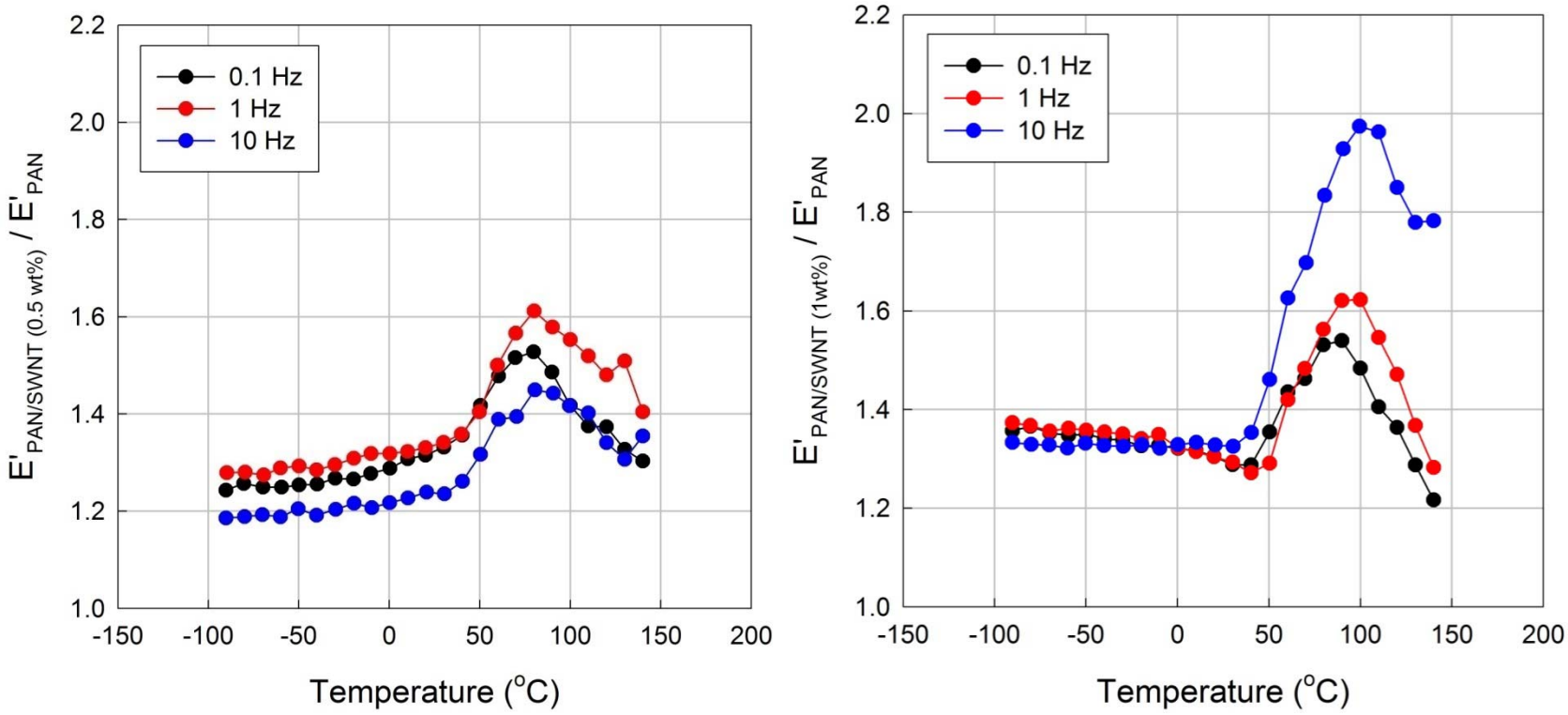


Figure C.3 Relative storage modulus of PAN/SWNT (0.5 wt%) fiber to control PAN fiber (left). The similar plots of PAN/SWNT (1 wt%) fiber to control PAN fiber (right). Both figures present the strong reinforcement around the glass transition temperature of PAN. The magnitude of reinforcement increases with increasing SWNT content.

# APPENDIX D

# DSC STUDIES OF PAN AND PAN/CNT FIBERS FOR STABILIZATION

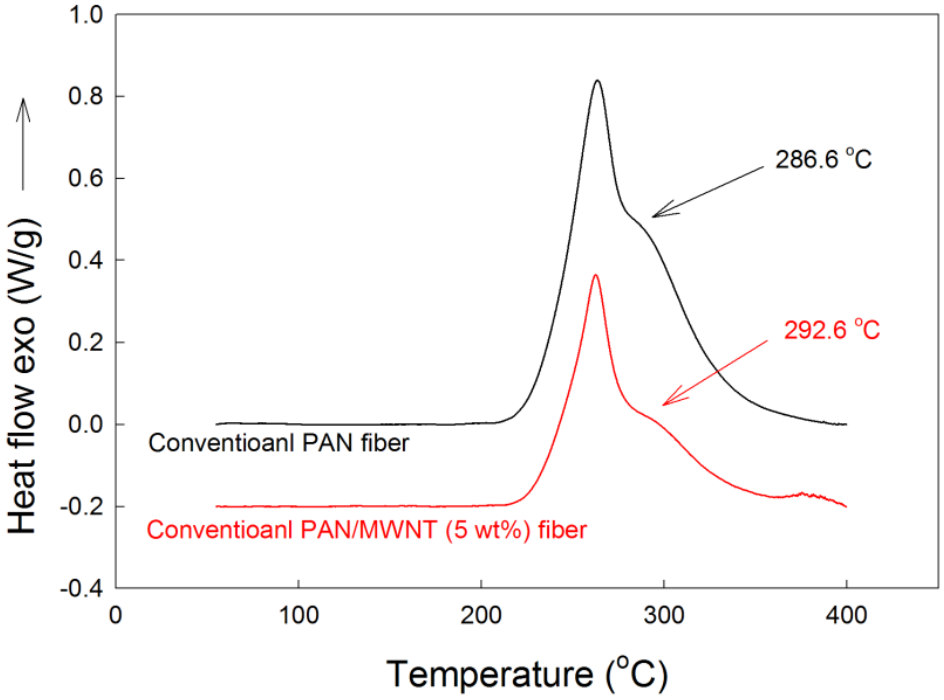


Figure D.1 DSC thermograms of PAN and PAN/MWNT (5 wt%) fibers spun by conventional solution spinning.

Table D.1 Analytical results of DSC thermograms in Figure D.1.

| | $T_{peak}$ (°C) | $\Delta H_{peak}$ (kJ/g) |
|---|---|---|
| PAN | 264 | 2.7 |
| PAN/MWNT (5 wt%) | 262 | 1.4 |

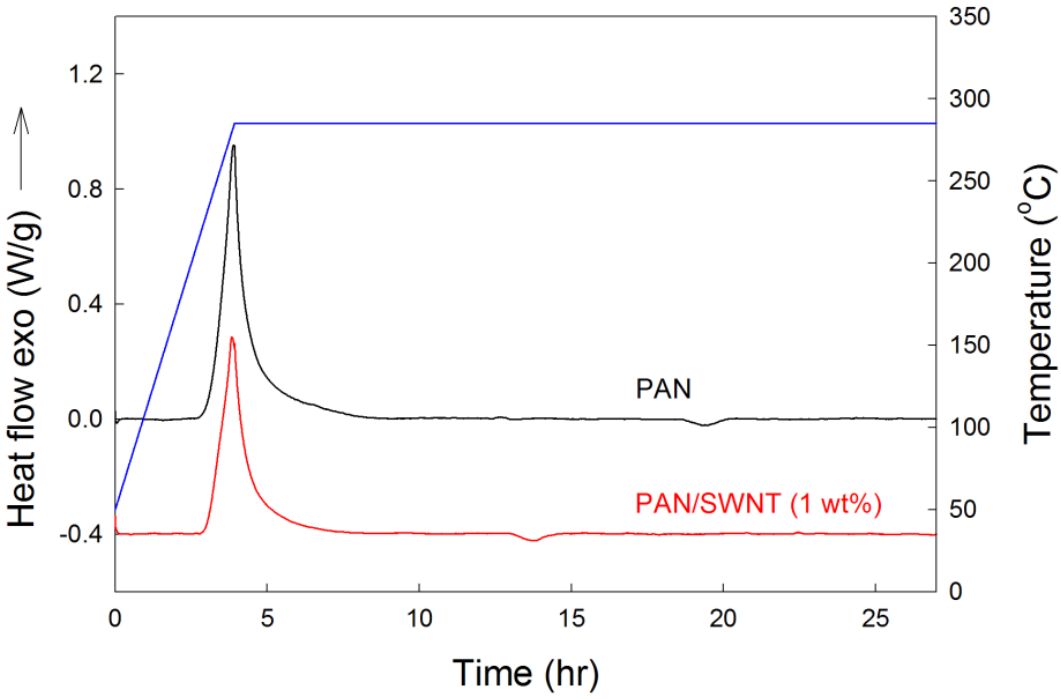


Figure D.2 Isothermal DSC thermograms of gel spun PAN and PAN/SWNT (1 wt%) fibers.

Table D.2 Analytical results of DSC thermograms in Figure D.2.

| | $T_{peak}$ (hr) | $\Delta H_{peak}$ (kJ/g) |
|---|---|---|
| PAN | 3.9 | 3.4 |
| PAN/SWNT (1 wt%) | 3.9 | 2.5 |

# APPENDIX E

# SEM MICROGRAPHS OF CARBONIZED BI-COMPONENT FIBERS

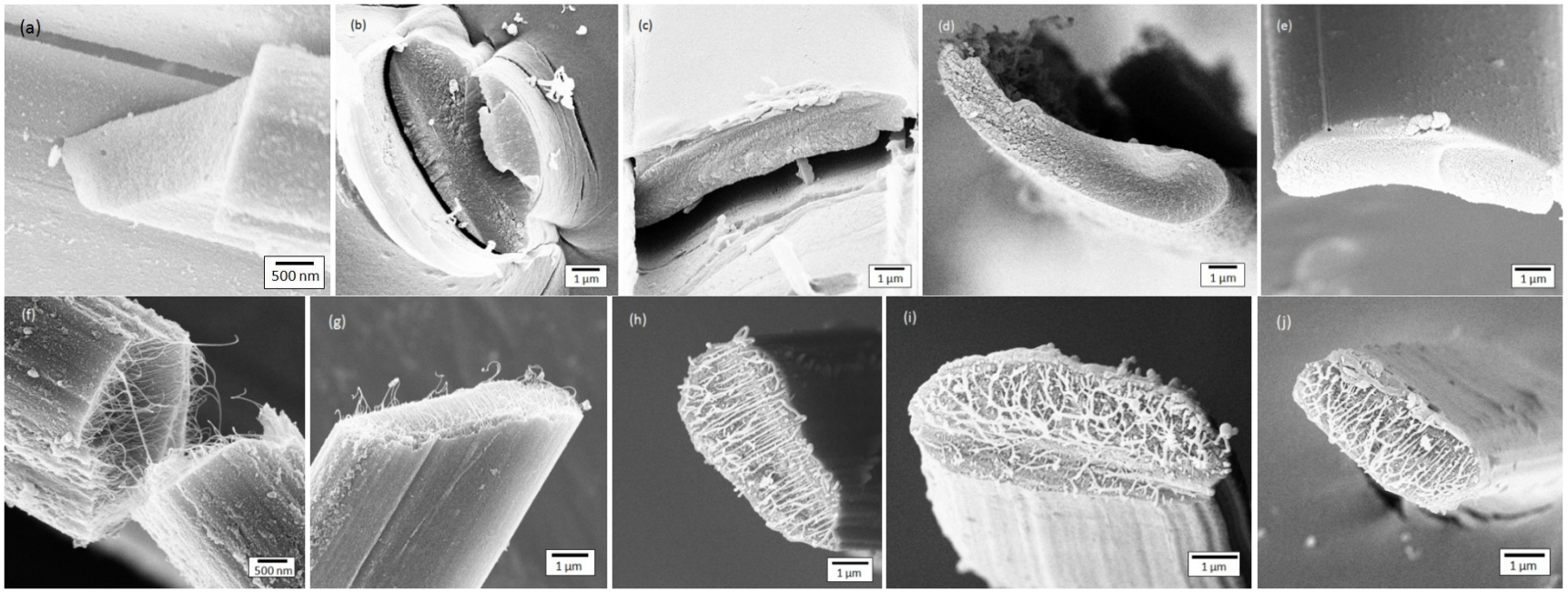


Figure E.1 SEM micrographs of carbonized core (a) - (e) PAN and (f) - (j) PAN/CNT (1 wt%) fibers.

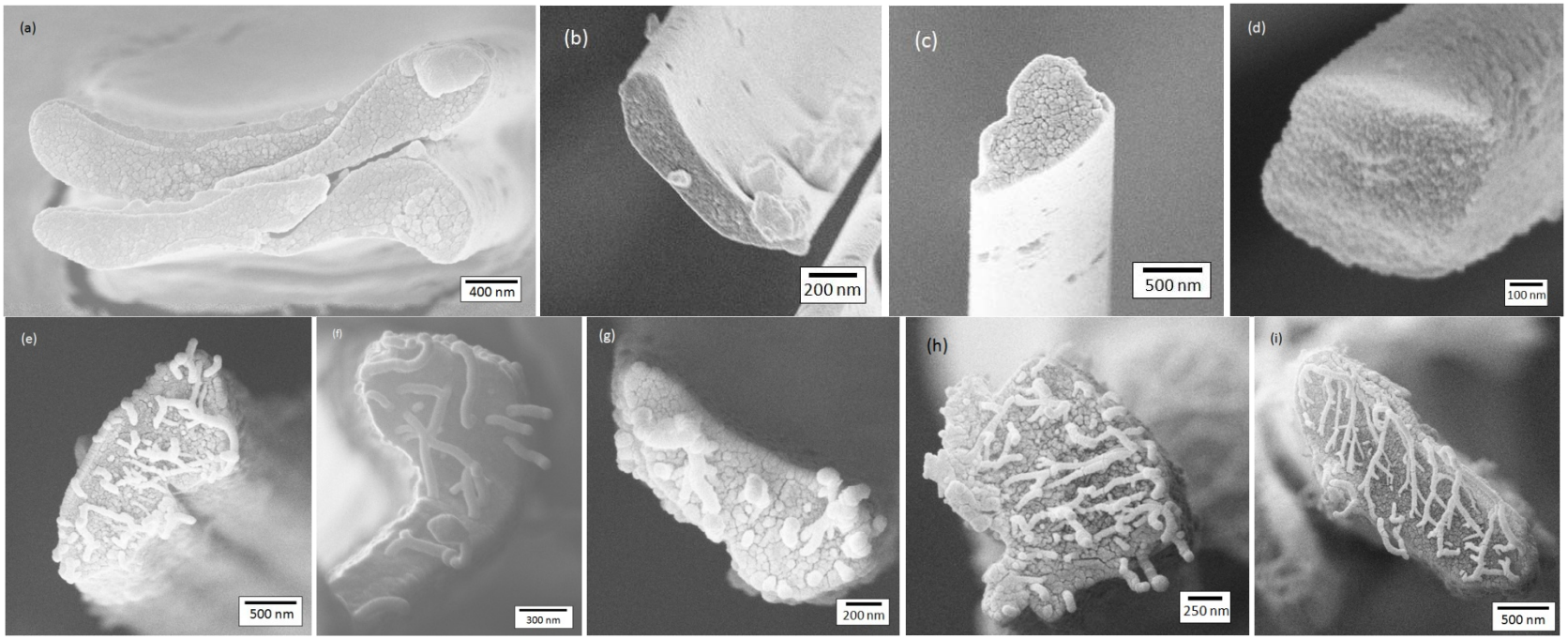


Figure E.2 SEM micrographs of carbonized islands (a) - (d) PAN and (e) - (i) PAN/CNT (1 wt%) fibers.

# REFERENCES


1. Edison, T. A. US patent 223898, 1880.

2. Kumar, S.; Gupta, V. B., Manufactured fibres for high performance, industrial and non-conventional applications. In *Manufactured Fibre Technology*, Gupta, V. B.; Kothari, V. K., Eds. Chapman & Hall: New York, 1997; pp 514-559.

3. Bajaj, P., Acrylic fibers. In *Manufactured Fibre Technology*, Gupta, V. B.; Kothari, V. K., Eds. Chapman & Hall: New York, 1997; p 406.

4. Gupta, A. K.; Paliwal, D. K.; Bajaj, P., Acrylic Precursors for Carbon-Fibers. *Journal of Macromolecular Science-Reviews in Macromolecular Chemistry and Physics* **1991,** C31, (1), 1-89.

5. Kratschmer, W.; Lamb, L. D.; Fostiropoulos, K.; Huffman, D. R., Solid C-60 - a New Form of Carbon. *Nature* **1990,** 347, (6291), 354-358.

6. Iijima, S., Helical Microtubules of Graphitic Carbon. *Nature* **1991,** 354, (6348), 56-58.

7. Iijima, S.; Ichihashi, T.; Ando, Y., Pentagons, Heptagons and Negative Curvature in Graphite Microtubule Growth. *Nature* **1992,** 356, (6372), 776-778.

8. Bethune, D. S.; Kiang, C. H.; Devries, M. S.; Gorman, G.; Savoy, R.; Vazquez, J.; Beyers, R., Cobalt-Catalyzed Growth of Carbon Nanotubes with Single-Atomic-Layerwalls. *Nature* **1993,** 363, (6430), 605-607.

9. Iijima, S.; Ichihashi, T., Single-Shell Carbon Nanotubes of 1-Nm Diameter. *Nature* **1993,** 363, (6430), 603-605.

10. Baughman, R. H.; Zakhidov, A. A.; de Heer, W. A., Carbon nanotubes - the route toward applications. *Science* **2002,** 297, (5582), 787-792.

11. Berber, S.; Kwon, Y. K.; Tomanek, D., Unusually high thermal conductivity of carbon nanotubes. *Physical Review Letters* **2000,** 84, (20), 4613-4616.

12. Harris, P. J., *Carbon Nanotubes and Related Structures*. Cambridge University Press: Cambridge, 1999.

13. Hone, J.; Whitney, M.; Zettl, A., Thermal conductivity of single-walled carbon nanotubes. *Synthetic Metals* **1999,** 103, (1-3), 2498-2499.

14. Krishnan, A.; Dujardin, E.; Ebbesen, T. W.; Yianilos, P. N.; Treacy, M. M. J., Young's modulus of single-walled nanotubes. *Physical Review B* **1998,** 58, (20), 14013-14019.

15. Saito, R.; Dresselhaus, G.; Dresselhaus, M. S., *Physical Properties of Carbon Nanotubes*. Imperial College Press: London, 1998.

16. Thess, A.; Lee, R.; Nikolaev, P.; Dai, H. J.; Petit, P.; Robert, J.; Xu, C. H.; Lee, Y. H.; Kim, S. G.; Rinzler, A. G.; Colbert, D. T.; Scuseria, G. E.; Tomanek, D.; Fischer, J. E.; Smalley, R. E., Crystalline ropes of metallic carbon nanotubes. *Science* **1996,** 273, (5274), 483-487.

17. Yu, M. F.; Files, B. S.; Arepalli, S.; Ruoff, R. S., Tensile loading of ropes of single wall carbon nanotubes and their mechanical properties. *Physical Review Letters* **2000,** 84, (24), 5552-5555.

18. http://www.seas.upenn.edu/mse/images/nanotube1.jpg

19. Ajayan, P. M.; Schadler, L. S.; Giannaris, C.; Rubio, A., Single-walled carbon nanotube-polymer composites: Strength and weakness. *Advanced Materials* **2000,** 12, (10), 750.

20. Belytschko, T.; Xiao, S. P.; Schatz, G. C.; Ruoff, R. S., Atomistic simulations of nanotube fracture. *Physical Review B* **2002,** 65, (23).

21. Li, F.; Cheng, H. M.; Bai, S.; Su, G.; Dresselhaus, M. S., Tensile strength of single-walled carbon nanotubes directly measured from their macroscopic ropes. *Applied Physics Letters* **2000,** 77, (20), 3161-3163.

22. Walters, D. A.; Ericson, L. M.; Casavant, M. J.; Liu, J.; Colbert, D. T.; Smith, K. A.; Smalley, R. E., Elastic strain of freely suspended single-wall carbon nanotube ropes. *Applied Physics Letters* **1999,** 74, (25), 3803-3805.

23. Yu, M. F.; Lourie, O.; Dyer, M. J.; Moloni, K.; Kelly, T. F.; Ruoff, R. S., Strength and breaking mechanism of multiwalled carbon nanotubes under tensile load. *Science* **2000,** 287, (5453), 637-640.

24. Dumitrica, T.; Hua, M.; Yakobson, B. I., Symmetry-, time-, and temperature-dependent strength of carbon nanotubes. *Proceedings of the National Academy of Sciences of the United States of America* **2006,** 103, (16), 6105-6109.

25. Gao, G. H.; Cagin, T.; Goddard, W. A., Energetics, structure, mechanical and vibrational properties of single-walled carbon nanotubes. *Nanotechnology* **1998,** 9, (3), 184-191.

26. Lu, J. P., Elastic properties of carbon nanotubes and nanoropes. *Physical Review Letters* **1997,** 79, (7), 1297-1300.

27. Popov, V. N.; Van Doren, V. E.; Balkanski, M., Elastic properties of crystals of single-walled carbon nanotubes. *Solid State Communications* **2000,** 114, (7), 395-399.

28. Salvetat, J. P.; Briggs, G. A. D.; Bonard, J. M.; Bacsa, R. R.; Kulik, A. J.; Stockli, T.; Burnham, N. A.; Forro, L., Elastic and shear moduli of single-walled carbon nanotube ropes. *Physical Review Letters* **1999,** 82, (5), 944-947.

29. Sinnott, S. B.; Shenderova, O. A.; White, C. T.; Brenner, D. W., Mechanical properties of nanotubule fibers and composites determined from theoretical calculations and simulations. *Carbon* **1998,** 36, (1-2), 1-9.

30. Li, Y. J.; Wang, K. L.; Wei, J. Q.; Gu, Z. Y.; Wang, Z. C.; Luo, J. B.; Wu, D. H., Tensile properties of long aligned double-walled carbon nanotube strands. *Carbon* **2005,** 43, (1), 31-35.

31. Johnson, W., The structure of PAN based carbon fibers and relationship to the physical properties. In *Handbook of composites. Strong fibers*, Watt, W.; Perov, B. V., Eds. Elsevier Science: New York, 1988; Vol. 1, p 393.

32. Liew, K. M.; He, X. Q.; Wong, C. H., On the study of elastic and plastic properties of multi-walled carbon nanotubes under axial tension using molecular dynamics simulation. *Acta Materialia* **2004,** 52, (9), 2521-2527.

33. Pan, Z. W.; Xie, S. S.; Lu, L.; Chang, B. H.; Sun, L. F.; Zhou, W. Y.; Wang, G.; Zhang, D. L., Tensile tests of ropes of very long aligned multiwall carbon nanotubes. *Applied Physics Letters* **1999,** 74, (21), 3152-3154.

34. Gaier, J. R.; Hambourger, P. D.; Slabe, M. E., Effect of Heat-Treatment Temperature of Vapor-Grown Graphite Fibers .1. Properties of Their Bromine Intercalation Compounds. *Synthetic Metals* **1989,** 31, (2), 229-240.

35. Gaier, J. R.; Slabe, M. E.; Stahl, M., Effect of Heat-Treatment Temperature of Vapor-Grown Graphite Fibers .2. Stability of Their Bromine Intercalation Compounds. *Synthetic Metals* **1989,** 31, (2), 241-249.

36. Subramoney, S., Novel nanocarbons - Structure, properties, and potential applications. *Advanced Materials* **1998,** 10, (15), 1157.

37. Uchida, T.; Anderson, D. P.; Minus, M. L.; Kumar, S., Morphology and modulus of vapor grown carbon nano fibers. *Journal of Materials Science* **2006,** 41, (18), 5851-5856.

38. Minus, M. L.; Kumar, S., The processing, properties, and structure of carbon fibers. *JOM* **2005,** 57, (2), 52-58.

39. Chae, H. G.; Kumar, S., Rigid-Rod Polymeric Fibers. *Journal of Applied Polymer Science* **2006,** 100, 791-802.

40. Toyobo; Inc., **(http://www.toyobo.co.jp/e/seihin/kc/pbo/menu)** (March/2005).

41. Honeywell; Inc., **(http://www.spectrafiber.com)** (March/2005).

42. Dupont; Inc., **(http://www.dupont.com/kevlar)** (March/2005).

43. Kim, P.; Shi, L.; Majumdar, A.; McEuen, P. L., Thermal transport measurements of individual multiwalled nanotubes. *Physical Review Letters* **2001,** 87, (21), Art. No. 215502.

44. Zhang, W.; Zhu, Z. Y.; Wang, F.; Wang, T. T.; Sun, L. T.; Wang, Z. X., Chirality dependence of the thermal conductivity of carbon nanotubes. *Nanotechnology* **2004,** 15, (8), 936-939.

45. Hone, J.; Batlogg, B.; Benes, Z.; Johnson, A. T.; Fischer, J. E., Quantized phonon spectrum of single-wall carbon nanotubes. *Science* **2000,** 289, (5485), 1730-1733.

46. Ericson, L. M.; Fan, H.; Peng, H. Q.; Davis, V. A.; Zhou, W.; Sulpizio, J.; Wang, Y. H.; Booker, R.; Vavro, J.; Guthy, C.; Parra-Vasquez, A. N. G.; Kim, M. J.; Ramesh, S.; Saini, R. K.; Kittrell, C.; Lavin, G.; Schmidt, H.; Adams, W. W.; Billups, W. E.; Pasquali, M.; Hwang, W. F.; Hauge, R. H.; Fischer, J. E.; Smalley, R. E., Macroscopic, neat, single-walled carbon nanotube fibers. *Science* **2004,** 305, (5689), 1447-1450.

47. Sreekumar, T. V.; Liu, T.; Min, B. G.; Guo, H.; Kumar, S.; Hauge, R. H.; Smalley, R. E., Polyacrylonitrile single-walled carbon nanotube composite fibers. *Advanced Materials* **2004,** 16, (1), 58-61.

48. Celzard, A.; McRae, E.; Deleuze, C.; Dufort, M.; Furdin, G.; Mareche, J. F., Critical concentration in percolating systems containing a high-aspect-ratio filler. *Physical Review B* **1996,** 53, (10), 6209-6214.

49. Munsonmcgee, S. H., ESTIMATION OF THE CRITICAL CONCENTRATION IN AN ANISOTROPIC PERCOLATION NETWORK. *Physical Review B* **1991,** 43, (4), 3331-3336.

50. Anglaret, E.; Righi, A.; Sauvajol, J. L.; Bernier, P.; Vigolo, B.; Poulin, P., Raman resonance and orientational order in fibers of single-wall carbon nanotubes. *Physical Review B* **2002,** 65, (16), 165426.

51. Bhattacharyya, A. R.; Sreekumar, T. V.; Liu, T.; Kumar, S.; Ericson, L. M.; Hauge, R. H.; Smalley, R. E., Crystallization and orientation studies in polypropylene/single wall carbon nanotube composite. *Polymer* **2003,** 44, (8), 2373-2377.

52. Liu, T.; Kumar, S., Quantitative characterization of SWNT orientation by polarized Raman spectroscopy. *Chemical Physics Letters* **2003,** 378, (3-4), 257-262.

53. Ichida, M.; Mizuno, S.; Kataura, H.; Achiba, Y.; Nakamura, A., Anisotropic optical properties of mechanically aligned single-walled carbon nanotubes in polymer. *Applied Physics a-Materials Science & Processing* **2004,** 78, (8), 1117-1120.

54. Monthioux, M.; Smith, B. W.; Burteaux, B.; Claye, A.; Fischer, J. E.; Luzzi, D. E., Sensitivity of single-wall carbon nanotubes to chemical processing: an electron microscopy investigation. *Carbon* **2001,** 39, (8), 1251-1272.

55. Girifalco, L. A.; Hodak, M.; Lee, R. S., Carbon nanotubes, buckyballs, ropes, and a universal graphitic potential. *Physical Review B* **2000,** 62, (19), 13104-13110.

56. An, K. H.; Jeong, S. Y.; Hwang, H. R.; Lee, Y. H., Enhanced sensitivity of a gas sensor incorporating single-walled carbon nanotube-polypyrrole nanocomposites. *Advanced Materials* **2004,** 16, (12), 1005.

57. Ausman, K. D.; Piner, R.; Lourie, O.; Ruoff, R. S.; Korobov, M., Organic solvent dispersions of single-walled carbon nanotubes: Toward solutions of pristine nanotubes. *Journal of Physical Chemistry B* **2000,** 104, (38), 8911-8915.

58. Baek, J. B.; Lyons, C. B.; Tan, L. S., Grafting of vapor-grown carbon nanofibers via in-situ polycondensation of 3-phenoxybenzoic acid in poly(phosphoric acid). *Macromolecules* **2004,** 37, (22), 8278-8285.

59. Bahr, J. L.; Mickelson, E. T.; Bronikowski, M. J.; Smalley, R. E.; Tour, J. M., Dissolution of small diameter single-wall carbon nanotubes in organic solvents? *Chemical communications* **2001**, (2), 193-194.

60. Bahr, J. L.; Tour, J. M., Highly functionalized carbon nanotubes using in situ generated diazonium compounds. *Chemistry of Materials* **2001,** 13, (11), 3823-3824.

61. Bahr, J. L.; Yang, J. P.; Kosynkin, D. V.; Bronikowski, M. J.; Smalley, R. E.; Tour, J. M., Functionalization of carbon nanotubes by electrochemical reduction of aryl diazonium salts: A bucky paper electrode. *Journal of the American Chemical Society* **2001,** 123, (27), 6536-6542.

62. Boul, P. J.; Liu, J.; Mickelson, E. T.; Huffman, C. B.; Ericson, L. M.; Chiang, I. W.; Smith, K. A.; Colbert, D. T.; Hauge, R. H.; Margrave, J. L.; Smalley, R. E., Reversible sidewall functionalization of buckytubes. *Chemical Physics Letters* **1999,** 310, (3-4), 367-372.

63. Bower, C.; Kleinhammes, A.; Wu, Y.; Zhou, O., Intercalation and partial exfoliation of single-walled carbon nanotubes by nitric acid. *Chemical Physics Letters* **1998,** 288, (2-4), 481-486.

64. Chen, G. Z.; Shaffer, M. S. P.; Coleby, D.; Dixon, G.; Zhou, W. Z.; Fray, D. J.; Windle, A. H., Carbon nanotube and polypyrrole composites: Coating and doping. *Advanced Materials* **2000,** 12, (7), 522-526.

65. Chen, J.; Hamon, M. A.; Hu, H.; Chen, Y. S.; Rao, A. M.; Eklund, P. C.; Haddon, R. C., Solution properties of single-walled carbon nanotubes. *Science* **1998,** 282, (5386), 95-98.

66. Chen, J.; Rao, A. M.; Lyuksyutov, S.; Itkis, M. E.; Hamon, M. A.; Hu, H.; Cohn, R. W.; Eklund, P. C.; Colbert, D. T.; Smalley, R. E.; Haddon, R. C., Dissolution of full-length single-walled carbon nanotubes. *Journal of Physical Chemistry B* **2001,** 105, (13), 2525-2528.

67. Chou, S. G.; Ribeiro, H. B.; Barros, E. B.; Santos, A. P.; Nezich, D.; Samsonidze, G. G.; Fantini, C.; Pimenta, M. A.; Jorio, A.; Plentz, F.; Dresselhaus, M. S.; Dresselhaus, G.; Saito, R.; Zheng, M.; Onoa, G. B.; Semke, E. D.; Swan, A. K.; Unlu, M. S.; Goldberg, B. B., Optical characterization of DNA-wrapped carbon nanotube hybrids. *Chemical Physics Letters* **2004,** 397, (4-6), 296-301.

68. Duesberg, G. S.; Muster, J.; Krstic, V.; Burghard, M.; Roth, S., Chromatographic size separation of single-wall carbon nanotubes. *Applied Physics a-Materials Science & Processing* **1998,** 67, (1), 117-119.

69. Gao, J. B.; Itkis, M. E.; Yu, A. P.; Bekyarova, E.; Zhao, B.; Haddon, R. C., Continuous spinning of a single-walled carbon nanotube-nylon composite fiber. *Journal Of The American Chemical Society* **2005,** 127, (11), 3847-3854.

70. Hamon, M. A.; Chen, J.; Hu, H.; Chen, Y. S.; Itkis, M. E.; Rao, A. M.; Eklund, P. C.; Haddon, R. C., Dissolution of single-walled carbon nanotubes. *Advanced Materials* **1999,** 11, (10), 834.

71. Hamon, M. A.; Hui, H.; Bhowmik, P.; Itkis, H. M. E.; Haddon, R. C., Ester-functionalized soluble single-walled carbon nanotubes. *Applied Physics a-Materials Science & Processing* **2002,** 74, (3), 333-338.

72. Hill, D. E.; Lin, Y.; Rao, A. M.; Allard, L. F.; Sun, Y. P., Functionalization of carbon nanotubes with polystyrene. *Macromolecules* **2002,** 35, (25), 9466-9471.

73. Huang, J. E.; Li, X. H.; Xu, J. C.; Li, H. L., Well-dispersed single-walled carbon nanotube/polyaniline composite films. *Carbon* **2003,** 41, (14), 2731-2736.

74. Islam, M. F.; Rojas, E.; Bergey, D. M.; Johnson, A. T.; Yodh, A. G., High weight fraction surfactant solubilization of single-wall carbon nanotubes in water. *Nano Letters* **2003,** 3, (2), 269-273.

75. Jang, Y. T.; Moon, S. I.; Ahn, J. H.; Lee, Y. H.; Ju, B. K., A simple approach in fabricating chemical sensor using laterally grown multi-walled carbon nanotubes. *Sensors and Actuators B-Chemical* **2004,** 99, (1), 118-122.

76. Jin, W. J.; Sun, X. F.; Wang, Y., Solubilization and functionalization of carbon nanotubes. *New Carbon Materials* **2004,** 19, (4), 312-318.

77. Jin, Z. X.; Huang, L.; Goh, S. H.; Xu, G. Q.; Ji, W., Characterization and nonlinear optical properties of a poly(acrylic acid)-surfactant-multi-walled carbon nanotube complex. *Chemical Physics Letters* **2000,** 332, (5-6), 461-466.

78. Jouguelet, E.; Mathis, C.; Petit, P., Controlling the electronic properties of single-wall carbon nanotubes by chemical doping. *Chemical Physics Letters* **2000,** 318, (6), 561-564.

79. Kim, H. J.; Jeon, K. K.; An, K. H.; Kim, C.; Heo, J. G.; Lim, S. C.; Bae, D. J.; Lee, Y. H., Exfoliation of single-walled carbon nanotubes by electrochemical treatment in a nitric acid. *Advanced Materials* **2003,** 15, (20), 1757-1760.

80. Kong, J.; Franklin, N. R.; Zhou, C. W.; Chapline, M. G.; Peng, S.; Cho, K. J.; Dai, H. J., Nanotube molecular wires as chemical sensors. *Science* **2000,** 287, (5453), 622-625.

81. Kumar, S.; Dang, T. D.; Arnold, F. E.; Bhattacharyya, A. R.; Min, B. G.; Zhang, X. F.; Vaia, R. A.; Park, C.; Adams, W. W.; Hauge, R. H.; Smalley, R. E.; Ramesh, S.; Willis, P. A., Synthesis, structure, and properties of PBO/SWNT composites. *Macromolecules* **2002,** 35, (24), 9039-9043.

82. Lee, G. W.; Kumar, S., Dispersion of nitric acid-treated SWNTs in organic solvents and solvent mixtures. *Journal of Physical Chemistry B* **2005,** 109, (36), 17128-17133.

83. Lin, Y.; Rao, A. M.; Sadanadan, B.; Kenik, E. A.; Sun, Y. P., Functionalizing multiple-walled carbon nanotubes with aminopolymers. *Journal of Physical Chemistry B* **2002,** 106, (6), 1294-1298.

84. Liu, J.; Casavant, M. J.; Cox, M.; Walters, D. A.; Boul, P.; Lu, W.; Rimberg, A. J.; Smith, K. A.; Colbert, D. T.; Smalley, R. E., Controlled deposition of

individual single-walled carbon nanotubes on chemically functionalized templates. *Chemical Physics Letters* **1999,** 303, (1-2), 125-129.

85. Liu, J.; Liu, T.; Kumar, S., Effect of solvent solubility parameter on SWNT dispersion in PMMA. *Polymer* **2005,** 46, (10), 3419-3424.

86. Mickelson, E. T.; Chiang, I. W.; Zimmerman, J. L.; Boul, P. J.; Lozano, J.; Liu, J.; Smalley, R. E.; Hauge, R. H.; Margrave, J. L., Solvation of fluorinated single-wall carbon nanotubes in alcohol solvents. *Journal of Physical Chemistry B* **1999,** 103, (21), 4318-4322.

87. Mickelson, E. T.; Huffman, C. B.; Rinzler, A. G.; Smalley, R. E.; Hauge, R. H.; Margrave, J. L., Fluorination of single-wall carbon nanotubes. *Chemical Physics Letters* **1998,** 296, (1-2), 188-194.

88. Moore, V. C.; Strano, M. S.; Haroz, E. H.; Hauge, R. H.; Smalley, R. E.; Schmidt, J.; Talmon, Y., Individually suspended single-walled carbon nanotubes in various surfactants. *Nano Letters* **2003,** 3, (10), 1379-1382.

89. Niyogi, S.; Hamon, M. A.; Hu, H.; Zhao, B.; Bhowmik, P.; Sen, R.; Itkis, M. E.; Haddon, R. C., Chemistry of single-walled carbon nanotubes. *Accounts of Chemical Research* **2002,** 35, (12), 1105-1113.

90. Park, C.; Ounaies, Z.; Watson, K. A.; Crooks, R. E.; Smith, J.; Lowther, S. E.; Connell, J. W.; Siochi, E. J.; Harrison, J. S.; Clair, T. L. S., Dispersion of single wall carbon nanotubes by in situ polymerization under sonication. *Chemical Physics Letters* **2002,** 364, (3-4), 303-308.

91. Penicaud, A.; Poulin, P.; Derre, A.; Anglaret, E.; Petit, P., Spontaneous dissolution of a single-wall carbon nanotube salt. *Journal of the American Chemical Society* **2005,** 127, (1), 8-9.

92. Petit, P.; Mathis, C.; Journet, C.; Bernier, P., Tuning and monitoring the electronic structure of carbon nanotubes. *Chemical Physics Letters* **1999,** 305, (5-6), 370-374.

93. Philip, B.; Xie, J. N.; Chandrasekhar, A.; Abraham, J.; Varadan, V. K., A novel nanocomposite from multiwalled carbon nanotubes functionalized with a conducting polymer. *Smart Materials & Structures* **2004,** 13, (2), 295-298.

94. Putz, K. W.; Mitchell, C. A.; Krishnamoorti, R.; Green, P. F., Elastic modulus of single-walled carbon nanotube/poly(methyl methacrylate) nanocomposites. *Journal of Polymer Science Part B-Polymer Physics* **2004,** 42, (12), 2286-2293.

95. Richard, C.; Balavoine, F.; Schultz, P.; Ebbesen, T. W.; Mioskowski, C., Supramolecular self-assembly of lipid derivatives on carbon nanotubes. *Science* **2003,** 300, (5620), 775-778.

96. Riggs, J. E.; Guo, Z. X.; Carroll, D. L.; Sun, Y. P., Strong luminescence of solubilized carbon nanotubes. *Journal of the American Chemical Society* **2000,** 122, (24), 5879-5880.

97. Rinzler, A. G.; Liu, J.; Dai, H.; Nikolaev, P.; Huffman, C. B.; Rodriguez-Macias, F. J.; Boul, P. J.; Lu, A. H.; Heymann, D.; Colbert, D. T.; Lee, R. S.; Fischer, J. E.; Rao, A. M.; Eklund, P. C.; Smalley, R. E., Large-scale purification of single-wall carbon nanotubes: process, product, and characterization. *Applied Physics a-Materials Science & Processing* **1998,** 67, (1), 29-37.

98. Satake, A.; Miyajima, Y.; Kobuke, Y., Porphyrin - Carbon nanotube composites formed by noncovalent polymer wrapping. *Chemistry of Materials* **2005,** 17, (4), 716-724.

99. Shaffer, M. S. P.; Fan, X.; Windle, A. H., Dispersion and packing of carbon nanotubes. *Carbon* **1998,** 36, (11), 1603-1612.

100. Sreekumar, T. V.; Liu, T.; Kumar, S.; Ericson, L. M.; Hauge, R. H.; Smalley, R. E., Single-wall carbon nanotube films. *Chemistry of Materials* **2003,** 15, (1), 175-178.

101. Star, A.; Han, T. R.; Joshi, V.; Stetter, J. R., Sensing with Nafion coated carbon nanotube field-effect transistors. *Electroanalysis* **2004,** 16, (1-2), 108-112.

102. Takahashi, T.; Tsunoda, K.; Yajima, H.; Ishii, T., Isolation of single-wall carbon nanotube bundles through gelatin wrapping and unwrapping processes. *Chemistry Letters* **2002**, (7), 690-691.

103. Xie, Y. H.; Soh, A. K., Investigation of non-covalent association of single-walled carbon nanotube with amylose by molecular dynamics simulation. *Materials Letters* **2005,** 59, (8-9), 971-975.

104. Xu, Z.; Chen, X.; Qu, X. H.; Jia, J. B.; Dong, S. J., Single-wall carbon nanotube-based voltammetric sensor and biosensor. *Biosensors & Bioelectronics* **2004,** 20, (3), 579-584.

105. Brown, S. D. M.; Jorio, A.; Corio, P.; Dresselhaus, M. S.; Dresselhaus, G.; Saito, R.; Kneipp, K., Origin of the Breit-Wigner-Fano lineshape of the tangential G-band feature of metallic carbon nanotubes. *Physical Review B* **2001,** 6315, (15), art. no.-155414.

106. Fischer, J. E.; Zhou, W.; Vavro, J.; Llaguno, M. C.; Guthy, C.; Haggenmueller, R.; Casavant, M. J.; Walters, D. E.; Smalley, R. E., Magnetically aligned single wall carbon nanotube films: Preferred orientation and anisotropic transport properties. *Journal of Applied Physics* **2003,** 93, (4), 2157-2163.

107. Zheng, L. X.; O'Connell, M. J.; Doorn, S. K.; Liao, X. Z.; Zhao, Y. H.; Akhadov, E. A.; Hoffbauer, M. A.; Roop, B. J.; Jia, Q. X.; Dye, R. C.; Peterson, D. E.; Huang, S. M.; Liu, J.; Zhu, Y. T., Ultralong single-wall carbon nanotubes. *Nature Materials* **2004,** 3, (10), 673-676.

108. Samuels, R. J., *Structured Polymer Properties*. John Wiley & Sons, Inc.: New York, 1974; p 28-41.

109. Wilchinsky, Z. W., Measurement of Orientation in Polypropylene Film. *Journal of Applied Physics* **1960,** 31, (11), 1969-1972.

110. Li, Y. L.; Kinloch, I. A.; Windle, A. H., Direct spinning of carbon nanotube fibers from chemical vapor deposition synthesis. *Science* **2004,** 304, (5668), 276-278.

111. Zhang, M.; Atkinson, K. R.; Baughman, R. H., Multifunctional carbon nanotube yarns by downsizing an ancient technology. *Science* **2004,** 306, (5700), 1358-1361.

112. Benoit, J. M.; Corraze, B.; Chauvet, O., Localization, Coulomb interactions, and electrical heating in single-wall carbon nanotubes/polymer composites. *Physical Review B* **2002,** 65, (24), 241405.

113. Biercuk, M. J.; Llaguno, M. C.; Radosavljevic, M.; Hyun, J. K.; Johnson, A. T.; Fischer, J. E., Carbon nanotube composites for thermal management. *Applied Physics Letters* **2002,** 80, (15), 2767-2769.

114. Cooper, C. A.; Ravich, D.; Lips, D.; Mayer, J.; Wagner, H. D., Distribution and alignment of carbon nanotubes and nanofibrils in a polymer matrix. *Composites Science and Technology* **2002,** 62, (7-8), 1105-1112.

115. Kim, B.; Lee, J.; Yu, I. S., Electrical properties of single-wall carbon nanotube and epoxy composites. *Journal of Applied Physics* **2003,** 94, (10), 6724-6728.

116. Shaffer, M. S. P.; Windle, A. H., Fabrication and characterization of carbon nanotube/poly(vinyl alcohol) composites. *Advanced Materials* **1999,** 11, (11), 937-941.

117. Zhang, X. F.; Liu, T.; Sreekumar, T. V.; Kumar, S.; Moore, V. C.; Hauge, R. H.; Smalley, R. E., Poly(vinyl alcohol)/SWNT composite film. *Nano Letters* **2003,** 3, (9), 1285-1288.

118. Dalton, A. B.; Collins, S.; Munoz, E.; Razal, J. M.; Ebron, V. H.; Ferraris, J. P.; Coleman, J. N.; Kim, B. G.; Baughman, R. H., Super-tough carbon-nanotube fibres - These extraordinary composite fibres can be woven into electronic textiles. *Nature* **2003,** 423, (6941), 703-703.

119. Dalton, A. B.; Collins, S.; Razal, J.; Munoz, E.; Ebron, V. H.; Kim, B. G.; Coleman, J. N.; Ferraris, J. P.; Baughman, R. H., Continuous carbon nanotube composite fibers: properties, potential applications, and problems. *Journal Of Materials Chemistry* **2004,** 14, (1), 1-3.

120. Zhang, X. F.; Liu, T.; Sreekumar, T. V.; Kumar, S.; Hu, X. D.; Smith, K., Gel spinning of PVA/SWNT composite fiber. *Polymer* **2004,** 45, (26), 8801-8807.

121. Mylvaganam, K.; Zhang, L. C., Chemical bonding in polyethylene-nanotube composites: A quantum mechanics prediction. *Journal of Physical Chemistry B* **2004,** 108, (17), 5217-5220.

122. Wu, M.; Shaw, L. L., On the improved properties of injection-molded, carbon nanotube-filled PET/PVDF blends. *Journal of Power Sources* **2004,** 136, (1), 37-44.

123. Sen, R.; Zhao, B.; Perea, D.; Itkis, M. E.; Hu, H.; Love, J.; Bekyarova, E.; Haddon, R. C., Preparation of single-walled carbon nanotube reinforced polystyrene and polyurethane nanofibers and membranes by electrospinning. *Nano Letters* **2004,** 4, (3), 459-464.

124. Martin, C. A.; Sandler, J. K. W.; Windle, A. H.; Schwarz, M. K.; Bauhofer, W.; Schulte, K.; Shaffer, M. S. P., Electric field-induced aligned multi-wall carbon nanotube networks in epoxy composites. *Polymer* **2005,** 46, (3), 877-886.

125. Pecastaings, G.; Delhaes, P.; Derre, A.; Saadaoui, H.; Carmona, F.; Cui, S., Role of interfacial effects in carbon nanotube/epoxy nanocomposite behavior. *Journal of Nanoscience and Nanotechnology* **2004,** 4, (7), 838-843.

126. Zhao, B.; Hu, H.; Haddon, R. C., Synthesis and properties of a water-soluble single-walled carbon nanotube-poly(m-aminobenzene sulfonic acid) graft copolymer. *Advanced Functional Materials* **2004,** 14, (1), 71-76.

127. Mrozek, R. A.; Kim, B. S.; Holmberg, V. C.; Taton, T. A., Homogeneous, coaxial liquid crystal domain growth from carbon nanotube seeds. *Nano Letters* **2003,** 3, (12), 1665-1669.

128. Thostenson, E. T.; Chou, T. W., Aligned multi-walled carbon nanotube-reinforced composites: processing and mechanical characterization. *Journal of Physics D-Applied Physics* **2002,** 35, (16), L77-L80.

129. Velasco-Santos, C.; Martinez-Hernandez, A. L.; Fisher, F. T.; Ruoff, R.; Castano, V. M., Improvement of thermal and mechanical properties of carbon nanotube composites through chemical functionalization. *Chemistry of Materials* **2003,** 15, (23), 4470-4475.

130. Coleman, J. N.; Cadek, M.; Blake, R.; Nicolosi, V.; Ryan, K. P.; Belton, C.; Fonseca, A.; Nagy, J. B.; Gun'ko, Y. K.; Blau, W. J., High-performance nanotube-reinforced plastics: Understanding the mechanism of strength increase. *Advanced Functional Materials* **2004,** 14, (8), 791-798.

131. Mamedov, A. A.; Kotov, N. A.; Prato, M.; Guldi, D. M.; Wicksted, J. P.; Hirsch, A., Molecular design of strong single-wall carbon nanotube/polyelectrolyte multilayer composites. *Nature Materials* **2002,** 1, (3), 190-194.

132. Ma, H. M.; Zeng, J. J.; Realff, M. L.; Kumar, S.; Schiraldi, D. A., Processing, structure, and properties of fibers from polyester/carbon nanofiber composites. *Composites Science and Technology* **2003,** 63, (11), 1617-1628.

133. Kumar, S.; Doshi, H.; Srinivasarao, M.; Park, J. O.; Schiraldi, D. A., Fibers from polypropylene/nano carbon fiber composites. *Polymer* **2002,** 43, (5), 1701-1703.

134. Zeng, J. J.; Saltysiak, B.; Johnson, W. S.; Schiraldi, D. A.; Kumar, S., Processing and properties of poly(methyl methacrylate)/carbon nanofiber composites. *Composites Part B-Engineering* **2004,** 35, (3), 245-249.

135. Ren, Y.; Fu, Y. Q.; Liao, K.; Li, F.; Cheng, H. M., Fatigue failure mechanisms of single-walled carbon nanotube ropes embedded in epoxy. *Applied Physics Letters* **2004,** 84, (15), 2811-2813.

136. Gong, X. Y.; Liu, J.; Baskaran, S.; Voise, R. D.; Young, J. S., Surfactant-assisted processing of carbon nanotube/polymer composites. *Chemistry of Materials* **2000,** 12, (4), 1049-1052.

137. Pham, J. Q.; Mitchell, C. A.; Bahr, J. L.; Tour, J. M.; Krishanamoorti, R.; Green, P. F., Glass transition of polymer/single-walled carbon nanotube composite films. *Journal of Polymer Science Part B-Polymer Physics* **2003,** 41, (24), 3339-3345.

138. Grunlan, J. C.; Mehrabi, A. R.; Bannon, M. V.; Bahr, J. L., Water-based single-walled-nanotube-filled polymer composite with an exceptionally low percolation threshold. *Advanced Materials* **2004,** 16, (2), 150-153.

139. Sandler, J. K. W.; Kirk, J. E.; Kinloch, I. A.; Shaffer, M. S. P.; Windle, A. H., Ultra-low electrical percolation threshold in carbon-nanotube-epoxy composites. *Polymer* **2003,** 44, (19), 5893-5899.

140. Shenogin, S.; Xue, L. P.; Ozisik, R.; Keblinski, P.; Cahill, D. G., Role of thermal boundary resistance on the heat flow in carbon-nanotube composites. *Journal of Applied Physics* **2004,** 95, (12), 8136-8144.

141. Guo, H.; Sreekumar, T. V.; Liu, T.; Minus, M.; Kumar, S., Structure and properties of polyacrylonitrile/single wall carbon nanotube composite films. *Polymer* **2005,** 46, (9), 3001-3005.

142. Potschke, P.; Fornes, T. D.; Paul, D. R., Rheological behavior of multiwalled carbon nanotube/polycarbonate composites. *Polymer* **2002,** 43, (11), 3247-3255.

143. Kymakis, E.; Alexandrou, I.; Amaratunga, G. A. J., High open-circuit voltage photovoltaic devices from carbon-nanotube-polymer composites. *Journal of Applied Physics* **2003,** 93, (3), 1764-1768.

144. Liu, T.; Sreekumar, T. V.; Kumar, S.; Hauge, R. H.; Smalley, R. E., SWNT/PAN composite film-based supercapacitors. *Carbon* **2003,** 41, (12), 2440-2442.

145. Xiao, Q. F.; Zhou, X., The study of multiwalled carbon nanotube deposited with conducting polymer for supercapacitor. *Electrochimica Acta* **2003,** 48, (5), 575-580.

146. Kim, J. Y.; Kim, M.; Choi, J. H., Characterization of light emitting devices based on a single-walled carbon nanotube-polymer composite. *Synthetic Metals* **2003,** 139, (3), 565-568.

147. Park, J. H.; Choi, J. H.; Moon, J. S.; Kushinov, D. G.; Yoo, J. B.; Park, C. Y.; Nam, J. W.; Lee, C. K.; Park, J. H.; Choe, D. H., Simple approach for the fabrication of carbon nanotube field emitter using conducting paste. *Carbon* **2005,** 43, (4), 698-703.

148. Wang, Q. H.; Setlur, A. A.; Lauerhaas, J. M.; Dai, J. Y.; Seelig, E. W.; Chang, R. P. H., A nanotube-based field-emission flat panel display. *Applied Physics Letters* **1998,** 72, (22), 2912-2913.

149. Abraham, J. K.; Philip, B.; Witchurch, A.; Varadan, V. K.; Reddy, C. C., A compact wireless gas sensor using a carbon nanotube/PMMA thin film chemiresistor. *Smart Materials & Structures* **2004,** 13, (5), 1045-1049.

150. Sayago, I.; Terrado, E.; Lafuente, E.; Horrillo, M. C.; Maser, W. K.; Benito, A. M.; Navarro, R.; Urriolabeitia, E. P.; Martinez, M. T.; Gutierrez, J., Hydrogen sensors based on carbon nanotubes thin films. *Synthetic Metals* **2005,** 148, (1), 15-19.

151. Zhao, Q.; Frogley, M. D.; Wagner, H. D., The use of carbon nanotubes to sense matrix stresses around a single glass fiber. *Composites Science and Technology* **2001,** 61, (14), 2139-2143.

152. Zhao, Q.; Frogley, M. D.; Wagner, H. D., Direction-sensitive stress measurements with carbon nanotube sensors. *Polymers for Advanced Technologies* **2002,** 13, (10-12), 759-764.

153. Raravikar, N. R.; Keblinski, P.; Rao, A. M.; Dresselhaus, M. S.; Schadler, L. S.; Ajayan, P. M., Temperature dependence of radial breathing mode Raman frequency of single-walled carbon nanotubes. *Physical Review B* **2002,** 66, (23), 235424.

154. Wood, J. R.; Zhao, Q.; Frogley, M. D.; Meurs, E. R.; Prins, A. D.; Peijs, T.; Dunstan, D. J.; Wagner, H. D., Carbon nanotubes: From molecular to macroscopic sensors. *Physical Review B* **2000,** 62, (11), 7571-7575.

155. Matarredona, O.; Rhoads, H.; Li, Z. R.; Harwell, J. H.; Balzano, L.; Resasco, D. E., Dispersion of single-walled carbon nanotubes in aqueous solutions of the anionic surfactant NaDDBS. *Journal of Physical Chemistry B* **2003,** 107, (48), 13357-13367.

156. Wang, H.; Zhou, W.; Ho, D. L.; Winey, K. I.; Fischer, J. E.; Glinka, C. J.; Hobbie, E. K., Dispersing single-walled carbon nanotubes with surfactants: A small angle neutron scattering study. *Nano Letters* **2004,** 4, (9), 1789-1793.

157. Potschke, P.; Bhattacharyya, A. R.; Janke, A., Melt mixing of polycarbonate with multiwalled carbon nanotubes: microscopic studies on the state of dispersion. *European Polymer Journal* **2004,** 40, (1), 137-148.

158. Cadek, M.; Coleman, J. N.; Barron, V.; Hedicke, K.; Blau, W. J., Morphological and mechanical properties of carbon-nanotube-reinforced semicrystalline and amorphous polymer composites. *Applied Physics Letters* **2002,** 81, (27), 5123-5125.

159. Jin, Z.; Pramoda, K. P.; Xu, G.; Goh, S. H., Dynamic mechanical behavior of melt-processed multi-walled carbon nanotube/poly(methyl methacrylate) composites. *Chemical Physics Letters* **2001,** 337, (1-3), 43-47.

160. Gojny, F. H.; Wichmann, M. H. G.; Kopke, U.; Fiedler, B.; Schulte, K., Carbon nanotube-reinforced epoxy-compo sites: enhanced stiffness and fracture toughness at low nanotube content. *Composites Science and Technology* **2004,** 64, (15), 2363-2371.

161. Schadler, L. S.; Giannaris, S. C.; Ajayan, P. M., Load transfer in carbon nanotube epoxy composites. *Applied Physics Letters* **1998,** 73, (26), 3842-3844.

162. Uchida, T.; Kumar, S., Single wall carbon nanotube dispersion and exfoliation in polymers. *Journal of Applied Polymer Science* **2005,** 98, (3), 985-989.

163. Min, B. G.; Sreekumar, T. V.; Uchida, T.; Kumar, S., Oxidative stabilization of PAN/SWNT composite fiber. *Carbon* **2005,** 43, (3), 599-604.

164. Ge, J. J.; Hou, H. Q.; Li, Q.; Graham, M. J.; Greiner, A.; Reneker, D. H.; Harris, F. W.; Cheng, S. Z. D., Assembly of well-aligned multiwalled carbon nanotubes in confined polyacrylonitrile environments: Electrospun composite nanofiber sheets. *Journal of the American Chemical Society* **2004,** 126, (48), 15754-15761.

165. Ye, H. H.; Lam, H.; Titchenal, N.; Gogotsi, Y.; Ko, F., Reinforcement and rupture behavior of carbon nanotubes-polymer nanofibers. *Applied Physics Letters* **2004,** 85, (10), 1775-1777.

166. Ko, F.; Gogotsi, Y.; Ali, A.; Naguib, N.; Ye, H. H.; Yang, G. L.; Li, C.; Willis, P., Electrospinning of continuons carbon nanotube-filled nanofiber yarns. *Advanced Materials* **2003,** 15, (14), 1161-1165.

167. Koganemaru, A.; Bin, Y.; Agari, Y.; Matsuo, M., Composites of polyacrylonitrile and multiwalled carbon nanotubes prepared by gelation/crystallization from solution. *Advanced Functional Materials* **2004,** 14, (9), 842-850.

168. Cadek, M.; Coleman, J. N.; Ryan, K. P.; Nicolosi, V.; Bister, G.; Fonseca, A.; Nagy, J. B.; Szostak, K.; Beguin, F.; Blau, W. J., Reinforcement of polymers with carbon nanotubes: The role of nanotube surface area. *Nano Letters* **2004,** 4, (2), 353-356.

169. Fornes, T. D.; Baur, J. W.; Sabba, Y.; Thomas, E. L., Morphology and properties of melt-spun polycarbonate fibers containing single- and multi-wall carbon nanotubes. *Polymer* **2006,** 47, (5), 1704-1714.

170. Chiang, I. W.; Brinson, B. E.; Smalley, R. E.; Margrave, J. L.; Hauge, R. H., Purification and characterization of single-wall carbon nanotubes. *Journal of Physical Chemistry B* **2001,** 105, (6), 1157-1161.

171. Shimamura, K.; Minter, J. R.; Thomas, E. L., Lattice Imaging of High Modulus Poly(Para-Phenylene Benzobisthiazole) Fibers. *Journal of Materials Science Letters* **1983,** 2, (2), 54-58.

172. Donald, A. M.; Windle, A. H., In *Liquid crystalline polymers*, Cahn, R. W.; Davis, E. A.; Ward, I. M., Eds. Cambridge University Press: Cambridge, 1992; p 250.

173. Ledbetter, H. D.; Rosenberg, S.; Hurtig, C. W. In Materials Research Society Symposium Proceedings, 1989; 1989; pp 253-264.

174. Luo, S.; Grubb, D. T.; Netravali, A. N., The effect of molecular weight on the lamellar structure, thermal and mechanical properties of poly(hydroxybutyrate-co-hydroxyvalerates). *Polymer* **2002,** 43, (15), 4159-4166.

175. Zimmerman, J.; Kohan, M. I., Nylon-selected topics. *Journal of Polymer Science Part a-Polymer Chemistry* **2001,** 39, (15), 2565-2570.

176. Endo, M.; Kim, Y. A.; Hayashi, T.; Yanagisawa, T.; Muramatsu, H.; Ezaka, M.; Terrones, H.; Terrones, M.; Dresselhaus, M. S., Microstructural changes induced in "stacked cup" carbon nanofibers by heat treatment. *Carbon* **2003,** 41, (10), 1941-1947.

177. Dumitrica, T.; Landis, C. M.; Yakobson, B. I., Curvature-induced polarization in carbon nanoshells. *Chemical Physics Letters* **2002,** 360, (1-2), 182-188.

178. Hamon, M. A.; Itkis, M. E.; Niyogi, S.; Alvaraez, T.; Kuper, C.; Menon, M.; Haddon, R. C., Effect of rehybridization on the electronic structure of single-walled carbon nanotubes. *Journal of the American Chemical Society* **2001,** 123, (45), 11292-11293.

179. Liu, T.; Kumar, S., Effect of orientation on the modulus of SWNT films and fibers. *Nano Letters* **2003,** 3, (5), 647-650.

180. Ward, I. M.; Hadley, D. W., *An Introduction to the mechanical properties of solid polymers*. Wiley: New York, 1995.

181. Provided by manufacturer.

182. Sugai, T.; Yoshida, H.; Shimada, T.; Okazaki, T.; Shinohara, H., New synthesis of high-quality double-walled carbon nanotubes by high-temperature pulsed arc discharge. *Nano Letters* **2003,** 3, (6), 769-773.

183. Koerner, H.; Liu, W. D.; Alexander, M.; Mirau, P.; Dowty, H.; Vaia, R. A., Deformation-morphology correlations in electrically conductive carbon nanotube thermoplastic polyurethane nanocomposites. *Polymer* **2005,** 46, (12), 4405-4420.

184. Shen, L. X.; Li, J., Transversely isotropic elastic properties of multiwalled carbon nanotubes. *Physical Review B* **2005,** 71, (3), Art. No. 035412.

185. Chawla, K. K., *Fibrous materials*. Cambridge University Press: Cambridge, 1998.

186. Smith, P.; Lemstra, P. J.; Booij, H. C., Ultradrawing of High-Molecular-Weight Polyethylene Cast from Solution .2. Influence of Initial Polymer Concentration. *Journal of Polymer Science Part B-Polymer Physics* **1981,** 19, (5), 877-888.

187. Smith, P.; Lemstra, P. J.; Kalb, B.; Pennings, A. J., Ultrahigh-Strength Polyethylene Filaments by Solution Spinning and Hot Drawing. *Polymer Bulletin* **1979,** 1, (11), 733-736.

188. Cha, W. I.; Hyon, S. H.; Ikada, Y., Gel Spinning of Poly(Vinyl Alcohol) from Dimethyl Sulfoxide/Water Mixture. *Journal of Polymer Science Part B-Polymer Physics* **1994,** 32, (2), 297-304.

189. Takahashi, T.; Suzuki, K.; Aoki, T.; Sakurai, K., Banded Structure of Gel-Drawn Poly(Vinyl Alcohol) Fibers. *Journal of Macromolecular Science-Physics* **1991,** B30, (1-2), 101-118.

190. Qian, B. J.; Lin, W. P.; He, J. M.; Hu, P. P.; Wu, C. X., The role of macromolecular entanglements in the gel spinning process and properties of high performance polyacrylonitrile fibers. *Journal of Polymer Engineering* **1996,** 15, (3-4), 327-345.

191. Sawai, D.; Kanamoto, T.; Porter, R. S., Differential scanning calorimetry evidence for the existence of a first-order thermal transition in ultraoriented at-poly(acrylonitrile). *Macromolecules* **1998,** 31, (6), 2010-2012.

192. Sawai, D.; Kanamoto, T.; Yamazaki, H.; Hisatani, K., Dynamic mechanical relaxations in poly(acrylonitrile) with different stereoregularities. *Macromolecules* **2004,** 37, (8), 2839-2846.

193. Sawai, D.; Yamane, A.; Kameda, T.; Kanamoto, T.; Ito, M.; Yamazaki, H.; Hisatani, K., Uniaxial drawing of isotactic poly(acrylonitrile): Development of oriented structure and tensile properties. *Macromolecules* **1999,** 32, (17), 5622-5630.

194. Sawai, D.; Yamane, A.; Takahashi, H.; Kanamoto, T.; Ito, M.; Porter, R. S., Development of high ductility and tensile properties by a two-stage draw of poly(acrylonitrile): Effect of molecular weight. *Journal of Polymer Science Part B-Polymer Physics* **1998,** 36, (4), 629-640.

195. Yamane, A.; Sawai, D.; Kameda, T.; Kanamoto, T.; Ito, M.; Porter, R. S., Development of high ductility and tensile properties upon two-stage draw of ultrahigh molecular weight poly(acrylonitrile). *Macromolecules* **1997,** 30, (14), 4170-4178.

196. Chae, H. G.; Kumar, S., Making strong fibers. *Science* **2008,** 319, 908-909.

197. Allen, R. A.; Ward, I. M.; Bashir, Z., The Variation of the D-Spacings with Stress in the Hexagonal Polymorph of Polyacrylonitrile. *Polymer* **1994,** 35, (19), 4035-4040.

198. Allen, R. A.; Ward, I. M.; Bashir, Z., An Investigation into the Possibility of Measuring an X-Ray Modulus and New Evidence for Hexagonal Packing in Polyacrylonitrile. *Polymer* **1994,** 35, (10), 2063-2071.

199. Colvin, B. G.; Storr, P., Crystal-Structure of Polyacrylonitrile. *European Polymer Journal* **1974,** 10, (4), 337-340.

200. Kumamaru, F.; Kajiyama, T.; Takayanagi, M., Formation of Single-Crystals of Poly(Acrylonitrile) during the Process of Solution Polymerization. *Journal of Crystal Growth* **1980,** 48, (2), 202-209.

201. Bashir, Z., Cocrystallization of Solvents with Polymers - the X-Ray-Diffraction Behavior of Solvent-Containing and Solvent-Free Polyacrylonitrile. *Journal of Polymer Science Part B-Polymer Physics* **1994,** 32, (6), 1115-1128.

202. Bashir, Z. In *Order and morphology in atactic polyacrylonitrile*, International conference on emerging trends in polymers and textiles, 2005; Jassal, M.; Agrawal, A. K., Eds. Indian Institute of Technology, Delhi: 2005; pp 17-28.

203. Minus, M. L.; Chae, H. G.; Kumar, S., Single wall carbon nanotube templated oriented crystallization of poly(vinyl alcohol). *Polymer* **2006,** 47, (11), 3705-3710.

204. Haggenmueller, R.; Zhou, W.; Fischer, J. E.; Winey, K. I., Production and characterization of polymer nanocomposites with highly aligned single-walled carbon nanotubes. *Journal of Nanoscience and Nanotechnology* **2003,** 3, (1-2), 105-110.

205. Potschke, P.; Brunig, H.; Janke, A.; Fischer, D.; Jehnichen, D., Orientation of multiwalled carbon nanotubes in composites with polycarbonate by melt spinning. *Polymer* **2005,** 46, (23), 10355-10363.

206. Miaudet, P.; Badaire, S.; Maugey, M.; Derre, A.; Pichot, V.; Launois, P.; Poulin, P.; Zakri, C., Hot-drawing of single and multiwall carbon nanotube fibers for high toughness and alignment. *Nano Letters* **2005,** 5, (11), 2212-2215.

207. Motta, M.; Li, Y. L.; Kinloch, I.; Windle, A., Mechanical properties of continuously spun fibers of carbon nanotubes. *Nano Letters* **2005,** 5, (8), 1529-1533.

208. Vigolo, B.; Penicaud, A.; Coulon, C.; Sauder, C.; Pailler, R.; Journet, C.; Bernier, P.; Poulin, P., Macroscopic fibers and ribbons of oriented carbon nanotubes. *Science* **2000,** 290, (5495), 1331-1334.

209. Zhou, W.; Vavro, J.; Guthy, C.; Winey, K. I.; Fischer, J. E.; Ericson, L. M.; Ramesh, S.; Saini, R.; Davis, V. A.; Kittrell, C.; Pasquali, M.; Hauge, R. H.;

Smalley, R. E., Single wall carbon nanotube fibers extruded from super-acid suspensions: Preferred orientation, electrical, and thermal transport. *Journal of Applied Physics* **2004,** 95, (2), 649-655.

210. Mcbriert.Vj; Ward, I. M., Investigation of Orientation Distribution Functions in Drawn Polyethylene by Broad Line Nuclear Magnetic Resonance. *Journal of Physics D-Applied Physics* **1968,** 1, (11), 1529-&.

211. Jiang, H.; Huang, Y.; Hwang, K. C., A finite-temperature continuum theory based on interatomic potentials. *Journal of Engineering Materials and Technology-Transactions of the Asme* **2005,** 127, (4), 408-416.

212. Raravikar, N. R.; Keblinski, P.; Rao, A. M.; Dresselhaus, M. S.; Schadler, L. S.; Ajayan, P. M., Temperature dependence of radial breathing mode Raman frequency of single-walled carbon nanotubes. *Physical Review B* **2002,** 66, (23), -.

213. Zhu, D.; Koganemaru, A.; Xu, C. Y.; Shen, Q. D.; Li, S. L.; Matsuo, M., Oxidative stabilization of PAN/VGCF composite. *Journal of Applied Polymer Science* **2003,** 87, (13), 2063-2073.

214. Zhu, D.; Xu, C. Y.; Nakura, N.; Matsuo, M., Study of carbon films from PAN/VGCF composites by gelation/crystallization from solution. *Carbon* **2002,** 40, (3), 363-373.

215. Devasia, R.; Reghunadhan, C. P.; Sivadasan, N. P.; Katherine, B. K.; Ninan, K. N., Cyclization reaction in poly(acrylonitrile/itaconic acid) copolymer: An isothermal differential scanning calorimetry kinetic study. *Journal of Applied Polymer Science* **2003,** 88, (4), 915-920.

216. Fochler, H. S.; Mooney, J. R.; Ball, L. E.; Boyer, R. D.; Grasselli, J. G., Infrared and Nmr Spectroscopic Studies of the Thermal-Degradation of Polyacrylonitrile. *Spectrochimica Acta Part a-Molecular and Biomolecular Spectroscopy* **1985,** 41, (1-2), 271-278.

217. Shimada, I.; Takahagi, T.; Fukuhara, M.; Morita, K.; Ishitani, A., Ft-Ir Study of the Stabilization Reaction of Polyacrylonitrile in the Production of Carbon-Fibers. *Journal of Polymer Science Part a-Polymer Chemistry* **1986,** 24, (8), 1989-1995.

218. Sivy, G. T.; Gordon, B.; Coleman, M. M., Studies of the Degradation of Co-Polymers of Acrylonitrile and Acrylamide in Air at 200-Degrees-C - Speculations on the Role of the Preoxidation Step in Carbon-Fiber Formation. *Carbon* **1983,** 21, (6), 573-578.

219. Usami, T.; Itoh, T.; Ohtani, H.; Tsuge, S., Structural Study of Polyacrylonitrile Fibers during Oxidative Thermal-Degradation by Pyrolysis-Gas Chromatography,

Solid-State C-13 Nuclear-Magnetic-Resonance, and Fourier-Transform Infrared-Spectroscopy. *Macromolecules* **1990,** 23, (9), 2460-2465.

220. Zhu, Y.; Wilding, M. A.; Mukhopadhyay, S. K., Estimation, using infrared spectroscopy, of the cyclization of poly(acrylonitrile) during the stabilization stage of carbon fibre production. *Journal of Materials Science* **1996,** 31, (14), 3831-3837.

221. Gallaher, K. L.; Lukco, D.; Grasselli, J. G., Investigations of the Assignment of the 2190 Cm-1 Infrared Band in Polyfumaronitrile. *Canadian Journal of Chemistry-Revue Canadienne De Chimie* **1985,** 63, (7), 1960-1966.

222. Coleman, M. M.; Petcavich, R. J., Fourier-Transform Infrared Studies on Thermal-Degradation of Polyacrylonitrile. *Journal of Polymer Science Part B-Polymer Physics* **1978,** 16, (5), 821-832.

223. Chang, T. E.; Jensen, L. R.; Kisliuk, A.; Pipes, R. B.; Pyrz, R.; Sokolov, A. P., Microscopic mechanism of reinforcement in single-wall carbon nanotube/polypropylene nanocomposite. *Polymer* **2005,** 46, (2), 439-444.

224. Haggenmueller, R.; Gommans, H. H.; Rinzler, A. G.; Fischer, J. E.; Winey, K. I., Aligned single-wall carbon nanotubes in composites by melt processing methods. *Chemical Physics Letters* **2000,** 330, (3-4), 219-225.

225. Kearns, J. C.; Shambaugh, R. L., Polypropylene fibers reinforced with carbon nanotubes. *Journal of Applied Polymer Science* **2002,** 86, (8), 2079-2084.

226. Mottaghitalab, V.; Spinks, G. M.; Wallace, G. G., The influence of carbon nanotubes on mechanical and electrical properties of polyaniline fibers. *Synthetic Metals* **2005,** 152, (1-3), 77-80.

227. Andrews, R.; Jacques, D.; Rao, A. M.; Rantell, T.; Derbyshire, F.; Chen, Y.; Chen, J.; Haddon, R. C., Nanotube composite carbon fibers. *Applied Physics Letters* **1999,** 75, (9), 1329-1331.

228. Jiang, K. L.; Li, Q. Q.; Fan, S. S., Nanotechnology: Spinning continuous carbon nanotube yarns - Carbon nanotubes weave their way into a range of imaginative macroscopic applications. *Nature* **2002,** 419, (6909), 801-801.

229. Koziol, K.; Vilatela, J.; Moisala, A.; Motta, M.; Cunniff, P.; Sennett, M.; Windle, A., High-performance carbon nanotube fiber. *Science* **2007,** 318, (5858), 1892-1895.

230. Motta, M.; Moisala, A.; Kinloch, I. A.; Windle, A. H., High performance fibres from 'Dog bone' carbon nanotubes. *Advanced Materials* **2007,** 19, (21), 3721-+.

231. Donnet, J.-B.; Wang, T. K.; Rebouillat, S.; Peng, J. C., *Carbon Fibers*. 3rd ed.; Marcel Dekker, Inc.: New York, 1998.

232. Bahl, O. P.; Shen, Z. M.; Lavin, J. G.; Ross, R. A., Manufacture of Carbon Fibers. In *Carbon Fibers*, Donnet, J.-B.; Wang, T. K.; Rebouillat, S.; Peng, J. C. M., Eds. Marcel Dekker: New York, 1998; p 1.

233. Peebles, L. H., *Carbon Fibers*. CRC Press: Boca Raton, 1995.

234. Pirlot, C.; Mekhalif, Z.; Fonseca, A.; Nagy, J. B.; Demortier, G.; Delhalle, J., Surface modifications of carbon nanotube/polyacrylonitrile composite films by proton beams. *Chemical Physics Letters* **2003,** 372, (3-4), 595-602.

235. Pirlot, C.; Willems, I.; Fonseca, A.; Nagy, J. B.; Delhalle, J., Preparation and characterization of carbon nanotube/polyacrylonitrile composites. *Advanced Engineering Materials* **2002,** 4, (3), 109-114.

236. Wang, B.; Li, J. W.; Wang, H. P.; Jiang, J. M.; Liu, Y. Q., Rheological behavior of spinning dope of multiwalled carbon nanotube/polyacrylonitrile composites. *Macromolecular Symposia* **2004,** 216, 189-194.

237. Weisenberger, M. C.; Grulke, E. A.; Jacques, D.; Rantell, T.; Andrews, R., Enhanced mechanical properties of polyacrylonitrile/multiwall carbon nanotube composite fibers. *Journal of Nanoscience and Nanotechnology* **2003,** 3, (6), 535-539.

238. Fennessey, S. F.; Farris, R. J., Fabrication of aligned and molecularly oriented electrospun polyacrylonitrile nanofibers and the mechanical behavior of their twisted yams. *Polymer* **2004,** 45, (12), 4217-4225.

239. Gu, S. Y.; Ren, J.; Vancso, G. J., Process optimization and empirical modeling for electrospun polyacrylonitrile (PAN) nanofiber precursor of carbon nanofibers. *European Polymer Journal* **2005,** 41, (11), 2559-2568.

240. Kang, Y. S.; Kim, H. Y.; Ryu, Y. J.; Lee, D. R.; Park, S. J., The effect of processing parameters on the diameter of electrospun polyacrylonitrile(PAN) nano fibers. *Polymer-Korea* **2002,** 26, (3), 360-366.

241. Qin, X. H.; Wan, Y. Q.; He, J. H.; Zhang, J.; Yu, J. Y.; Wang, S. Y., Effect of LiCl on electrospinning of PAN polymer solution: theoretical analysis and experimental verification. *Polymer* **2004,** 45, (18), 6409-6413.

242. Vaisman, L.; Wachtel, E.; Wagner, H. D.; Marom, G., Polymer-nanoinclusion interactions in carbon nanotube based polyacrylonitrile extruded and electrospun fibers. *Polymer* **2007,** 48, (23), 6843-6854.

243. Wang, T.; Kumar, S., Electrospinning of polyacrylonitrile nanofibers. *Journal of Applied Polymer Science* **2006,** 102, (2), 1023-1029.

244. Cho, H. H.; Kim, K. H.; Kang, Y. A.; Ito, H.; Kikutani, T., Fine structure and physical properties of polyethylene/poly(ethylene terephthalate) bicomponent fibers in high-speed spinning. I. Polyethylene sheath/poly(ethylene terephthalate) core fibers. *Journal of Applied Polymer Science* **2000,** 77, (10), 2254-2266.

245. Cho, H. H.; Kim, K. H.; Kang, Y. A.; Ito, H.; Kikutani, T., Fine structure and physical properties of poly(ethylene terephthalate)/polyethylene bicomponent fibers in high-speed spinning. II. Poly(ethylene terephthalate) sheath/polyethylene core fibers. *Journal of Applied Polymer Science* **2000,** 77, (10), 2267-2277.

246. Godshall, D.; White, C.; Wilkes, G. L., Effect of compatibilizer molecular weight and maleic anhydride content on interfacial adhesion of polypropylene-PA6 bicomponent fibers. *Journal of Applied Polymer Science* **2001,** 80, (2), 130-141.

247. Huang, J. H.; Baird, D. G.; Loos, A. C.; Rangarajan, P.; Powell, A., Filament winding of bicomponent fibers consisting of polypropylene and a liquid crystalline polymer. *Composites Part a-Applied Science and Manufacturing* **2001,** 32, (8), 1013-1020.

248. Kikutani, T.; Radhakrishnan, J.; Arikawa, S.; Takaku, A.; Okui, N.; Jin, X.; Niwa, F.; Kudo, Y., High-speed melt spinning of bicomponent fibers: Mechanism of fiber structure development in poly(ethylene terephthalate)/polypropylene system. *Journal of Applied Polymer Science* **1996,** 62, (11), 1913-1924.

249. Radhakrishnan, J.; Ito, H.; Kikutani, T.; Okui, N., Enhancement of fiber structure formation of a liquid crystalline copolyester via ultra-high speed bicomponent spinning with poly(ethylene terephthalate). *Polymer Engineering and Science* **1999,** 39, (1), 89-98.

250. Radhakrishnan, J.; Kikutani, T.; Okui, N., Thinning behavior of the spinline in high-speed bicomponent spinning of high molecular weight and low molecular weight poly(ethylene terephthalate). *Sen-I Gakkaishi* **1996,** 52, (11), 618-622.

251. Wang, Z.; Ciselli, P.; Peijs, T., The extraordinary reinforcing efficiency of single-walled carbon nanotubes in oriented poly(vinyl alcohol) tapes. *Nanotechnology* **2007,** 18, (45).

252. Kozey, V. V.; Jiang, H.; Mehta, V. R.; Kumar, S., COMPRESSIVE BEHAVIOR OF MATERIALS .2. HIGH-PERFORMANCE FIBERS. *Journal of Materials Research* **1995,** 10, (4), 1044-1061.

253. Kozey, V. V.; Kumar, S., COMPRESSION BEHAVIOR OF MATERIALS .1. GLASSY-POLYMERS. *Journal of Materials Research* **1994,** 9, (10), 2717-2726.